Functionalized nanomaterials : their use as contrast agents in bioimaging : mono- and multimodal approaches

Quentin Le Trequesser, Hervé Seznec, Marie-Hélène Delville

Functionalized Nanomaterials: Their Use As Contrast Agents In Bio-imaging: Mono- And Multimodal Approaches

Le Trequesser Quentin,[1,2,3] Seznec Hervé,[2,3] Delville Marie-Hélène[1,*]

[1] CNRS, Université de Bordeaux, ICMCB, 87 avenue du Dr. A. Schweitzer, F-33608, Pessac, France

[2] Université de Bordeaux, CNRS/IN2P3, UMR5797, Centre d'Etudes Nucléaires de Bordeaux Gradignan, Chemin du Solarium, BP120, F-33175, Gradignan, France

[3] CNRS/IN2P3, Université de Bordeaux, UMR5797, Centre d'Etudes Nucléaires de Bordeaux Gradignan, Chemin du Solarium, BP120, F-33175, Gradignan, France

Correspondence should be addressed to MHD (delville@cicmcb-bordeaux.cnrs.fr)

Abstract

The successful development of nanomaterials illustrates the considerable interest in the development of new molecular probes for medical diagnosis and imaging. Substantial progress was made in synthesis protocol and characterization of these materials whereas toxicological issues are sometimes incomplete. Nanoparticle-based contrast agents tend to become efficient tools for enhancing medical diagnostics and surgery for a wide range of

imaging modalities. Multimodal nanoparticles (NPs) are much more efficient than conventional molecular-scale contrast agents. They provide new abilities for *in vivo* detection and enhanced targeting efficiencies through longer circulation times, designed clearance pathways, and multiple binding capacities. Properly protected, they can safely be used for the fabrication of various functional systems with targeting properties, reduced toxicity and proper removal from the body. This review mainly describes the advances in the development of mono- to multimodal NPs and their *in vitro* and *in vivo* relevant biomedical applications ranging from imaging and tracking to cancer treatment. Besides specific applications for classical imaging, (MRI, PET, CT, US, PAI) are also mentioned less common imaging techniques such as terahertz molecular imaging (THMI) or ion beam analysis (IBA). Perspectives on multimodal theranostic NPs and their potential for clinical advances are also mentioned.

Keywords. Nanoparticles, Multimodal Bio-imaging, Characterization, Multifunctionality, Theranostic.

Contenu

Introduction

Nanoparticles as contrast agents tend to become standard practice in the field of imaging, for both bio-imaging and medical imaging [1]. They are used to improve the enhancement of image contrast as compared to molecular species and improve the visibility of features that would otherwise be difficult to detect. They go on receiving considerable attention in this

field for their potential as contrast agents, [2-9] offering many advantages compared to more conventional chemical agents such as greater biocompatibility and reduced toxicity [8, 10-13]. Noninvasive imaging and minimally invasive *in vivo* bio-imaging techniques are of course the most valuable tools for clinical diagnostics. Clinical Imaging modalities generally include complementary techniques [14] such as: optical imaging, [15-23] magnetic resonance imaging (MRI), [24-27] computed tomography (CT), [28] ultrasound imaging (USI) [29-33] positron emission tomography (PET) [34-37] and single photon emission computed tomography (SPECT) [38-40]. Other techniques are also scrutinized, for example multi-photon plasmon resonance microscopy, [41] optical coherence tomography (OCT), [42] surface enhanced Raman spectroscopy (SERS), [15, 43-47] and diffuse optical spectroscopy [48]. Some of these techniques enable entire-organism anatomical imaging (e.g. MRI or PET) and others provide more specific molecular imaging (*e.g.*, optical fluorescence or USI) at subcellular resolution. Combination of these different tools should allow a better early-stage cancer diagnosis, guided stem cell therapies, drug delivery, pathogen detection, gene therapy, image-guided surgery, and cancer staging, [49] in addition to many other clinically relevant procedures, diagnostics, and therapies.

To help improving these techniques resolution, nanoparticles (NPs) emerge as very powerful probes for both *in vivo* imaging in medical and biological diagnostics. Several NP-based contrast agents (CAs) have helped generating breakthroughs as compared to common CAs improving their properties and detection limits, in a broad array of imaging modalities. The specifications of an ideal NP CA are numerous. It should exhibit colloidal stability in biological *in vivo* media, non-dependence on solvent polarity, ionic strength, pH, or temperature. Other properties such as limited nonspecific binding, resistance to reticulo-endothelial system (RES) uptake, and easy clearance mechanisms are also required. High sensitivity and selectivity for the target (*e.g.*, antigen, cell, tissue) with good contrast quality (high signal-to-noise ratio, (SNR)) and sufficiently long blood circulation times are also mandatory. In other words, this NP should have the adapted long-term quantitative imaging at low doses and be safely cleared from the body after imaging completion.

In Table 1 besides the characteristics of the most commonly used *in vivo* imaging modalities in the clinical field are also gathered some more recent ones such as TeraHetz molecular imaging (THMI), Particle induced x-ray emission (PIXE), Rutherford Backscattering Spectrometry (RBS), and Scanning Transmission Ion Microscopy (STIM). Each type of *in*

vivo imaging technique has its own advantages and limitations, which include spatial and/or temporal resolution, sensitivity, SNR, penetration depth in tissue, and quantitative accuracy.

Table 1. List of commonly used bio-imaging techniques (partly adapted from Refs [50] and [51]).

Technique	Typical NP label	Signal measured	Resolution	Depth	Sensitivity (moles of label detected)	Advantages	Cost	Main limitation
Optical and NIRF	QDs, dye-doped NPs, upconverting NPs, SWNTs and other carbon-based nanomaterials (dots, diamonds, graphene)	Light, particularly in the near-infrared	1–3 mm	<1 cm	10^{-12}	High sensitivity Multicolor imaging	Low	Poor depth penetration Poor spatial resolution
MRI	Iron oxide NPs, Gd(III)-doped NPs, NP-based CEST and hyperpolarized probes (*e.g.,* ^{129}Xe)	Alterations in magnetic fields	25–100 µm	No limit	10^{-9}–10^{-6}	High spatial resolution	High	Low sensitivity, cannot follow many labels, time consuming
PET	NPs incorporating radioisotopes (*e.g.,* ^{18}F, ^{11}C, ^{64}Cu, ^{124}I)	Positron from radionuclides	1–2 mm	No limit	10^{-15}	High sensitivity quantitative entire body scanning	High	Can detect only one radionuclide, requires radioactivity
SPECT	NPs incorporating radioisotopes (*e.g.,* ^{99m}Tc, ^{111}In)	γ-rays	1–2 mm	No limit	10^{-14}	High sensitivity	High	Uses radioactivity Poor spatial resolution
CT	Iodinated NPs, gold NPs, iron oxide-doped nanomaterials	X-rays	50 µm	No limit	10^{-6}	High spatial resolution	High	Poor resolution of soft tissues Not quantitative
US	Microbubbles, nanoemulsions, silica NPs, polystyrene NPs	Sound	50 µm	Several cm	10^{-8}	Real-time measurement	Low	Poor image contrast, works poorly in air-containing organs
PAT[a]	Gold nanoshells, gold nanocages, gold nanorods, gold NPs, SWNTs, dye-doped NPs	Sound	50 µm	<5 cm	10^{-12}	multiscale imaging anatomical, functional, molecular and fluid-dynamic imaging	Low	Information processing and machines still being optimized
THMI[b]	Gold nanorods Metal oxide NPs	Heat variation	100 µm	No limit	10^{-6}	High sensitivity molecular network information based on hydrogen bonding		
Ion beam Analysis [52] (PIXE,[c] **RBS,**[d] **STIM**[e] **[53])**	Metal Metal oxide NPs	H^+ beam He^+ ions	>1 µm 50-200nm 250 nm	20 µm	Traces of elements 0.1 to 10 ppm	High sensitivity Elemental mapping Quantitative	high	Restricted to *in vitro* studies

a) PAT: photoacoustic tomography
b) THMI: TeraHetz molecular imaging
c) PIXE: Particle induced x-ray emission
d) RBS: Rutherford Backscattering Spectrometry

e) STIM: Scanning Transmission Ion Microscopy

A close look at the literature reveals that basically there are some types of NPs which always appear as contrast agents: metal NPs (mostly gold) and metal oxide NPs. They appear either as active agents such as iron oxide in MRI for example, or as carriers of the active agent like silica NPs.

In this review, our aim is to give a state of the art of the most recent works on the subject including the most recent techniques, and to categorize these NPs according to their field of activities: MRI, near-infrared fluorescence (NIRF) imaging, positron emission tomography (PET), computed tomography (CT), ultrasound (US), photoacoustic imaging (PAI) and TeraHetz molecular imaging (THMI). Table 1 highlights the current NP-based contrast labels for each of these techniques. The accent will be stressed on multifunctional/multimodal NPs and theranostic NPs; their potential for clinical use, will also be discussed. The reader can also get information on numerous imaging techniques in various reviews [14, 16, 28, 54-56].

1 Magnetic resonance imaging (MRI)

MRI is typically *the* noninvasive and nonionizing imaging method that provides both physiological and pathological information about living tissue, usually by measuring water proton relaxation rates. MRI offers high soft tissue contrast especially with contrast agents (CAs) and provides deep tissue imaging with high spatial resolution (~ 50 μm). The major drawback of this technique is its low sensitivity requiring the use of these CAs whose role is to alter relaxation processes. CAs are divided in two classes: those that increase the T_1 signal in T_1-weighted images (so-called positive contrast agents, giving a bright contrast), and those that reduce the T_2 signal in T_2-weighted images (so-called negative contrast agents, leading to a dark contrast). The effectiveness of a particular probe is defined by its longitudinal (r_1) and transverse (r_2) relaxivities. T_2 agents are not so convenient for diagnosis because they provide dark contrast which is not so easy to interpret for clinicians. In contrast, the signal produced by T_1 (paramagnetic) contrast agents, can easily be detected with high spatial resolution.

1.1 T_1 NPs-based contrast agents

Three important requirements for the design of highly sensitive paramagnetic NPs have been identified: (i) a large number of labile water molecules coordinated to the metal; (ii) optimum residence lifetime at the metal site; and (iii) a slow tumbling motion of the NP containing the

contrast agent.[57] To fulfill these requirements, a well-known T_1 CA, Gd(III), has been incorporated into various nanomaterials, for example silica and perfluorocarbon nanoparticles, carbon nanotubes, [58] carbon nanodots, [59] and nanodiamonds, [60] which all exhibit high MR contrast because of a high payload of gadolinium ions and a slow tumbling motion of particles. For a Gd(III) complex attached to nanodiamonds, a 10-fold relaxivity increase was observed compared with the monomeric Gd(III) complex. Gadolinium chelates were grafted on to gold for dual imaging [61] and mesoporous silica NPs, [62, 63] leading to a high local concentration of CA as compared to molecular complexes. They were associated with other lanthanides to provide particles capable of dual imaging, [64, 65] with drug for therapeutic function [66] or with gene in microglial cells for therapy [67].

However, gadolinium loading on these systems strongly depends on the number of anchoring sites available on the surface of the NPs even if Gd (III) could also recently be dispersed in a carbon matrix [59]. A way to solve this problem relies in the synthesis of Gd–based paramagnetic NPs, [68] such as Ln_2O_3, GdF_3, and $GdPO_4$ [26, 69, 70] which yield high magnetic moments because of the abundance of paramagnetic ions on their surfaces.

Transition metal oxide (MnO) NPs have recently been developed by various groups for T_1-contrast imaging of brain tumors, [71] in addition to the liver and kidney [58, 72]. Hollow MnO NPs could also carry drug molecules in their cavities for simultaneous imaging and therapy applications [73].

Silica has been recognized as a good candidate for a coating material because it is relatively biocompatible and resistant to biodegradation [74, 75]. Among others, mesoporous silica-coated hollow MnO NPs (HMnO@mSiO_2) have been synthesized and characterized. These nanoparticles show a significantly higher r_1 relaxivity than other existing manganese oxide nanoparticle based contrast agents. The porous SiO_2 coating enables water exchange across the shell and the high surface-to-volume ratio of the hollow structure increases the water accessibility to the manganese core and consequently enhances T_1contrast. HMnO@mSiO_2 nanoparticles also showed potential MRI cell tracking using positive contrast [75].

With relaxivities that depend on the biological environment, “smart” T_1 MR probes that respond to their surroundings have been pursued extensively [57]. This class of probe primarily consists of Gd(III)-based complexes; incorporation of these smart probes into NPs will further enhance their efficiency in molecular imaging applications. Very recently, the use of an improved hydrolysis method of inorganic salts assisted by incubation in a water bath, led to water-soluble extremely small-sized metal-iron oxide nanoparticles iron oxide based NPs: MFe_2O_4 (ESIONs) (M = Fe, Zn, Ni) NPs with average sizes of 4 to 5 nm [76, 77]. The r_1

relaxivities and the r_2/r_1 ratios of these nanoparticles were more than 5 and less than 3, respectively, which indicated that they were good candidates as T_1-weighted MRI contrast agents. As an example, the γ-Fe_2O_3 ESIONs were synthesized by controlled thermal decomposition of iron-oleate complex in the presence of oleyl alcohol *via* heat-up process. These ESIONs revealed a maghemite crystal structure with a magnetization much smaller than that of 12 nm-sized iron oxide NPs due to their small magnetic moment and a spin canting effect. ESIONs have a large number of surface Fe^{3+} ions with 5 unpaired electrons exhibited high r_1 relaxivities of > 4.7 mM^{-1} s^{-1} and low r_2/r_1 ratios of < 6.2. Their high r_1 relaxivity and long blood circulation time enabled high-resolution blood pool T_1-weighted MR imaging of various blood vessels with sizes down to 0.2 mm. With their low toxicity, high r_1 relaxivity, long blood half-life, they could become the new T_1 MRI contrast agents for various clinical applications including diagnosis of the myocardial infarction, renal failure, atherosclerotic plaque, thrombosis, and angiogenesis of tumor cells.

1.2 T_2 NPs-based contrast agents

Beside these lanthanide derivatives, magnetic NP-based probes have been developed for MRI to achieve high tissue contrast and to improve imaging sensitivity. The most popular material studied for T_2 (superparamagnetic) contrast agents is based on iron oxide NPs (maghemite and magnetite), which are generally coated with dextran, PEG, or other polymers, and are used for clinical MRI [78-82]. Based on their size, these NPs have been classified as magnetic iron oxide NPs (MION, μm), superparamagnetic iron oxide (SPIO, hundreds of nm), ultra-small paramagnetic iron oxide (USPIO, <50 nm) and down.

SPIO contrast agents have been essentially used clinically for diagnosis of liver diseases, [83] whereas USPIO probes are generally used for lymph-node imaging, angiography, and blood-pool imaging [84-89]. Besides their clinical use, MRI contrast agents based on iron oxide nanoparticles are actually developed for studying biological processes: Significant contributions in this research area have illustrated the potential use of these particles for molecular and cellular imaging applications [78, 80, 82, 90-94].

As an example, [95] Transferrin(Tf)-SPIONs were injected intravenously in a rat bearing two tumors with different levels of Transferrin receptor (TfR) and MRI performed (Figure 1). The decrease in T_2 relaxation time was much more pronounced for the tumor expressing high levels of the TfR compared to the tumor expressing low levels of the receptor showing that both *in vitro* and *in vivo* MRI can be significantly improved when iron oxide NPs are targeted

towards cell surface receptors that are overexpressed in tumors. A better understanding of imaging biology could significantly influence the design, synthesis, and efficacy of MRI probes.

Figure 1 here

The efficiency of iron oxide probes as T_2 contrast agent is size-dependent and increases with higher particle crystallinity [26, 79, 86, 96, 97]. However, these NPs generally synthesized at low temperatures, have poor crystallinity associated with small size, and lack of monodispersity, as also found for other nanomaterials [98].

Another challenge for this class of contrast agents is the development of efficient methods for their dispersion in biological media and surface functionalization for biological targeting. Their encapsulation in a silica coating [99] may be a good option since it provides colloidal stability in biological solutions by avoiding inter-particle interactions and agglomeration. Furthermore, it can act as an anchor for the binding of biological vectors at the NPs surface. The thickness of the silica shell has also a strong influence on the physical properties of the NPs, especially in terms of contrast agent efficacy for magnetic resonance imaging. An ideal shell thickness was determined to be around 35 nm [100].

The inherent negative contrast associated with iron oxide NPs has limited their use in low-signal regions of the body or in organs with intrinsically high magnetic susceptibilities, for example the lungs. To solve this problem, specific methods based on either pulse sequences [101, 102] design [103] or size control [76] of nanoparticles have been developed by researchers to generate bright contrast from iron oxide NPs.

Other T_2-based NPs contrast agents with improved magnetic and physicochemical properties have been developed such as paramagnetic dysprosium nanomaterials (nanoparticles and nanorods) [104, 105]. Their negligible r_1 relaxivity enhances T_2 MR imaging because in that case protons are nearly exclusively induced for T_2 MR imaging at a negligible r_1. Bimetallic ferrite NPs such as $CoFe_2O_4$, $MnFe_2O_4$, and $NiFe_2O_4$ NPs have been investigated as potential T_2 contrast agents, and some of them, especially $MnFe_2O_4$ NPs have been found to display a very high magnetization and large T_2 relaxivity values [106]. However, long term toxicity issues of these new nanomaterials have yet to be assessed. The key point for these NPs to serve as T_1 or T_2 agents is their size. Indeed, some of these ferrites (Fe_3O_4, $ZnFe_2O_4$ and $NiFe_2O_4$) when displaying a 4-5 nm size have recently been used as T_1-weighted contrast agents for magnetic resonance imaging (MRI), see ref. [77].

1.3 Other probes

1.3.1 PARACEST nanoparticles

Nanoparticle CAs are also now used as paramagnetic chemical exchange saturation transfer (PARACEST) agents when they display bound water signals that can exchange protons with the bulk water. PARACEST magnetic resonance imaging (MRI) relies on these exchangeable protons that resonate at a chemical shift which is clearly distinguishable from the bulk water signal due the paramagnetism of the particle. Radiofrequency pre-pulses when applied at an appropriate frequency saturate the exchangeable protons, which transfer into the bulk water pool and lead to reduced equilibrium magnetization allowing the image contrast to be switched 'on' and 'off' by a simple change of the pulse sequence parameters. To enhance the inherent insensitivity of MRI to PARACEST agents and improve the limit of detection for these agents, nanoscale carriers have been developed such as liposomes, dendrimers, polymers, adenovirus particles, and perfluorocarbon nanoparticles [79, 107-109]. The unique MRI properties of such nanoparticle systems generate a large interest in potential medical applications.

1.3.2 Metal nanoparticles

Ferromagnetic cobalt particles coated with gold (Au) for biocompatibility with a unique shape that enables optical absorption over a broad range of frequencies were used for MRI and photoacoustic tomography (PAT) so as to detect picomolar concentrations of nanoparticles. This dual-modality probe revealed very useful for detection of trace amounts of nanoparticles in biological tissues, in which MRI provides volume detection, whereas PAT performs edge detection [110]. Water-soluble cobalt oxide nanocrystals (CoO NCs) were obtained *via* a phase-transfer method with amphiphilic surfactants, such as anionic (sodium dodecyl sulfate, SDS), neutral (Pluronic F127, PF127) and cationic (cetyltrimethyl ammonium bromide, CTAB) [111]. A field-dependence of the magnetization on the type of surfactants showed the crucial role of the later. The longitudinal relaxivities (r_1) and transverse relaxivities (r_2) of the functionalized CoO NCs gave a r_2/r_1 of about 26 for CoO NCs functionalized with PF127 showing some potential as T_2 contrast agents. Cobalt ferrite NPs were also probed and displayed $r_2$values higher than those of commercial ferumoxytol (91 mM^{-1} s^{-1}) [111].

2 Near-infrared fluorescence (NIRF) imaging

Fluorescence imaging is a powerful molecular imaging technique, in which specific probes (*i.e.*, fluorophores) are excited by incident radiation, usually in the visible or NIR, and emit energy at a (usually) lower energy than that of the excitation one. Despite its extremely high-sensitivity detection and location of individual cells, mRNA, DNA, proteins, peptides, receptors, low-expressing cellular markers, it lacks the ability to provide anatomical resolution which is limited to 2-3 mm. As long as noninvasive imaging is concerned, fluorescence in the visible region is usable only for thin tissue sections. Deeper penetration depths required for most clinical applications need fluorescence-based techniques working in the NIR region (650-950 nm). In this NIR window, the absorption of water, hemoglobin, and lipids are at their minimum while auto-fluorescence and tissue scattering are low, enabling maximum light penetration and therefore high SNRs and sensitive detection. The light penetration depth depends on the type of tissue imaged; indeed skin and muscles are more transparent than organs with lots of vasculature (*e.g.*, liver and spleen) because of absorption by hemoglobin. However, new advances in optical microscopy imaging techniques [18] have increased light penetration depths. The fluorophores must be bright with large Stokes shifts and high fluorescence quantum yields in the NIR, photostable as well as resistant to degradation in biological systems. Reviews on NPs used in *in vivo* fluorescence imaging are available [112-114].

2.1 Quantum dots

Quantum dots (QDs) exhibit broad absorption spectra, large absorption cross-sections, narrow and tunable emission spectra, high fluorescence quantum yields, and high photostability. [115] For all these reasons they are extremely popular in fluorescence imaging application. Their optical properties enable bi- [116] and even multicolor imaging, with different colored QDs used in a single assay with only one excitation source [117]. This is illustrated in Figure 2, which clearly shows one of the first demonstrations of an *in vivo* simultaneous imaging of five different lymphatic flows and their trafficking to distinct lymph nodes. The versatility and use of multiple QDs in a single assay to visualize several lymphatic drainages in a mouse give rise to a new powerful tool.

Figure 2 here

NIR emitting QDs comprise II–VI, IV–VI, and III–V compounds, such as CdSe, CdTe, HgTe, PbS, PbSe, PbTe, InAs, InP, and GaAs, as well as alloys of these materials, and core@shell structures, which can allow the emission tuning further and alter fluorescence lifetimes. Interesting probes are based on self-illuminating QDs, using fluorescence resonance energy transfer (FRET) from bioluminescent proteins conjugated to the QD [118, 119]. However, potential toxicity due to heavy metal ions has to be taken into account and may be detrimental for their use in clinical bio-imaging [120] and limit their use to *in vitro* and diagnostic assays. However, they have been used successfully in a sentinel lymph node mapping using intraoperative NIRF imaging [121] and more recently in non-human primates. [122] The authors showed that rhesus macaques injected with phospholipid micelle encapsulated CdSe/CdS/ZnS quantum dots did not exhibit evidence of toxicity. Blood and biochemical markers remained within normal ranges following treatment, and histology of major organs after 90 days showed no abnormalities. They deduced that acute toxicity of these quantum dots *in vivo* can be minimal even if chemical analysis revealed that most of the initial dose of cadmium still remained in the liver, spleen and kidneys after 90 days significant of slow breakdown and clearance of quantum dots.

2.2 Dye-doped nanoparticles

NIR dye-doped silica NPs are becoming popular choices of contrast agent for several reasons: silica NPs are optically transparent, water dispersible, biologically inert, nontoxic in the amorphous form, with well-established conjugation strategies to modify the surface to proteins, peptides, and other ligands for cellular receptors using silane chemistry. The use of such as matrix, in which many NIR fluorophores can be encapsulated, reduces the potential toxicity of these fluorescent probes and shields the NIR emitter from the aqueous environment, where the dye usually suffers from low fluorescence quantum yield, degradation, and unsatisfactory photostability. NIR-emitting dyes such as polymethines (Cy5.5, Cy7), indocyanine green (ICG), Alexa Fluor 750, and IRDye78 have already been incorporated into silica NPs. Encapsulation of multiple dyes within a single silica NP generates much brighter and more stable probes than those loaded with a single one. Dye-doped silica NPs are usually synthesized by a sol–gel Stöber process or in microemulsion by simply adding the dye (or a modified form of the dye) to the silica-forming solution.[123] In addition, the use of mesoporous silica NPs enables the loading of an additional functions into the resulting pores, for example imaging probes of sentinel lymph nodes (SLNs) known as the first defense against primary tumor metastasis, [124] sensing [125] or a therapeutic agent

capable of photothermal ablation or a controlled drug release [126]. The covalent chemical grafting of lanthanide complexes on metal oxide nanoparticles was also recently performed and introduction of two different lanthanides gave bimodal contrast agents [64, 65, 127].

2.3 Upconverting nanomaterials

Fluorescence imaging for small animals has received an increasing attention due to its ability to obtain anatomical and physiological details of living systems [128]. Most of the conventional fluorescence probes for bio-imaging are based on single-photon excitation, emitting low energy fluorescence when excited by high energy light. These single-photon probes exhibit some limitations such as (i) DNA damages with cell death due to long-term exposure to high energy excitation; (ii) low signal-to-noise ratio (SNR) due to the significant auto-fluorescence of the biological tissues; (iii) low penetration depth in the biological tissues. As opposed to visible light excitation, near-infrared (NIR) light excitation for *in vivo* imaging provides several advantages, such as deep penetration, weak autofluorescence, minimal photobleaching and low phototoxicity. In particular, two-photon-excited fluorescence imaging based on the anti-Stokes luminescence process revealed a useful strategy for imaging of the living brain to reduce autofluorescence [129].

Nanocrystals with both excitation and photoluminescence (PL) in the biological optical transparency window combined with high quantum efficiency, spectral sharpness, and photostability, makes them extremely promising as optical bio-imaging probes. Rare-earth upconversion nanophosphors (UCNPs) belong to this new generation of luminescent probes for small-animal imaging. When excited by continuous-wave near-infrared light, they exhibit a unique narrow photoluminescence with higher energy. This upconversion luminescence (UCL) makes UCNPs promising as bio-imaging probes with attractive features, such as suppression of the auto-fluorescence from biological samples and a large penetration depth. As a result, UCNPs have emerged as novel imaging agents for small animals. Rules suitable to develop new optical labels for *in vivo* near-infrared optical imaging procedures were reported [130]. Later on, in their critical review, [131] Li *et al.* have recently reviewed the recent developments in the preparation, surface modification and bioconjugation chemistry of these UCNPs, and their applications in bio-imaging and multimodality imaging of small animals.

Among others, upconverting NPs developed as agents for *in vivo* fluorescence imaging, are doped with rare-earth ions derivatives.[132] They absorb NIR light (usually around 980 nm) and emit upconverted light at a higher energy, usually in the green or far-red/NIR, with long

fluorescence lifetime (μs to ms) [133, 134]. For example, polyethyleneimine-coated $NaYF_4$: Yb,Er and $NaYF_4$:Yb,Tm NPs when exposed to a 980-nm NIR laser could be used as upconverting NPs and evidence the first demonstration of use of upconversion fluorophores for cellular and tissue imaging *via* the imaging of visible fluorescence through mouse thigh muscle down to 10 mm depth [135]. Er-doped or Yb/Er-doped ceramic phosphors were synthesized and partly modified with polyethylene glycol to give dispersion and controlled interaction with the biological objects. Near infrared fluorescence of nematodes, mouse tissue and M1 cells was observed by detecting 1.5 μm emission from Er-doped in the ceramic phosphor [136]. In the same way, a new generation of ^{18}F-labeled co-doped with $Gd^{3+}/Yb^{3+}/Er^{3+}$ lanthanide nanoparticles of $NaYF_4$ proved to be multimodality nanoprobes for UCL but also for PET, and MR imaging [137]. The presence of Yb^{3+} and Er^{3+} co-doped in the $NaYF_4$ nanoparticles gave rise to intense UCL emission in the visible relaxivity for MRI. Successful labeling of the lanthanide nanoparticles with ^{18}F gave a particle suitable for PET imaging. *In vivo* PET/MR entire-body imaging of small animals and *ex vivo* UCL imaging experiments on the biodistribution of ^{18}F-labeled lanthanide NPs in small animals indicated the effectiveness of such NPs as a multimodality nanoprobe as discussed later on. Functionalized Y_2O_3-based upconverting NPs also form a promising platform for *in vivo* optical-based diagnostic imaging with an excellent photostability in the NIR as well as a low toxicity [138]. The Yb and Er-doped version of the yttrium oxide nanoparticles (Y_2O_3:YbEr-NPs) exhibit beside a visible UCL, a strong NIR emission under NIR excitation (NIR-NIR emission): the particles shows bright green (550 nm) and red (660 nm) upconversion (UC) as well as near infrared (NIR) fluorescence (1550 nm) under 980 nm excitation [139, 140]. These NPs with NIR fluorescence at energies lower than their excitation wavelength could provide more advantages for bio-imaging applications.

When judiciously coated some YF_3:Yb^{3+}/Er^{3+} NPs lead to upconversion luminescence in the NIR (831 nm) rather than in the visible, which enables greater penetration of the light. [141] Other examples include core@shell $NdF_3@SiO_2$, (α-$NaYbF_4$:Tm^{3+})@CaF_2, $NaGdF_4$: Nd^{3+}@$NaGdF_4$ NPs which also have excitation and emission in the NIR range, and efficient deep tissue imaging of small animals. [133, 142] All of these materials were modified as to become dispersible in aqueous solutions and conjugated to relevant biomolecules for targeting purposes.

2.4 Carbon nanomaterials

Carbon-based nanomaterials are also potential NIR contrast agents for *in vivo* imaging. The near-infrared photoluminescence intrinsic to the semiconducting single-walled carbon nanotubes (SWNTs) is ideal for biological imaging through the low autofluorescence and deep tissue penetration in the near-infrared region beyond 1 μm [143]. Their NIR fluorescence also offers a powerful approach for sensor development and *in vivo* or real-time imaging of biological systems [144]. They present an emission in the second IR window (1000-1350 nm), which would enable even deeper light penetration. The toxicity of SWNTs is still a controversy; their surface chemistry, therapeutics applications and toxicology as well as their use in biomedical imaging were reviewed [145]. A recent strategy to functionalize CNTs with bioactive glycoproteins, glycolipids and glycodendrimers led to a series of biocompatible and water-soluble CNTs which exhibit highly selective interactions with proteins and living cells. Their biomedical applications in cell sensing, gene delivery, bio-imaging , biosensors and bone tissue engineering were analyzed in a review paper [146]. Bioanalytical applications and bio imaging of carbon dots (CDs) have been reviewed [147]. They exhibit the advantages of being excited by single-photon (ultraviolet or near-ultraviolet) as well as multi-photon (red or near-infrared) excitation, and their luminescence properties are essentially due to surface defects. CDs were found to have emission in the visible region when they are passivated by polymer chains [148], doped with inorganic salts or photosensitizer [59, 149-152]. These materials are being investigated for optical imaging agents using both one and two-photon excitation [153]. Despite the fact that small animal or thin tissue imaging has been largely illustrated, clinical applications have not been yet proven.

Colloidal diamond NPs (i.e., nanodiamonds) are yet another nanomaterial being investigated as potential *in vivo* fluorescent probes for biological and medical imaging. They have been shown to be biocompatible, not cytotoxic, and to have a highly reactive surface that is easily functionalized with biological entities [154]. These nanodiamonds emit single photon luminescence when stimulated by laser light owing to a number of different point defects based on different types of vacancies. Comprehensive reviews on nanodiamonds [155] their use as biolabels [156] and in nanomedecine [157] have been published.

Similar to these luminescent carbon dots (C-dots), graphene quantum dots or graphene quantum discs (GQDs) have generated enormous excitement because of their superiority in chemical inertness, biocompatibility and low toxicity. Besides, GQDs, consisting of a single atomic layer of nano-sized graphite, have the excellent performances of graphene, such as high surface area, large diameter and better surface grafting using π–π conjugation and surface groups [158, 159].

2.5 Other probes and NIRF techniques

Luminescent porous silicon NPs (LPSiNPs) emitting at ~ 800 nm are also attractive candidates, excitable by NIR or two-photon excitation (Figure 3) and as opposed to most optically active nanomaterials (carbon nanotubes, gold nanoparticles and quantum dots), they can self-destruct in a mouse model into kidney cleared components in a relatively short period of time with no evidence of toxicity [160].

Figure 3 here

3 Positron emission tomography (PET)

PET is a nuclear medicine imaging technique that produces a three-dimensional (3D) image or picture of functional processes in the body. The system detects pairs of gamma rays emitted indirectly by which is introduced into the body on a biologically active molecule. It relies on the detection of a positron emitted by radioisotopes (tracer); 3D images of the tracer concentration within the body are then constructed by computer analysis. Approved and used on a daily basis as a clinical molecular imaging technique with a resolution of 1-2 mm, [54] it presents however a relatively low spatial resolution which needs be improved. However, PET exhibits the highest sensitivity of all imaging modalities which enables quantification of the local concentration of radionuclide tracer, with only a few trace isotopes [55, 161]. Furthermore, PET penetration depth is unlimited, so the probe can always be imaged, irrespective of the target location. Especially important in cancer imaging and research, PET is capable of detecting molecular changes that are occurring in the body before the macroscopic disease is observed [37, 89, 162] and of monitoring disease progression after treatment (i.e., tumor response to therapy) [163].

Over the past decades, positron emitter labeled nanoparticles have been widely used and substantially improved in a wide range of diagnostic biomedical research. One of the main challenges in this field is now to develop disease-specific nanoprobes with facile and robust radiolabeling strategies. These nanoprobes should also provide (i) imaging stability, (ii) enhanced sensitivity for disease early stage detection, (iii) optimized *in vivo* pharmacokinetics for reduced nonspecific organ uptake, and (iv) improved targeting for high efficacy. A variety of nanoparticles have been engineered and explored for diagnostic and therapeutic potential in various diseases and lately reviewed [164]. They are essentially labeled with PET isotopes for

cardiovascular, pulmonary, and tumor imaging, as well as for pharmacokinetic evaluation [161].

3.1 Radionuclide Labeled Nanoparticles

Common isotopes that can be chelated on to or incorporated within NPs (in an analogous way to the gadolinium ions used for MRI) include ^{18}F, ^{11}C, ^{15}O, ^{13}N, ^{64}Cu, ^{124}I, ^{68}Ga, ^{82}Rb, and ^{86}Y. PET imaging using ^{18}F, which is the most widespread radionuclide probe used in this field, has become an established clinical tool for whole-body imaging. In light its short half-life, its quick conjugation into the probe with a high reaction yield is necessary to improve its efficiency and to reduce cost. A general synthesis strategy for such ^{18}F-labeled rare-earth nanoparticles was developed through a facile inorganic reaction between rare-earth cations (Y^{3+} and Gd^{3+}) and fluoride ions [165]. The ^{18}F-labeled rare-earth NPs were further evaluated by PET imaging, for their *in vivo* distribution and their application in lymph monitoring. There are, however, other types of probes and the main nanoparticle-based PET ones and their labeling radionuclide are reported in Table 2.

Table 2. Labeling Strategies and Specific Activities of PET Radionuclides Labeled Nanoparticles and the Nuclear Characteristics of the corresponding PET Radionuclides. Adapted from Ref. [164] and up-dated.

NPs	**labeling strategy**	**radionuclide**	$T_{1/2}$	**β energy (KeV)**			**main photon KeV (%)**	**Ref.**
				decay (%)	**max.**	**Mean.**		
QDs	nucleophilic substitution	^{18}F	109.7 min	β^+ (96.7) EC (0.1)	634	245	511 (193.5)	[166]
	DOTA	^{64}Cu	12.7 h	β^+ (17) EC (44)	653	278	511 (34.8)	[167]
	DO3A	^{64}Cu						[168]
Iron oxide	Click chemistry	^{18}F						[34, 169]
	DOTA	^{64}Cu						[170] [171] [172]
	dithiocarbamatebisphosphonate	^{64}Cu						[173]
	Direct labeling	^{68}Ga	67.7 min	β^+ (89) EC (11)	1899	829	511 (178.3)	[174]
	Chelation	^{64}Cu						[175]
	NOTA	^{68}Ga						[176]
	Tyrosine	^{124}I	4.18 d	β^+ (23) EC (77)	2138	820	511 (46); 603 (62.9) 723 (10.3)	[177]
Aluminum hydroxide	Inorganic interaction	^{18}F						[178]
Upconversion nanophosphors	Inorganic interaction	^{18}F						[137] [165] [179]
Gold	DOTA	^{64}Cu						[161]

nanoparticle								
Gold nanoshells (SiO_2@Au)	DOTA	^{64}Cu						[180] [181]
Latex	Direct labeling	^{68}Ga						[182]
	DOTA	^{64}Cu						[183]
	TETA, CB-TE2A	^{64}Cu						[184]
	BAT	^{64}Cu						[185]
Liposome	Encapsulation	^{18}F						[186]
	Chelation	^{64}Cu						[185]
	Encapsulation	^{64}Cu						[187]
Solid lipid nanoparticle	Encapsulation	^{18}F						[188]
	DTPA	^{68}Ga						[189]
	BAT chelate	^{64}Cu						[190]
Polymer	Tyrosine	^{76}Br	16.2 h	β^+ (55) EC (45)	3941	1180	511 (109); 559 (74) 657 (15.9); 185	[191]
	DOTA	^{64}Cu						[192]
	[^{18}F] FETos	^{18}F						[193]
		^{124}I						[194]
Nanotube	DOTA	^{64}Cu						[195]
	desferrioxamine B	^{89}Zr	3.3 d	β^+ (23) EC(77)	901	397		[196]
	DOTA	^{86}Y	14.7 h	β^+ (33)	3141	664	511 (63.9); 1077 (82.5)	[197]
Graphene oxide	1,4,7-triazacyclononane-1,4,7-triacetic acid,	^{66}Ga	9.3 h	β^+ (56.5) EC(43.5)	4150	-	-	[198]

The pharmacokinetic and *in vivo* cancer targeting issues of $^{64}Cu^{2+}$ ions functionalized gold nanocages (NCs) (^{64}Cu-DOTA-PEGAuNCs) when followed by PET imaging in normal rodents revealed Au NCs size dependent [161]. 30 nm Au NCs showed much-improved *in vivo* pharmacokinetics with decreased RES system uptake and enhanced blood circulation as compared to 55 nm ones. The PET/CT imaging demonstrated rapid accumulation and centralized distribution of the 30 nm Au NCs in tumors and, more importantly, high tumor-to-muscle ratios. PET/CT images (Figure 4) clearly showed this rapid localization of the 30 nm ^{64}Cu-DOTAPEG-Au NCs in tumors at 1 h post-injection even only with the administration of a trace amount (23.8 fmol).

Figure 4 here

Most of the time PET tracers are incorporated with another modality in NPs, most notably CT [199-202]. Figure 5 illustrates the use ^{18}F-doped cross-linked iron oxide modified tri-modal NPs (18F-CLIO) to image the liver and blood pool of a mouse. The *in vivo* dynamic PET imaging showed very high signal-to-noise ratios for injected ^{18}F-CLIO. The nanoparticle had a vascular half-life of 5.8 h in mice and was internalized into macrophages of liver, spleen,

and phagocytic cells of other lymphatic organs. The NP is additionally biodegradable and breaks down into elemental components within months. PET/CT allows concentrations at 2-4 orders of magnitude lower than those required for MR imaging which likely makes PET imaging an important platform for clinical molecular.

Figure 5 here

Biocompatible inorganic NPs such as hydroxyapatite NPs also revealed as useful PET/CT probes [178]. They showed particularly avid and stable binding of ^{18}F-fluoride in various biological media. The *in vivo* behaviour of the ^{18}F-labelled hydroxyapatite particles determined by PET-CT imaging in mice showed that hydroxyapatite was stable in circulation but its accumulation in liver *via* reticuloendothelial clearance was followed by gradual degradation and release of ^{18}F-fluoride (over a period of 4 h) which then accumulated in bone.

3.2 Coupling with other contrast agents

Among the other modalities that have been combined with PET, should be mentioned ultra-small cancer-selective silica particles grafted with iodine and dye-doped polymers which were recently approved by FDA for in-human clinical trials [203], NIRF agents within the silica NPs [204] or QDs [168, 205, 206] and MRI [199] agents in conjunction with iron oxide nanomaterials [35, 171]. A bifunctional chelator (dithiocarbamate bisphosphonate, (dtcbp)) containing a dithiocarbamate group for binding the PET isotope ^{64}Cu, and a bisphosphonate group for strong binding to Fe_3O_4 was elaborated. Dtcbp efficiently binds ^{64}Cu to form the [^{64}Cu(dtcbp)$_2$] complex which is then grafted on the iron oxide NPs leading to a PET-MR dual modality imaging capabilities of which *in vivo* accumulates in draining lymph nodes (Figure 6) [173].

Figure 6 here

However, the ratio between PET tracer and MRI contrast agent must be carefully controlled, because PET is extremely sensitive whereas MRI is not.

Single-photon emission computed tomography (SPECT), a similar technique which can also detect nanomoles of tracer. SPECT is based on the detection of lower energy γ-emitting radioisotopes such as ^{99m}Tc, ^{111}In, ^{123}I, and ^{131}I [14, 207-209]. As compared to PET, SPECT has the advantage to be more sensitive and versatile, it is cheaper and more widely available

as it does not rely on a local cyclotron for production of isotopes even if it is an order of magnitude less sensitive than PET.

Covalent functionalization of radionuclide-filled single-walled carbon nanotubes were used as radio-probes [210]. The intravenous administration of these ^{125}I loaded SWNTs was tracked *in vivo* using SPECT. Specific tissue accumulation (here lung) coupled with high *in vivo* stability prevented leakage of radionuclide to high-affinity organs (thyroid/stomach) or excretion, and resulted in ultrasensitive imaging and delivery of unprecedented radio-dose density. The nano-encapsulation of iodide within SWNTs enabled its biodistribution to be completely redirected from tissue with innate affinity (thyroid) to lung (Figure 7).

Figure 7 here

4 X-ray imaging and computed tomography (CT)

X-ray computed tomography (CT) is one of the most powerful noninvasive diagnostic imaging techniques in modern medicine. It has been a clinical tool for more than half a century and the first widespread clinical use of NPs as X-ray contrast agents in humans were 3 to 10-nm thorium dioxide nanoparticles [12, 211]. However due to the long-term radiation effects and significant carcinogenicity of the ^{232}Th, its clinical application was rapidly given up.

Iodinated molecules were then used as CT contrast agents in the clinics. They however have relatively short *in vivo* circulation times, which significantly restrict the applications of this technique in target-specific imaging and angiography. The use of large dose of these agents, which may induce serious adverse effects as well as a hypersensitivity to iodine of some patients, led researchers to address these issues. Over the past decade, advances in nanoscience brought some solutions thanks to the unique properties of nanomaterials, such as their prolonged circulating half-life, passive accumulation at the tumor sites, facile surface modification, and integration of multiple functions into a single particle, make them advantageous for *in vivo* applications [212].

4.1 Iodinated nanoparticles

The widespread clinical use of iodinated compounds has encouraged the development of iodinated nanomaterials. Research essentially focuses [213, 214] on the incorporation of iodinated organic compounds into NPs, with designs ranging from emulsions, [215-218]

liposomes, [214, 219-223] and lipoproteins, [224, 225] to insoluble nano objects, [214, 226-228] and polymeric NPs, [215, 229-233]; many of them have been successfully applied *in vivo* [28, 56]. The purpose of these nanomaterials is to locally increase iodine concentrations, resulting in higher local contrast compared with conventional water-soluble CT contrast agents. A key feature of many of these NPs is their pharmacokinetics, which are often markedly different from those of small iodinated molecules in clinical use. They have increased circulation time with the subsequent implications for targeting because longer circulation times increase the chance of interaction and binding of the contrast agent to a target.

Some multimodal nanoparticles were doped with an iodinated compound and used to enhance X-ray contrast [216, 224, 234, 235] as discussed in later on in the review. Iodine has a lower atomic number than gold and bismuth, it however exhibits higher elemental mass attenuation coefficient and incident X-ray energies so that when compared to gold NPs under conditions used for coronary angiography, iodinated contrast agents had equivalent performance [236]. When a contrast agent was developed by combining the two radio-dense elements iodine and gold within a single PAMAM dendrimer, it was demonstrated that the incorporation of both Au NPs and iodine-containing small molecules resulted in a significant cooperative enhancing effect in X-ray attenuation [237].

4.2 Gold nanoparticles

In addition to the clinically used iodine, the element gold has received much attention due to its higher atomic number than iodine, and thus, a larger contribution of photoelectron effect to X-ray attenuation generating a substantial interest in gold NP-based contrast agents for *in vivo* X-ray CT. Gold nano-objects contain a large number of the contrast element (Au) as opposed to iodine-based nanoparticles in which iodinated molecules are often only covalently grafted onto the NP surface thereby lowering the concentration of the agent. Various gold, [10, 61, 238-240] gold@dielectric hybrids, [10, 241-246] and multimodal materials, [96, 246-248] have been fabricated and their *in vivo* functionality as X-ray CT contrast agents for cancer, tissue-specific, and blood-pool imaging. Gold nanomaterials are currently being explored in multiple clinical trials and they constitute a promising next generation candidate for X-ray contrast materials, radiotherapy [249-251] and cancer therapy [252].

4.3 Other contrast materials

Other CT molecular imaging agents have also been studied besides iodinated and gold-based ones. These NPs consist of bismuth sulfide and composite ceramics containing iron oxide and lanthanide materials. Bismuth sulfide NPs have recently been shown to have superior performance to iodine on a molar basis [253-255]. Even if bismuth displays similar mass attenuation coefficients to that of gold and a higher *k*-edge transition, its toxicity may prevent bismuth-based nanomaterials clinical use as CT agents. Other types of CT contrast agents, are those based on iron oxide [256] and have recently been reviewed [94, 257, 258]. A facile approach for fabrication of Fe_3O_4@Au NPs as a dual mode contrast agent for both magnetic resonance (MR) and computed tomography (CT) imaging applications has been performed *via* the combination of a LbL (layer by layer) self-assembly process and dendrimer chemistry [259]. The use of Fe_3O_4@Au NPs as a contrast agent for dual mode MR/CT imaging has been demonstrated not only for *in vitro* imaging of cancer cells, but also for *in vivo* liver imaging *via* MR and subcutaneous tissue imaging *via* CT.

The high atomic weight and large number of unpaired electron makes Gadolinium an excellent contrasting agent both for MRI and CT imaging [12, 260-262]. Therefore, most of the time, NPs are at least dual probe: CT/MRI or CT/NIRF [261, 263, 264]. As an example Gd^{3+} complex-modified $NaLuF_4$-based upconversion nanophosphors were success fully applied for UCL, MR and CT multi-modal imaging, by integrating NIR-to-NIR UCL, X-ray attenuation and paramagnetic function in one single nanoparticle. The property of NIR-to-NIR UCL enhances the high signal-to-noise ratio of *in vivo* imaging of small animal. Moreover, Gd^{3+} grafting on the surface of NPs generates high r_1 relaxivity for the core–shell nanoparticles which become suitable for T_1 MR imaging. In addition, this nanoparticle with the core of Yb^{3+} and Tm^{3+}-doped $NaLuF_4$ shows a high X-ray attenuation and are good for CT imaging. The SiO_2 shell reduces the toxicity of these lanthanide-based nanoparticles for small animals, which was confirmed by MTT assays and histological analyses. The incorporation of different lanthanide ions of Lu^{3+}, Yb^{3+}, Tm^{3+} and Gd^{3+} into one particle, $NaLuF_4$:Yb^{3+},Tm^{3+}@SiO_2-GdDTPA, provides a facile design strategy to fabricate multimodality imaging agents [261].

Yb-based NPs (NaYbF4:Er) which already revealed to be efficient upconversion nanophosphors (UCNPs) have also recently been identified as CT contrasts agents [265]. When encapsulated in a polymer (PEG) shell they showed low cytotoxicity and long circulation time in vivo. And a much higher efficacy as compared to the clinical iodinate agents commonly used. This improvement was attributed to the K-edge energy of Yb that locates within the higher energy region of the X-ray spectrum. Furthermore, a gadolinium

doping in these nanoparticles endowed them with enhanced fluorescence as well as NMR imaging capabilities providing clearance issues are solved.

By virtue of its high atomic number and this well-positioned K-edge, Yb provides excellent spectral CT contrast both *in vitro* and *in vivo*.[266] To partly solve bioelimination and preliminary biodistribution issues Yb nanocolloids were used as spectral CT contrast agents. The synthetic approach involved an organically soluble organometallic Yb(III)-2,4-pentadionate complex to produce polysorbate encapsulated nanocolloids of Yb incorporating a high density of Yb (>500K/nanoparticle) into a stable metal particle. Such high payloads of the Yb in the form of hydrophobic small molecule metal complexes could be obtained and stably concentrated into lipid-encapsulated nanocolloids and provide novel molecular imaging for use for spectral“multicolor” computed tomography (CT).

5 Ultrasound (US)

US is also a well-established clinical imaging modality. In particular, it is routinely used to characterize lesions in liver, urogenital tract, head and neck and soft tissues. Its main advantages are (i) the ability to extract molecular information (ii) portability, (iii) cost-effectiveness, (iv) absence of ionizing irradiation, (v) high spatial and temporal resolution (real-time examination) and (vi) global availability. It is based on the pulse–echo principle, with emitted and received wave’s frequencies higher than 20 kHz. US clinical application involves sound waves in the range of 2–3 MHz for pediatric imaging and 5–12 MHz for adult imaging, providing spatial resolution in the range 0.2 to 1 mm [28].

Contrast in US is provided by the variable ability of sound to propagate through media, resulting in reflection and refraction of the sound waves. Reflection and refraction depend on the sound itself but also on the nature of the medium and of its density. Therefore several microbubble-based contrast agents have been developed and are applied clinically to enhance the echogenicity of vasculature and organ-specific regions [267-272]. These microbubbles composed of surfactant, protein, and/or polymer shells containing gas cores, for example air, perfluorocarbons, or nitrogen should have an optimum size of 2-3 μm for common imaging practice [273]. Contrast agents for ultrasound imaging echogenic liposomes, [274-276] perfluorocarbon droplets, [277] and other materials such as gold particles, which have a density and compressibility substantially different from that of blood and tissue.

The use of nanobubbles [29, 278-286] as US contrast agents is in constant progress. Even if named nanobubbles they are typically in the range 150 to 1000-nm in diameter. They are generally composed of a perfluorocarbon gas encapsulated by a surfactant, protein, and/or polymer shell. The clinical significance of ultrasound as well as the labeling advantages of nanomaterials prompted a continued interest in developing smaller ultrasound contrast agents. [287-289] Despite this increasing interest, one should mention that due to lower scattering cross sections and often low mechanical properties of the shell, the performance of these nanomaterials is often inferior to that of microbubbles.

As for other imaging techniques, there is a general trend to combine both imaging and therapy. A solution was proposed which consisted in a medical imaging contrast agent combining both NPs and microbubbles for imaging and therapy applications in a single agent resulting in more accurate diagnosis and local treatment of diseased tissue. Various silica-coated NPs (*e.g.,* CdSe/ZnS QDs, Au NRs, Fe_3O_4, and Gd-loaded silica NPs) were incorporated into highly monodisperse, microfluidic-generated compressible protein-lipid-coated, perfluorobutane microbubbles (with size control down to 3 μm) [290]. When diluted in saline the NP-incorporated microbubbles are detectable using low-pressure ultrasound. They can be produced at high-throughput, sufficient for *in vivo* usage (106 MB/s).

Polymeric micelles and perfluorocarbon nano/microbubble systems that encapsulated a drug, which can be released locally within tumor cells were also obtained; US was then used to determine the efficacy of this drug therapy [278, 279]. Designed redox polymer NPs were shown to reduce intra-cerebral hemorrhage induced by 1-MHz focused ultrasound sonication coupled with microbubble treatment. Sonication coupled with redox polymer NPs loaded microbubbles produced intra-cerebral hemorrhage but the incorporated redox polymer nanoparticles had a significant neuro-protective on the intra-cerebral hemorrhage-induced brain [291].

Microbubbles can potentially be used as carriers for nanoscale US contrast agents and the incorporation of multimodal probes with potential therapeutic applications: sonodynamic therapy, ultrasound-induced apoptosis, sonoporation/sonotransfection, ultrasound-induced drug/gas delivery, and focused ultrasound-induced thermal ablation [32, 33, 280, 292-299]. Very recently mesoporous silica nanocapsules were also used as ultrasound contrast agents and can be can be potentially used as the inorganic theranostic platform for contrast-intensified ultrasound imaging, ultrasound-induced cytoclasis and drug release, and ultrasound-guided efficient HIFU tumor ablation therapy [300].

6 Photoacoustic imaging (PAI)

Photoacoustic imaging, PAI, [301] also known as laser optoacoustic imaging, is an emerging noninvasive, nonionizing, imaging modality that combines the high sensitivity of optical methods with the excellent resolution of acoustic methods [302, 303]. When illuminated by a short-pulsed laser, the biological sample absorbs the given light and this excitation is followed by a transient increase in temperature (~10 mK) and subsequent thermo-elastic expansion of the absorbent. This generates an ultrasonic acoustic signal, which is detected by wideband transducers surrounding the object and used to determine its geometry. Electromagnetic energy in the optical from visible to near-IR and radio-frequency regions is often utilized for PA excitation in soft tissues. This is not only because electromagnetic waves in these regions are nonionizing and safe for human use but also because they provide both high contrast and adequate penetration depths in biological tissues. PAI is generally performed using two main techniques, photoacoustic microscopy (PAM) and photoacoustic computed tomography (PAT). [301, 303, 304] PAM uses a coupled, focused ultrasonic detector–confocal optical illumination system [302] to generate multidimensional tomographic images without any reconstruction algorithms, whereas the detectors in PAT scan the laser-illuminated object in a circular path and use inverse algorithms to construct three-dimensional images [301, 305-307].

While *in vivo* imaging with optical techniques, suffers from hemoglobin absorption and tissue scatter, which limit overall light penetration depth, PAI can overcome this primary drawback thanks to the lower ultrasonic scattering coefficients (by 2-3 orders of magnitude) of absorbents compared with their optical equivalents leading to ~ 5 cm depth analysis with a resolution of < 1 mm [308, 309]. The depth issue can even be completely eliminated when microwaves or radio waves (referred to as thermo-acoustic tomography (TAT)) are used as illumination sources [310-313].

6.1 Gold-based nanomaterials

Gold-based nanomaterials are the most significant class of materials explored for PAT applications. Some of those commonly used for PAT include spherical gold NPs, [304, 314-320] nanorods, [321-327] nanostars, [328] nanocages, [305, 329-334] hollow nanoshells, [335] and composite materials with gold nanoshells: SiO_2@Au, [306, 336, 337] Fe_3O_4@Au,

[314] cobalt@gold NPs, [110] gold-speckled silica, [316, 320] and gold nanobeacons.[338, 339] The reasons for such an attention to gold nanosystems are many fold: they have tunable size- and shape-dependent plasmonic properties [340, 341] which allow them to absorb and scatter light from the visible to NIR region, and make them suitable for image-guided therapy [325, 342-344] and photothermal ablation of tumors.[345-347] A comparison of gold plasmonic nanostructures (surface plasmon resonance (SPR) tuned to 800 nm), revealed that gold nanorods and nanocages have much larger absorption and scattering cross sections than gold nanoshells [348].

Gold nanorods have similarly been used as NIR photoacoustic contrast agents with high sensitivity [349]. Manipulation of the aspect ratio enables tuning of the SPR of the resulting nanorods, which has led to multiplexing applications [321, 324, 326, 327, 344]. Gold nanorods are also effective as tracers for noninvasive *in vivo* spectroscopic photoacoustic SLN mapping in a rat model [350].

When they are silica-coated, gold nanorods show increased photoacoustic [344] and photothermal stability and retain their superior optical properties under much higher fluences [323, 325] when compared to PEG-coated gold nanorods which implies better imaging capabilities and make silica-coated gold nanorods a promising imaging and therapeutic nano-agent for photoacoustic imaging and image-guided photothermal therapy. A recent paper reported the use of silica-coated gold nanorods in photoacoustic imaging for quantitation of mesenchymal stem cells MSCs in rodent muscle tissue. The silica coating increased the uptake of gold into the cell more than 5-fold, without any sign of proliferation changes in cells suggesting that the therapeutic benefit of the MSCs will be retained despite the presence of contrast agent [351].

Gold-based compounds have a low toxicity [13, 345, 352-355] t which makes them good candidates for clinical and medicinal applications [252, 354, 356]. Gold nano-objects are also used as multimodal systems which will be addressed later on.

6.2 Carbon nanomaterials

Carbon nanomaterials have been considered as potential biomedical materialsfor pharmaceutical, biomedical, [357, 358] and bio-imaging applications, [359-362] including PAI [363-372] and thermo-acoustic imaging [373]. The characteristic optical properties of SWNTs, particularly those with optical properties in the NIR region, [374] play an important role in photoacoustic imaging [375].

As an example, single-walled carbon nanotubes conjugated with cyclic Arg-Gly-Asp (RGD) peptides can be used as a contrast agent for photoacoustic imaging of tumours. Intravenous administration of these targeted SWNTs (~ 2 nm in diameter and 50–300 nm in length) nanotubes to mice bearing tumors showed eight times greater photoacoustic signal in the tumor than mice injected with non-targeted nanotubes [376]]. Antibody-conjugated SWNTs targeted to integrins αvβ3-positive U87 human glioblastoma tumors in mice generated a high photoacoustic contrast *in vivo* [377] As an alternative and noninvasive approach to detection of the SLN, SWNTs have been shown to result in significant signal enhancement for detection by PAI [378]. To overcome the limitation of their relatively low absorption coefficients, the nanotubes are modified enhancing their NIR absorption and, thus, photoacoustic contrast. In one report, nanotubes were plated with a thin layer (4-8 nm) of gold; use of these golden carbon nanotubes (GNTs) resulted in a 100-fold increase in photoacoustic signal enhancement [379, 380]. The photoacoustic signals of GNTs as compared to other NIR contrast agents exhibited higher PA signals and correspondingly lower bubble-formation thresholds than those of pristine carbon nanotubes and gold nanoparticles, and comparable properties to those of gold nanorods and nanoshells [380-382]. The antibody-conjugated GNTs were used to target lymphatic vessels *in vivo* by PAI. In another modification of SWNTs, ICG dye molecules were attached to the surface of the nanotubes by π–π stacking interactions and showed 20-fold higher absorbance than bare SWNTs as illustrated in Figure 8 [371]. The synergy between the NIR absorption property of the dye and SWNT led to SWNT-ICG nanomaterials which provide an ~300× improvement in photoacoustic sensitivity compared with unmodified SWNTs *in vivo*.

Figure 8 here

In a recent work, [383] novel probe based on reduced graphene oxide (RGO)-iron oxide NPs(IONP) nanocomposite, was non-covalently functionalized with a biocompatible polymer, polyethylene glycol (PEG), for applications in multimodal imaging guided photothermal therapy of cancer base on PAT. Using this theranostic nanoprobe, *in vivo* triple modal fluorescence, photoacoustic, and magnetic resonance imaging are carried out, uncovering high passive tumor targeting, which is further used for effective photothermal ablation of tumors in mice.

6.3 Other types of nanoparticles

The encapsulation of dyes within protective NPs would certainly provide additional advantages in improving image contrast [384] due to signal amplification, reduced chemical

as well as photo-degradation, and additional ability to target specific biologically relevant sites [385-387]. In the selection of a dye, the relevant absorption profile is a key point but others can also be crucial, such as fluorescence imaging or therapeutic function such as photodynamic therapy (PDT) [126, 388-391]. ICG is the most commonly used for photoacoustic imaging in molecular and nanoparticulate formulations because it is the only FDA-approved dye for human applications. Its absorption peak at ~780 nm lies within the biological NIR window and enables deep tissue imaging only if encapsulated in NP matrices: organically modified silica (ORMOSIL), poly(lactic-co-glycolic acid) (PLGA), and calcium phosphate) due to its short plasma half-life (4 min). As such it has shown an improved stability and longer blood circulation time [392].

Superparamagnetic iron oxide nanoparticles (SPION) which have been widely used as FDA approved contrast agents for magnetic resonance imaging (MRI) and are known to have an excellent safety profile [80, 81] were also analyzed for photoacoustic applications. With such NPs photoacoustic imaging which enhances imaging contrast by visualizing the optical absorption of either tissue or injected contrast agents could be coupled with magneto-motive ultrasound (MMUS) imaging which enhances the sensitivity and specificity of ultrasound based on the detection of magnetic nanoparticles perturbed by an external magnetic field. This integrated magneto-photo-acoustic (MPA) imaging helped identifying morphological properties, molecular information and complementary functional information of tissues [393]. The same MPA imaging used to noninvasively detect the delivery and endocytosis of NPs could differentiate endocytosed nanoparticles from extracellular nanoparticles in background tissue, and is promising for *in vivo* studies of cellular functionality [394]. Another study demonstrated the potential of core-shell iron oxide nanoparticles with silica coating as PA contrast agents under 1064-nm laser excitation; the increased thermo-elastic response of the silica-coated SPION compared to the bare ones was assumed to be due to enhanced opto-thermal properties of the core-shell structure [395]. Besides inorganic nanoparticles there are also studies on the use polymeric nanoobjects for PAI.[386, 387, 396, 397]

7 TeraHertz molecular imaging (THMI)

Terahertz (THz, 1 THz = 10^{12}Hz) molecular imaging (THMI) is a new analytic technique that detects changes in surface plasmons (SPs) emerging from nanoparticles following irradiation with an optical laser beam. Due to the high absorption of THz radiation in water, which is the

main component of biological tissues, high contrast between skin, muscle, fat, veins, nerves, etc can be obtained. In particular, this high sensitivity of THz to the concentration of water provides a high contrast between tumor (high water content) and normal tissues. Thus, characterizing the refractive index and absorption of various tissues is the key to the use of THz in the Life Sciences both for spectroscopy and imaging and in the design of biochips.

Terahertz (THz) technology has then been advancing rapidly because of these tremendous potential applications. Among them, THz cancer diagnosis is drawing much attention as THz waves can detect the variation of cells caused by cancer, thereby rendering a new modality of medical imaging. Conventional THz imaging for cancer diagnosis assesses the difference in water content or structural changes between tumor and normal tissues. However, use of THMI nanoprobes improved the sensitivity of conventional THz imaging by providing a target-specific THz image and by enabling assessment of molecular and cellular activities *via* analysis of THz waveforms [398, 399]. The sensitivity of THz electromagnetic (EM) waves to water molecules allows the utilization of the THz technique in diagnosing cancers because in cancerous tumors, diseased tissues contain more interstitial water than healthy tissues. This higher water content, combined with structural changes such as increased cell and protein density, leads to a larger THz absorption and refractive index for tissues with tumors.

7.1 Gold nanoobjects

THz spectroscopy is advantageous in analytical chemistry because it can detect and identify intermolecular interactions in chemical compounds, such as hydrogen bonds and hydrations, and molecular networks. Recent advances in THz components, such as ultrashort pulsed lasers and photoconductive antennas, have improved the sensitivity of THz time-domain (TDS) spectroscopy and have made the THz chemical imaging much efficient. THz chemical imaging can reveal hydrogen bond distributions and will be a very powerful tool in biology, pharmacology, and life sciences. The problem with THz cancer diagnosis is the difficulty in identifying the tumor in tissues at an early stage. Antibody-conjugated contrast agents for THz EM waves, similar to the technique adopted in MRI, may solve the problem. This was first performed using the so called nanoparticle-*c*ontrast *a*gent-enabled *t*era*h*ertz *i*maging (CATHI) technique by targeting metal NPs such as gold nano-rods (GNRs) to cancer cells in tumors The THz reflection amplitude from the cancer cells with gold nano-rods (GNRs) increased by 20% upon infrared (IR) laser irradiation compared to cancer cells without GNRs. In a differential mode, the difference between the two cases was more evident because the

THz signal from the cancer cells with GNRs was 30 times higher than that from cancer cells without GNRs [398].

Cancer diagnosis by the terahertz molecular imaging (THMI) technique was also demonstrated by *in vivo* imaging A431 cancerous tumors in mice. The change in the THz response is due to the activation of the surface plasmon resonance on the surface of nanoparticle probes when illuminated with NIR beams. The development of a differential measurement technique in which the NIR beam is directly modulated instead of numerical subtraction of two images led to high signal-to-noise ratio (SNR) eliminating the background noise and generating a high sensitivity capable of identifying the miniscule differences at a cellular level [399].

7.2 Metal oxide based Nanoparticles

Very recently, the commercially available suspension of SPIO–dextran composites (Feridex) was also used as not only a MRI probe but also as a THMI one. They were transfected into SKOV3 cancer cells, at various concentrations, and both the magnetic and optical properties of the particles were examined by MR and THz reflection imaging. Mice were inoculated with Feridex-labeled SKOV3 cells, and *in vivo* MR and THz images were taken 1, 3, 7, and 14 days after inoculation. The THz images and T2* -weighted MR images showed similar patterns; the signal intensities of both image sets increased with Feridex concentration and decreased over time [93].

Another MRI contrast agent based on gadolinium oxide (Gd_2O_3) nanoparticles (GONPs) is receiving attention as potential multi-functional contrast agents also active in THMI [400]. The optical constants of GONPs were found concentration-dependent by terahertz time domain spectroscopy THz-TDS. Even a few μM of GONPs could be detected due to their power absorption capacity, which is almost three orders of magnitude larger than that of water. Therefore, GONPs can significantly improve the contrast in THz images. Their encapsulation with biocompatible materials would probably prevent aggregation problem of GONPs.

As opposed to MRI technology, which has difficulty to acquire images from a surface that is not surrounded by water such as human skin or digestive organs, THz medical imaging technology, however, has uniqueness on the surface measurement of biological samples such as epithelial cancers. Therefore, THz imaging along with nanoparticle contrast agents will probably be one of the strongest imaging technique for certain diagnosis.

8 Ion Beam Analysis Techniques

Besides quantum dots and gold NPs, many other inorganic nanoparticles suffer from a lack of fluorescence in the optical regime, and cannot be followed by light microscopy; therefore, there was a need for the development of X-ray fluorescence mapping which is the main way to detect, track and quantify nanoparticles *in vitro* in biological specimens.

Ion beam analysis techniques have been widely used for the determination of chemical element composition of diverse types of specimens. Particle induced x-ray emission (PIXE) has proven to be a reliable and a highly sensitive technique for the detection and quantification of chemical elements in living organism. The direct analysis of biological samples is particularly convenient when ion beam analysis is performed with high-resolution microbeam, also called nuclear microprobe. The use of high-resolution microbeam offers the opportunity to reveal the *in vitro* chemical imaging of the whole cell compartments (nucleus, cytoplasm) and to perform trace elements quantification at the single cell level. PIXE could also be performed on multicellular organisms deciphering the whole elemental composition of defined anatomic structures of interest to address the particular questions of bioaccumulation and biopersistence of endogenous/exogenous chemical elements, such as metal oxide nanoparticles. In addition, because *in vitro* cell culture or microorganisms prepared for PIXE do not require sectioning, they can be investigated close to their natural state using cryogenic preparation methods.

PIXE provides multi-elemental capability, which allows the simultaneous comparison of distribution of several elements inside the same specimen [401-410].

TiO_2 is one of these nanomaterials which were largely examined by PIXE, the main reason being due to its extensive use in cosmetics and sunscreens. Analyses performed on the penetration depth and on pathways of the TiO_2 particles into the skin showed a penetration of TiO_2 particles through the *stratum corneum* into the underlying *stratum granulosum via* intercellular space. The TiO_2 particle concentration in the *stratum spinosum* was below the minimum detection limit of about 1 particle/μm^2 [411]. The state of aggregation of TiO_2 NPs revealed to be crucial with regard to lungs toxicity [412]. The biodistributions of Pt and TiO_2 micro- and nano-sized particles in mice were estimated and visualized by X-ray scanning analytical microscopy. The study indicated that the difference in chemical character had a greater effect than did particle size. We predict that X-ray scanning analytical microscopy will be a useful method for studying biodistribution of micro- and nano-sized particles, because

this method requires no labeling or treatment of the target particles [413].

PIXE can even been used as a therapeutic tool because metallic nanoparticles (MNPs) are able to release localized x-rays when activated with a high-energy proton beam. The exploitation of this phenomenon in the therapeutic irradiation of tumors was then investigated. PIXE-based x-ray emission was directed at CT26 tumor cells *in vitro*, which were administered with either gold (average diameter 2 and 13 nm) or iron (average diameter 14 nm) nanoparticles (GNPs or SNPs). It increased with MNPs solution concentration over the range of 0.1-2 mg ml^{-1}. An *in vivo* study in CT26 mouse tumor models with tumor regression assay demonstrated significant tumor dose enhancement, thought to be a result of the PIXE effect when compared to conventional proton therapy (PT) without MNP (radiation-only group). Mice which received GNPs or SNPs injection doses of 300 mg kg^{-1} body weight before proton beam therapy exhibited from 75% to 90% tumor volume reduction (TVR) in 20 days post-PT while the radiation-only group showed only 18% TVR and re-growth of tumor volume after the same timing. This approach may result in new treatment options for infiltrative metastatic tumors and other diffuse inflammatory diseases (Figure 9) [414].

Figure 9 here

In some situations under investigation, the use of complementary PIXE and RBS facilities allows information to be obtained at high level of detail, yielding new understanding of the affected tissues and the progression of disease [406, 415].

The methods can produce quantitative distributions of the chemical elements obtained by combining PIXE with other ion beam techniques, RBS (Rutherford Backscattering Spectrometry) and STIM (Scanning Transmission Ion Microscopy) even if STIM is also used by itself [416, 417].

RBS is then used for sample mass normalization of PIXE signal as it provides the quantitative determination of the different elements in biological samples. The accurate concentration of the chemical elements requires the determination of the initial mass of the sample done by STIM analysis [411, 418-420]. As an example, visualization of the penetration of sunscreen formulations containing TiO_2 NPs (about 20 nm primary particle size) into hair follicles of both human and porcine skin using these complementary methods of ion microscopy (PIXE, RBS, STIM) showed that the NPs were found as deep as approx. 400 µm in the follicle, obviously introduced mechanically rather than by a diffusive process (Figure 10) [418].

Figure 10 here

Figure 10 shows a sagittal cut through a hair follicle of porcine skin which was exposed to an

isopropylmyristate gel containing TiO_2 NPs and subsequently washed with water. The PIXE-maps for P (red), S (green) and Ti (blue) are superimposed. The Ti is clearly observed on top of the *stratum corneum* as well as in the follicle surrounding the hair. The left and right images are identical with the Ti color code over-modulated to better visualize the Ti spots.

More recent studies have used high-resolution nuclear microprobe to investigate the interaction of metal oxide nanoparticles with cells and multicellular organisms (Figure 11). Up to now, nuclear microprobe still lacks sufficient spatial resolution to resolve individual nanoparticles, but permit to determine detect, track and quantify metal oxide nanoparticle aggregates, and to assess the effect of nanoparticles on trace element homeostasis, such as calcium [421, 422].

Figure 11 here

Another promising research area is the study of intracellular localization of functionalized NPs by combining *in vivo* optical/epifluorescence imaging and high resolution PIXE/RBS/STIM analysis (Figure 12) [423].

Figure 12 here

We can predict that X-ray scanning analytical microscopy will be a useful method for studying biodistribution of micro- and nano-sized particles, because this method requires no labeling or treatment of the target particles.

9 Multimodal bio-imaging

9.1 Multimodal techniques and instrumentation

Multimodal bio-imaging became possible not only because of multimodal NPs [424] but also because the development of adapted techniques capable of combining two even three types of analysis in a single machine. MRI/PET probes [35] for example are powerful emerging tools, combining the sensitive, metabolically functional PET with the high-resolution, anatomical detail provided by MRI. They had a real expansion with the development of MR/PET scanner [425-427]. This is not the only example and this domain of multiple modality techniques will most likely go on growing in the future [90, 172].

The improvement in instrumentation and detection systems is also a crucial point enhancing the sensitivity of these emerging imaging techniques. Improved image-analysis software and expanded data storage can make existing technologies even more powerful.

9.2 Multimodal nanoprobes

Imaging modalities in the clinic generally include optical imaging, magnetic resonance imaging (MRI), computed tomography (CT), ultrasound (US) and positron emission tomography (PET) or single photon emission computed tomography (SPECT). A current popular approach to overcome their specific limitations results in combining two or more CAs into a single NP entity which can then be imaged by these multiple techniques either consecutively or simultaneously depending on the degree of development of the techniques [19, 171, 199-201, 281, 383, 428-438]. Combining the anatomical resolution of MRI with the sensitivity of optical imaging is common and constitutes a powerful technique for finding and quantifying the size of tumors, especially tumors or metastases that are too small for MRI detection alone. These MR/optical imaging agents can be used to monitor enzyme activity, in brain tumor imaging, and to detect and monitor apoptosis and atherosclerosis [439]. Other types of multimodal contrast agents [5, 25, 74, 200, 201, 281, 430, 432, 433, 436, 437, 440-442] such as probes with three modes of imaging are considered, for example MRI/NIRF/PET [439], and even four [425, 439, 443, 444] which are gathered in Table 3. As an example, difficulty in delineating brain tumor margins is a major obstacle for further efficient treatment [445]. Current imaging methods are often limited by inadequate sensitivity, specificity and spatial resolution. To overcome this issue, Kircher *et al.* recently showed that a unique triple-modality magnetic resonance imaging/photoacoustic imaging/Raman imaging nanoparticle (MPRNPs) could accurately help delineate the margins of brain tumors in living mice both preoperative and intraoperative ways. The probes were detected by all three modalities with a picomolar sensitivity both *in vitro* and in living mice. Intravenous injection of MPRs into glioblastoma-bearing mice led to MPRNP accumulation and retention only by the tumors. This provided non-invasive tumor delineation by the three modalities and through the intact skull. Raman imaging helped for guidance of intraoperative tumor resection because it could accurately delineate the tumor margins.

Table 3. List of the different multimodal NPs and the type of techniques they are used for.

Number of	Type	Nanoobjects	ref

modality			
2	MRI/CT	Gold NPs/ Gd^{3+}	[245]
		Fe_3O_4@Au nanocomposite particles	[259]
		Au–Fe_3O_4 Janus NPs	[446]
	MRI/Fluorescence	QDs / iron oxide and Gd^{3+} NPs	[447]
		Silica NPs, Gd^{3+} Eu^{3+} and Tb^{3+}complexes	[64, 65]
		Hydroxyapatite Gd^{3+} and Eu^{3+} complexes	[448]
		Iron-doped silicon nanoparticles	[449]
	MRI/NIRF	Fe_3O_4@Au	[450]
		Iron oxide and Cy5.5 dye	[451]
	MRI/MRI (T_1/ T_2)	SPIO and	[452]
		Carbon dots and Gd^{3+}	[59]
	MRI/PAT	See the reviews	[110, 200]
	MRI/PET		[35, 425, 426, 453, 454]
	MRI/PET	Gd^{3+} ^{64}Cu	[455]
	MRI/SPECT/Fluorescence	Gd_2O_3@SiO_2 and Cy 5	[171]
	MRI/ THMI	SPIOs	[93]
	MRI/US	Perfluorocarbon NPS and Gd^{3+}	[456]
		Magnetite and PLA microbubbles	[293]
		iron oxide and ^{64}Cu	[36, 173, 175]
	CT/Fluorescence	TaO_x NPs and rhodamine-B	[457]
	CT/PAT	Gold@PEG NPs	[239, 343]
	CT/NIRF	$NaYbF_4$ and Tm^{3+}	[263]
	PET/NIRF	QDs and ^{64}Cu DOTA	[205]
	PAT/US	Gold nanorods and microbubbles	[32]
		Gold Nnanorods	[458]
	SPECT/fluorescence	See reviews	[439, 459]
	TAT/PAT	SWNTs	[378]
	US/NIRF	Proteins/Gold NPs, Iron oxide NPs, QD,	[460]
3	MRI/NIRF/PET	SPIO and ^{64}Cu and Cy5.5	[439] [171]
	MRI/NIRF/PET	Mesoporous SiO_2 near-IR dye ZW800 and Gd^{3+} and ^{64}Cu	[124]
		SPIO and ^{18}F	[34]
		SPIO and ^{124}I	[235]
		^{18}F Yb,Er,Tm codoped $NaYF_4$	[137]
	MRI/CT/NIRF	NaY/GdF_4:Yb,Er,Tm@SiO2-Au@PEG	[436]

		$NaLuF_4:Yb^{3+},Tm^{3+}@SiO_2$-GdDTPA	[261]
		$Fe_3O_4@NaLuF_4$:Yb,Er/Tm Core-shell NPs	[461]
	MRI/PAT/Raman	SWNTs@PEG and iron metal NPs and Protamine	[34]
		Gd^{3+} and Gold NPs and *trans*-1,2-bis(4-pyridyl)-ethylene	[445]
	MRI/PAT/ fluorescence	Graphene oxide and iron oxide and dye	[383]
	MRI/CT/NIRF	Perfluoro-NPs, ^{19}F	[462]
≥ 4	MRI/PET/BRET/ fluorescence	Cobalt–ferrite $MNP@SiO_2$(RITC)-PEG/NH_2 and Luciferase protein and ^{68}Ga	[176]
	MRI/MM-OCT[a]/US/ fluorescence	SPION and RGD peptide and Nile red	[463]
	MRI/ Optic	MNPs and QDs	[464]
	PET–CT/MRI/NIRF	^{64}Cu and Iron oxide and NIR dye	[202]

[a] MM-OCT: magnetomotive optical coherence tomograph.

y

All these combinations are expected to provide very precise and detailed information for clear diagnosis and to be more efficient than a single modality. However, it should be stated that the rational selection of the different imaging modalities to put on a single probe is highly crucial. During the design of these multimodal imaging probes, the enhancement of one modality must not be at the expense of another and researchers should rationally avoid overlapping of advantages and rather compensate for the weak points of each modality so as to maximize the overall synergistic effect. Generally, imaging modalities with high sensitivity (PET, optical, etc.) are combined with others which will exhibit high spatial resolution (MR, CT, etc.) (Table 1).

Furthermore, these bio-imaging techniques require different administered doses, based on the technique's sensitivity, host biology, route of delivery, and the targeting strategy used. The controlling the ratios of the different types of agents on a single probe, becomes compulsory so as to obtain the perfect SNR for each modality. Additionally, the incorporation of more than one modality may cause interferences between the two, iron-based MRI agents quenching fluorescence agents for example, and complicate the synthetic aspect. Succeeding in this approach would lead to the administration of a single dose of multiple agents to the patient, resulting in a potential reduction of side effects.

10 Functionalization

Most disease processes occur at the molecular and cellular levels, therefore researchers have to face breakthrough in precisely viewing and understanding these processes. The ideal imaging resolution they want to reach is a few nanometers, the length scale of most biological. With this in mind the functionalization of NPs becomes crucial for their use in diagnostic and therapeutic applications. The research on the functionalization of NPs for bio-imaging applications has been reviewed [25, 98, 360, 465-471]. The preparation of NPs for bio-imaging applications can include a variety of steps: synthesis, coating, surface functionalization, and bioconjugation. The most common strategies of engineering NP surfaces involve physical adsorption or chemisorption of the desired ligands onto the surface. Chemisorption or covalent linkages are preferred, and the coated NPs should possess high colloidal stability, biocompatibility, water solubility, as well as functional groups for further bioconjugation. Functionalization techniques reported in the literature suffer from limitations such as complex synthesis steps, poor biocompatibility, low stability, and hydrophobic products. Therefore, coating strategies based on chemisorption and ligand exchange often provide a better way to finely tune the surface properties of NPs. After conjugation with the appropriate targeting ligands, antibodies, or proteins, fluorescent NPs also exhibit highly selective binding, making them useful for targeting and imaging.

Table 4. List of the different functionalization processes of NPs from [465].

Reaction type	Functionalized NP	Reactant	Final NP
Michael addition	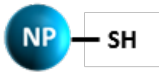	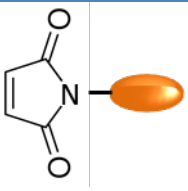	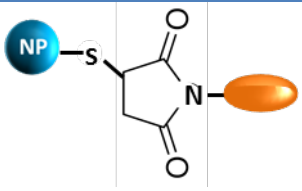
Epoxide opening		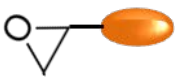	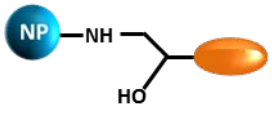
Addition of amine to cyanates			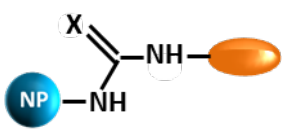

Amide bond formation		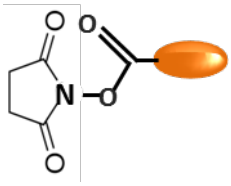	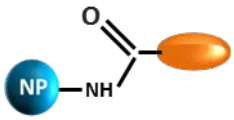
Amide bond formation			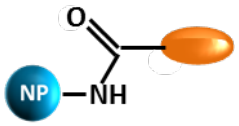
Amide bond formation	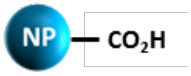		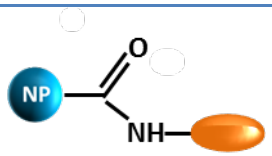
Imine bond formation		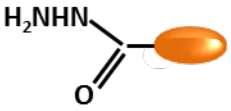	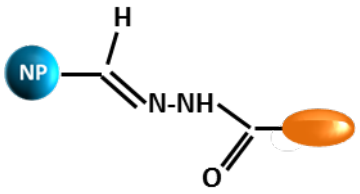
Imine bond formation		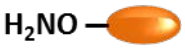	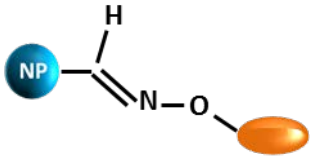
Click chemistry		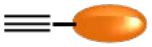	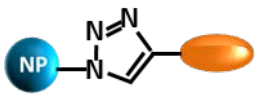
Ring closing or opening metathesis		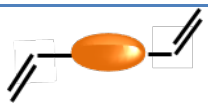	
Diels-Alder reaction	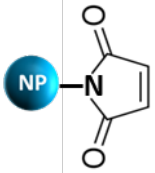	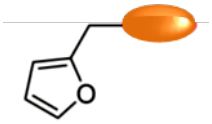	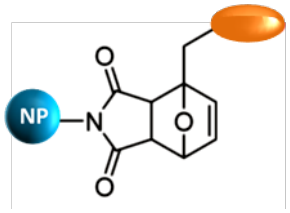

Synthesis of NPs leads to two major categories: hydrophobic and hydrophilic NPs, respectively. Many NPs, mainly QDs and metal NPs are hydrophobic in nature, causing insolubility in water and preventing further functionalization. Thus, water solubilization and functionalization become key points prior to any applications of the NPs. Their coating chemistry is critical to provide colloidal stability and water-soluble, robust NPs with flexible

surface chemistry. The most common functionalization strategies are (i) direct encapsulation of the hydrophobic NPs by hydrophilic polymers or a silica coating and (ii) ligand exchange of the original surfactant with hydrophilic ligands, such as thiols.

Regardless of composition, surface functionalization of the nanomaterial is required to enable targeting and stealth for long circulation times with minimal nonspecific binding [239]. There is a plethora of entities that can be incorporated onto a NP's surface, with covalent bonding preferred over electrostatic interactions: DNA, RNA, [472] oligonucleotides (aptamers), [29, 434, 473-476] peptides, [36, 175, 201, 477-482] proteins, [483-487] enzymes, [488-491] antibodies [492]. No matter what the surface moiety, its activity must not be altered once anchored to the NP surface (Figure 13).

Figure 13 here

Routes of delivery and bioavailability are also important concerns in which functionalization is crucial. The most common delivery route is intravenous injection which requires an optimization of NPs circulation time since they must be able to pass through the bloodstream and reach their desired target intact. Their surface functionalization generally results in size increase due to the added shell (silica, PEG, poloxamines, poloxamers, polysaccharides). This size increase may be detrimental for vasculature permeability and may affect bloodstream circulation especially through thin capillaries.

In addition to intravenous (IV) administration, intramuscular injections, oral, transdermal, and inhalation routes are also possible and NPs must be able to survive their particular delivery route. The probe, to be effective must perform the desired function or bind properly to the desired target so that any loss of biological activity of the component conjugated to the NP surface must be determined beforehand.

Functionalization can also help addressing NPs toxicity aspects [12, 354, 358, 465, 468, 493, 494]. Indeed, properly protected NPs conjugated or coated with biocompatible materials can be used for the fabrication of various functional systems with multimodality as well as targeting properties, reduced toxicity and proper removal from the body.

Furthermore, governmental institutions should require a standardization process of NPs characterizations (as particle size, shape, dissolution rate, agglomeration state, and surface area and chemistry) [495] as well as toxicity assays. It has generally been assumed that *in vitro* toxicity tests designed for soluble chemicals are appropriate for nanomaterials. However extrapolation of *in vitro* toxicology findings to humans is not so obvious when the mode of action and/or metabolic conditions in the cell culture model may not be relevant in humans

[496-498]. This is not an easy task, since the standardized established tests should work for multiple particle types, despite the fact that these NPs have different characteristics and behaviors (fluorescence, magnetism, metallic nature…) but it should definitely be undertaken. When such NPs are used in bio-imaging , it is also crucial to have accurate characterization to fully understand (i) their structure–function relationship such as particle number and dose administered so as to make the right balance between safety and good SNRs, (ii) their behavior in the biological environment (*e.g.*, dispersibility or aggregation), and (iii) the interactions between the functionalized surface of the NP and the target of interest (i.e., binding kinetics and thermodynamics).

11 Perspectives: Multimodal Theranostic NPs

To successfully translate multimodal NPs into clinical treatment, several issues have to be taken into consideration such as (i) reasonable blood half-life; (ii) favorable physiological behavior with minimal off-target; (iii) any possible metabolism to clearable components; (iv) effective clearance of NPs from the human body; and (v) their potential toxicity for living subjects and humans. So when adequately modified multimodal nanoprobes can also become theranostic NPs. They are then essentially found in cancer research where they provide the diagnostic capability using an imaging modality to detect a tumor, while supplying the component for therapy against this specific tumor type, commonly utilizing photothermal ablation (PTA) or photodynamic therapy (PDT). PTA works by exciting a NP with a large absorption cross section (*e.g.*, gold), which causes a localized heating that then kills the tumor cells into which the NPs have been injected [337]. Once more gold-based nanoobjects are numerous: gold nanoshells and nanocages surrounding a silica core have been used in photo-ablative therapies [329, 345-347, 356, 499-503] even if PTA has also been used with SWNTs [504].

PDT uses photosensitizers that, when excited by light, react with molecular oxygen in the biological environment to produce ROS, which are cytotoxic to cells. Multifunctional NPs used for multimodal imaging and theranostic applications have been reviewed [8, 126, 150, 388-391, 416, 481, 505-508]. One material that may prove useful in combining a dual imaging and therapy is mesoporous silica NPs; with their large surface areas and pore

volumes, one or two modalities (optical imaging agent and an anticancer drug) can be incorporated into the silica matrix while loading the other modality into its pores. [509-511]

Encapsulating drug payloads in NPs can prevent exposure of healthy cells to the cytotoxic drug and may prove more beneficial (*e.g.*, lower toxicity and fewer side effects) at lower doses than the free drug. However, this can reveal much more complex than the use of simple small-molecule drugs that are easily characterized. In addition, the NP must remain intact until reaching the tumor site and then release the drug controllably through its desired mechanism—issues that will require further research and development.

Due to their nanoscale dimensions and high aspect ratio, single-walled carbon nanotubes (SWCNTs) have been used as a high drug loading transporter for anti-cancer drugs, as they are capable of penetrating mammalian cell membranes. The triple functionalization of oxidized SWCNTs with the anti-cancer drug doxorubicin, a monoclonal antibody, and a fluorescent marker at non-competing binding sites allowed for targeted delivery of drug to cancer cells and visualization of their cellular uptake by confocal microscopy. An intracellular release of doxorubicin (DOX).was observed which then translocated to the nucleus while the nanotubes remain in the cytoplasm [512].

Other important areas in which multimodal NPs can be beneficial include (i) tumor imaging for guided surgery, [323, 513-516] imaging of gene expression *in vivo* to elucidate disease development, [287, 288, 296, 370, 517-520] drug delivery [471] and efficacy of anti-cancer drugs [234, 337, 429, 498, 521-525].

In the next future, NPs will not only be used as contrast agents not simply to find and delineate tumors, but also aim at elucidating the biological processes and cellular mechanisms so as to understand and hopefully cure other diseases than cancer, such as Alzheimer's, Parkinson's, multiple sclerosis, rheumatoid arthritis, and diabetes.

Major developments of the future should then concern diagnosis as well as treatment with therapeutic NPs. These new agents to be developed from a societal point of view will have to prove as highly superior to any currently existing system with the same function. Therefore, the development of CAs incorporating an additional functionality (i.e., therapeutic agent, measure of disease progression, or evaluation of treatment effectiveness) with the classical *in-vivo* imaging modality will most likely be expanded, especially if based on some already-approved material.

Additional types of NP contrast agents may see development in the future. These smart responsive probes that turn "on" or "off" when exposed to the target or given conditions are

being developed. Two fluorochromes (Cy5.5) cleavable by proteases, and (Cy7) which serves as an internal standard were grafted on superparamagnetic iron oxide NPs leading to a dual fluorochrome optical probe which reacted to the presence of protease enzymes in its environment with a change in signal (700% increase in fluorescence) [526].

Tumor cells have a more acidic internal environment compared with normal cells (most cancer tissues have lower extracellular pH values (pH 6.0–7.0) than normal tissues (pH 7.4), and the pH drops further in tumor cells, especially inside endosomes (4.5–5.5), which provides a high possibility to control the drug release behaviors through the use of pH-sensitive vehicles. Many systems exploiting this pH modification are under scrutiny [527].

Well-defined core@shell (MCNC@PAA) nanospheres based on a 100 nm sized magnetic colloid nanocrystal cluster core and across-linked poly(acrylic acid) (PAA) shell were for example loaded with of doxorubicin (DOX). [528] The experimental results showed that (i) the MCNC@PAA NPS could achieve a high drug loading content and entrapment efficiency; (ii) a synergistic pH-responsive effect derived from the entrapped DOX and PAA network was found to effectively manipulate the drug releasing behavior at 37 °C. In fact the premature release was highly restricted at a pH of 7.4, while upon more acidic ones pH (from 7.4 to 5.0 or 4.0), a large amount of the drug was rapidly released. The *in vitro* cellular cytotoxicity test proved they are highly biocompatible and suitable for use as a drug carrier in CDDS and that MCNC/PAA–DOX show a higher cytotoxicity compared with that of free DOX to HeLa cells. Other pH-sensitive based NPs have been used such as chitosan [529] polymers, [530] core@shell NPs [527], nanogels [531]. Among stimuli sensitive NPs are light sensitive one. For example, light-stimulated remote release of nucleic acid has been attempted by utilizing the tunable optical properties and moderating Au–S bond strength of various gold nanomaterials [532, 533]. For example, temporally and spatially controlled delivery of siRNA using (NIR)-sensitive gold nanoshell-siRNA conjugates was explored [534]. Pulsed NIR laser irradiation, after their easy cellular uptake by TAT-lipid attached on the gold nanoshell, triggered siRNA release and resulted in efficient gene silencing *in vitro*. A remote optical switch for localized and selective control of RNA interference was also achieved using gold nanorods conjugated with thiol-modified sense strand of double stranded oligonucleotides [535]. Some of these NPs are dual probes with both photo- and pH- responsive properties [536].

A recent review by Kwon et al. on stimuli-responsive polymers and nanomaterials for gene delivery and imaging applications came out in which they introduces the recent advances in tackling the key challenges in achieving efficient, targeted, and safe non-viral gene delivery

using various nucleic acid-containing nanomaterials that are designed to respond to various extra- and intracellular biological stimuli (pH, redox potential, and enzyme) as well as external artificial triggers (light and ultrasound). Nanomaterials platform for combined imaging and gene therapy, nanotheranostics, using stimuli-responsive materials was also highlighted in this review. It is clear that developing novel multifunctional l vectors, which transform their physico-chemical properties in response to various stimuli in a timely and spatially controlled manner, is highly desired to translate the promise of gene therapy for the clinical success. Temperature-sensitive NPs have been identified many of them including heat activable iron oxide and thermo-sensitive polymers, [537-547] silica NPs, [542, 544, 548] liposomes, [548-550] micelles, [551] multifunctional nanoparticles containing both CdTe quantum dots (QDs) and Fe_3O_4 magnetic particles [552].

These nanomaterials CAs will certainly find more than numerous applications as tunable, remotely controlled platforms for drug delivery, hyperthermia cancer treatment, and various other biomedical applications. The basis for the interest lies in their unique properties achieved at the nanoscale that can be accessed *via* remote stimuli. These properties could then be exploited to simultaneously activate secondary systems that are not remotely actuatable [440, 535, 536, 553-561]. Despite all the work already performed, Richard Feynman is still more than right: “There is still Plenty of Room at the Bottom”.

Acknowledgments:

The authors are grateful to the financial support from the CNRS, IN2P3/CNRS, University of Bordeaux, the Région Aquitaine and the French National Research Institution (ANR CES2010, TITANIUMS).

REFERENCES

[1] Suetens P. Fundamentals of Medical Imaging. 2nd edition ed. New York, NY, USA,: Cambridge
University Press; 2009.
[2] Naz S, Qadir MI, Ali M, Janbaz KH. Nanotechnology for imaging and drug delivery in cancer. *J. Chem. Soc. Pak.* 2012, 34, 107-111.
[3] Chi X, Huang D, Zhao Z, Zhou Z, Yin Z, Gao J. Nanoprobes for in vitro diagnostics of cancer and infectious diseases. *Biomaterials* 2012, 33, 189-206.

[4] Dykman L, Khlebtsov N. Gold nanoparticles in biomedical applications: recent advances and perspectives. *Chemical Society Reviews* 2012, 41, 2256-2282.
[5] Lee D-E, Koo H, Sun I-C, Ryu JH, Kim K, Kwon IC. Multifunctional nanoparticles for multimodal imaging and theragnosis. *Chemical Society Reviews* 2012, 41, 2656-2672.
[6] Re F, Moresco R, Masserini M. Nanoparticles for neuroimaging. *J. Phys. D: Appl. Phys.* 2012, 45, 073001/073001-073001/073012.
[7] Saha K, Agasti SS, Kim C, Li X, Rotello VM. Gold Nanoparticles in Chemical and Biological Sensing. *Chemical Reviews* 2012, 112, 2739-2779.
[8] Smith L, Kuncic Z, Ostrikov K, Kumar S. Nanoparticles in cancer imaging and therapy. *J. Nanomater.* 2012, 891318, 891317 pp.
[9] Cormode DP, Klink A, Fayad ZA, Mulder WJM. Nanoparticle contrast agents for cardiovascular medical imaging. Science Publishers, Inc.; 2012. p. 3-24.
[10] Kojima C, Cho S-H, Higuchi E. Gold nanoparticle-loaded PEGylated dendrimers for theragnosis. *Res. Chem. Intermed.* 2012, 38, 1279-1289.
[11] Li K, Liu B. Polymer encapsulated conjugated polymer nanoparticles for fluorescence bioimaging. *Journal of Materials Chemistry* 2012, 22, 1257-1264.
[12] Jakhmola A, Anton N, Vandamme TF. Inorganic Nanoparticles Based Contrast Agents for X-ray Computed Tomography. *Advanced Healthcare Materials* 2012, 1, 413-431.
[13] Taylor A, Wilson KM, Murray P, Fernig DG, Levy R. Long-term tracking of cells using inorganic nanoparticles as contrast agents: are we there yet? *Chem. Soc. Rev.* 2012, 41, 2707-2717.
[14] Patel V, Papineni RVL, Gupta S, Stoyanova R, Ahmed MM. A realistic utilization of nanotechnology in molecular imaging and targeted radiotherapy of solid tumors. *Radiat Res* 2012, 177, 483-495.
[15] Lucas M, Riedo E. Combining scanning probe microscopy with optical spectroscopy for applications in biology and materials science. *Rev. Sci. Instrum.* 2012, 83, 061101/061101-061101/061135.
[16] Peti-Peterdi J, Burford JL, Hackl MJ. The first decade of using multiphoton microscopy for high-power kidney imaging. *Am. J. Physiol.* 2012, 302, F227-F233.
[17] Johnston LJ. Fluorescence imaging on the nanoscale: bioimaging using near-field scanning optical microscopy. *Photochemistry* 2011, 39, 191-210.
[18] Ntziachristos V. Going deeper than microscopy: the optical imaging frontier in biology. *Nat. Methods* 2010, 7, 603-614.
[19] Huff TB, Shi Y, Fu Y, Wang H, Cheng J-X. Multimodal nonlinear optical microscopy and applications to central nervous system imaging. *IEEE J. Sel. Top. Quantum Electron.* 2008, 14, 4-9.
[20] Wabuyele MB, Vo-Dinh T. Nanoimaging of biomolecules using near-field scanning optical microscopy. CRC Press LLC; 2007. p. 12/11-12/13.
[21] Kawata S, Inouye Y, Ichimura T. Near-field optics and spectroscopy for molecular nano-imaging. *Sci. Prog. (St. Albans, U. K.)* 2004, 87, 25-49.
[22] Bragas AV, Scarpettini AF, Masip M. Optical nanoimaging with plasmonic probes. American Chemical Society; 2010. p. PHYS-713.
[23] Sokolov K, Follen M, Aaron J, Pavlova I, Malpica A, Lotan R, Richards-Kortum R. Real-time vital optical imaging of precancer using anti-epidermal growth factor receptor antibodies conjugated to gold nanoparticles. *Cancer Res.* 2003, 63, 1999-2004.
[24] Elliott AM, Stafford RJ, Schwartz J, Wang J, Shetty AM, Bourgoyne C, O'Neal P, Hazle JD. Laser-induced thermal response and characterization of nanoparticles for cancer treatment using magnetic resonance thermal imaging. *Med. Phys.* 2007, 34, 3102-3108.
[25] Gao J, Gu H, Xu B. Multifunctional Magnetic Nanoparticles: Design, Synthesis, and Biomedical Applications. *Accounts of Chemical Research* 2009, 42, 1097-1107.

[26] Xu W, Kattel K, Park JY, Chang Y, Kim TJ, Lee GH. Paramagnetic nanoparticle T1 and T2 MRI contrast agents. *Phys. Chem. Chem. Phys.* 2012, 14, 12687-12700.
[27] Wallnofer EA, Thurner GC, Abdelmoez AA, Rohr I, Klammsteiner N, Talasz H, Kremser C, Jaschke W, Debbage P. MRI molecular imaging with nanoparticles: a technical platform for early diagnosis of cancer. *Int J Clin Pharmacol Ther* 2011, 49, 73-74.
[28] Kircher MF, Willmann JK. Molecular body imaging: MR imaging, CT, and US. part I. principles. *Radiology* 2012, 263, 633-643.
[29] Wang C-H, Huang Y-F, Yeh C-K. Aptamer-Conjugated Nanobubbles for Targeted Ultrasound Molecular Imaging. *Langmuir* 2011, 27, 6971-6976.
[30] Ke H, Wang J, Dai Z, Jin Y, Qu E, Xing Z, Guo C, Yue X, Liu J. Gold-Nanoshelled Microcapsules: A Theranostic Agent for Ultrasound Contrast Imaging and Photothermal Therapy. *Angew. Chem., Int. Ed.* 2011, 50, 3017-3021, S3017/3011-S3017/3015.
[31] Deshpande N, Willmann JK. Microparticle- anmd nanoparticle-based contrast-enhanced ultrasound imaging contrast-enhanced ultrasound imaging. John Wiley & Sons, Inc.; 2011. p. 233-262.
[32] Wang Y-H, Liao A-H, Chen J-H, Lee Y-H, Wang C-R, Li P-C. Thermotherapy with a photoacoustic/ultrasound dual-modality agent. *Proc. SPIE* 2011, 7899, 78993V/78991-78993V/78995.
[33] Caissie A, Karshafian R, Hynynen K, Czarnota GJ. Ultrasound contrast microbubbles: in vivo imaging and potential therapeutic applications. *Pan Stanford Ser. Biomed. Nanotechnol.* 2011, 2, 267-291.
[34] Devaraj NK, Keliher EJ, Thurber GM, Nahrendorf M, Weissleder R. 18F Labeled Nanoparticles for in Vivo PET-CT Imaging. *Bioconjugate Chem.* 2009, 20, 397-401.
[35] Werner MK, Schmidt H, Schwenzer NF. MR/PET: A New Challenge in Hybrid Imaging. *American Journal of Roentgenology* 2012, 199, 272-277.
[36] Lee H-Y, Li Z, Chen K, Hsu AR, Xu C, Xie J, Sun S, Chen X. PET/MRI dual-modality tumor imaging using arginine-glycine-aspartic (RGD)-conjugated radiolabeled iron oxide nanoparticles. *J. Nucl. Med.* 2008, 49, 1371-1379.
[37] Phelps ME. Positron emission tomography provides molecular imaging of biological processes. *Proc. Natl. Acad. Sci. U. S. A.* 2000, 97, 9226-9233.
[38] Sensale-Rodriguez B, Yan R, Kelly MM, Fang T, Tahy K, Hwang WS, Jena D, Liu L, Xing HG. Broadband graphene terahertz modulators enabled by intraband transitions. *Nat Commun* 2012, 3, 780.
[39] Patil RR, Yu J, Banerjee SR, Ren Y, Leong D, Jiang X, Pomper M, Tsui B, Kraitchman DL, et al. Probing In Vivo Trafficking of Polymer/DNA Micellar Nanoparticles Using SPECT/CT Imaging. *Mol. Ther.* 2011, 19, 1626-1635.
[40] Kryza D, Taleb J, Janier M, Marmuse L, Miladi I, Bonazza P, Louis Cd, Perriat P, Roux Sp, et al. Biodistribution Study of Nanometric Hybrid Gadolinium Oxide Particles as a Multimodal SPECT/MR/Optical Imaging and Theragnostic Agent. *Bioconjugate Chemistry* 2011, 22, 1145-1152.
[41] Yelin D, Oron D, Thiberge S, Moses E, Silberberg Y. Multiphoton plasmon-resonance microscopy. *Opt Express* 2003, 11, 1385-1391.
[42] Wang C, Kim J, Jin CT, Leong PHW, McEwan A. Near infrared spectroscopy in optical coherence tomography. *J. Near Infrared Spectrosc.* 2012, 20, 237-247.
[43] Rodriguez-Lorenzo L, Fabris L, Alvarez-Puebla RA. Multiplex optical sensing with surface-enhanced Raman scattering: A critical review. *Anal. Chim. Acta* 2012, 745, 10-23.
[44] Hankus ME, Cullum BM. SERS nano-imaging probes for characterizing extracellular surfaces. *Proc. SPIE-Int. Soc. Opt. Eng.* 2007, 6759, 675908/675901-675908/675910.

[45] Hankus ME, Cullum BM. SERS probes for the detection and imaging of biochemical species on the nanoscale. *Proc. SPIE-Int. Soc. Opt. Eng.* 2006, 6380, 638004/638001-638004/638012.
[46] Vo-Dinh T, Wang H-N, Scaffidi J. Plasmonic nanoprobes for SERS biosensing and bioimaging. *J. Biophotonics* 2010, 3, 89-102.
[47] Kiser JB, Cullum BM, Porterfield DM, Booksh KS. Optical cross-talk and surface characterization of SERS nanoimaging bundle substrates. *Proc. SPIE* 2010, 7674, 76740D/76741-76740D/76748.
[48] Zaman RT, Diagaradjane P, Wang JC, Schwartz J, Rajaram N, Gill-Sharp KL, Cho SH, Rylander HG, III, Payne JD, et al. In vivo detection of gold nanoshells in tumors using diffuse optical spectroscopy. *IEEE J. Sel. Top. Quantum Electron.* 2007, 13, 1715-1720.
[49] Majumdar D, Peng X-H, Shin DM. The medicinal chemistry of theragnostics, multimodality imaging and applications of nanotechnology in cancer. *Curr. Top. Med. Chem. (Sharjah, United Arab Emirates)* 2010, 10, 1211-1226.
[50] Sosnovik D, Weissleder R. Magnetic resonance and fluorescence based molecular imaging technologies
Imaging in Drug Discovery and Early Clinical Trials. In: *Herrling PL, Matter A, Rudin M,* editors.: Birkhäuser Basel, 2005, pp. 83-115.
[51] Baker M. Whole-animal imaging: The whole picture. *Nature (London, U. K.)* 2010, 463, 977-980.
[52] Jeynes C, Bailey MJ, Bright NJ, Christopher ME, Grime GW, Jones BN, Palitsin VV, Webb RP. "Total IBA" – Where are we? *Nuclear Instruments and Methods in Physics Research Section B: Beam Interactions with Materials and Atoms* 2012, 271, 107-118.
[53] Breese MBH, Landsberg JP, King PJC, Grime GW, Watt F. Applications of scanning transmission ion microscopy. *Nuclear Instruments and Methods in Physics Research Section B: Beam Interactions with Materials and Atoms* 1992, 64, 505-511.
[54] Massoud TF, Gambhir SS. Molecular imaging in living subjects: seeing fundamental biological processes in a new light. *Genes Dev.* 2003, 17, 545-580.
[55] Debbage P, Jaschke W. Molecular imaging with nanoparticles: giant roles for dwarf actors. *Histochem. Cell Biol.* 2008, 130, 845-875.
[56] Kircher MF, Willmann JK. Molecular body imaging: MR imaging, CT, and US. Part II. Applications. *Radiology* 2012, 264, 349-368.
[57] Terreno E, Delli CD, Viale A, Aime S. Challenges for Molecular Magnetic Resonance Imaging. *Chem. Rev. (Washington, DC, U. S.)* 2010, 110, 3019-3042.
[58] Na HB, Hyeon T. Nanostructured T1 MRI contrast agents. *J. Mater. Chem.* 2009, 19, 6267-6273.
[59] Bourlinos AB, Bakandritsos A, Kouloumpis A, Gournis D, Krysmann M, Giannelis EP, Polakova K, Safarova K, Hola K, et al. Gd(iii)-doped carbon dots as a dual fluorescent-MRI probe. *Journal of Materials Chemistry* 2012, 22, 23327-23330.
[60] Manus LM, Mastarone DJ, Waters EA, Zhang X-Q, Schultz-Sikma EA, MacRenaris KW, Ho D, Meade TJ. Gd(III)-Nanodiamond Conjugates for MRI Contrast Enhancement. *Nano Letters* 2009, 10, 484-489.
[61] Alric C, Taleb J, Le DG, Mandon C, Billotey C, Le M-HA, Brochard T, Vocanson F, Janier M, et al. Gadolinium Chelate Coated Gold Nanoparticles As Contrast Agents for Both X-ray Computed Tomography and Magnetic Resonance Imaging. *J. Am. Chem. Soc.* 2008, 130, 5908-5915.
[62] Voisin P, Ribot EJ, Miraux S, Bouzier-Sore A-K, Lahitte J-F, Bouchaud V, Mornet S, Thiaudiere E, Franconi J-M, et al. Use of Lanthanide-Grafted Inorganic Nanoparticles as Effective Contrast Agents for Cellular Uptake Imaging. *Bioconjugate Chem.* 2007, 18, 1053-1063.

[63] Ribot EJ, Miraux S, Konsman JP, Bouchaud V, Pourtau L, Delville M-H, Franconi J-M, Thiaudiere E, Voisin PJ. In vivo MR tracking of therapeutic microglia to a human glioma model. *NMR Biomed* 2011, 24, 1361-1368.
[64] Pinho SLC, Faneca H, Geraldes CFGC, Delville M-H, Carlos LD, Rocha J. Lanthanide-DTPA grafted silica nanoparticles as bimodal-imaging contrast agents. *Biomaterials* 2012, 33, 925-935.
[65] Pinho SLC, Faneca H, Geraldes CFGC, Rocha J, Carlos LD, Delville M-H. Silica Nanoparticles for Bimodal MRI–Optical Imaging by Grafting Gd3+ and Eu3+/Tb3+ Complexes. *European Journal of Inorganic Chemistry* 2012, 2012, 2828-2837.
[66] Taylor KML, Kim JS, Rieter WJ, An H, Lin W, Lin W. Mesoporous Silica Nanospheres as Highly Efficient MRI Contrast Agents. *J. Am. Chem. Soc.* 2008, 130, 2154-2155.
[67] Ribot E, Bouzier-Sore AK, Bouchaud V, Miraux S, Delville MH, Franconi JM, Voisin P. Microglia used as vehicles for both inducible thymidine kinase gene therapy and MRI contrast agents for glioma therapy. *Cancer Gene Ther.* 2007, 14, 724-737.
[68] Hahn M, Singh A, Sharma P, Brown S, Moudgil B. Nanoparticles as contrast agents for in-vivo bioimaging: current status and future perspectives. *Analytical and Bioanalytical Chemistry* 2011, 399, 3-27.
[69] Lux F, Roux S, Perriat P, Tillement O. Biomedical applications of nanomaterials containing gadolinium. *Curr. Inorg. Chem.* 2011, 1, 117-129.
[70] Kattel K, Park JY, Xu W, Kim HG, Lee EJ, Bony BA, Heo WC, Lee JJ, Jin S, et al. A Facile Synthesis, In vitro and In vivo MR Studies of d-Glucuronic Acid-Coated Ultrasmall Ln2O3 (Ln = Eu, Gd, Dy, Ho, and Er) Nanoparticles as a New Potential MRI Contrast Agent. *ACS Applied Materials & Interfaces* 2011, 3, 3325-3334.
[71] Na HB, Lee JH, An K, Park YI, Park M, Lee IS, Nam D-H, Kim ST, Kim S-H, et al. Development of a T1 Contrast Agent for Magnetic Resonance Imaging Using MnO Nanoparticles. *Angewandte Chemie International Edition* 2007, 46, 5397-5401.
[72] Baek MJ, Park JY, Xu W, Kattel K, Kim HG, Lee EJ, Patel AK, Lee JJ, Chang Y, et al. Water-Soluble MnO Nanocolloid for a Molecular T1 MR Imaging: A Facile One-Pot Synthesis, In vivo T1 MR Images, and Account for Relaxivities. *ACS Applied Materials & Interfaces* 2010, 2, 2949-2955.
[73] Shin J, Anisur RM, Ko MK, Im GH, Lee JH, Lee IS. Hollow manganese oxide nanoparticles as multifunctional agents for magnetic resonance imaging and drug delivery. *Angew. Chem., Int. Ed.* 2009, 48, 321-324.
[74] Lee JE, Lee N, Kim T, Kim J, Hyeon T. Multifunctional Mesoporous Silica Nanocomposite Nanoparticles for Theranostic Applications. *Accounts of Chemical Research* 2011, 44, 893-902.
[75] Kim T, Momin E, Choi J, Yuan K, Zaidi H, Kim J, Park M, Lee N, McMahon MT, et al. Mesoporous Silica-Coated Hollow Manganese Oxide Nanoparticles as Positive T1 Contrast Agents for Labeling and MRI Tracking of Adipose-Derived Mesenchymal Stem Cells. *Journal of the American Chemical Society* 2011, 133, 2955-2961.
[76] Kim BH, Lee N, Kim H, An K, Park YI, Choi Y, Shin K, Lee Y, Kwon SG, et al. Large-Scale Synthesis of Uniform and Extremely Small-Sized Iron Oxide Nanoparticles for High-Resolution T1 Magnetic Resonance Imaging Contrast Agents. *Journal of the American Chemical Society* 2011, 133, 12624-12631.
[77] Zeng L, Ren W, Zheng J, Cui P, Wu A. Ultrasmall water-soluble metal-iron oxide nanoparticles as T1-weighted contrast agents for magnetic resonance imaging. *Phys. Chem. Chem. Phys.* 2012, 14, 2631-2636.
[78] Corot C, Robert P, Idee J-M, Port M. Recent advances in iron oxide nanocrystal technology for medical imaging. *Adv. Drug Delivery Rev.* 2006, 58, 1471-1504.

[79] Na HB, Song IC, Hyeon T. Inorganic Nanoparticles for MRI Contrast Agents. *Advanced Materials* 2009, 21, 2133-2148.
[80] Rosen JE, Chan L, Shieh D-B, Gu FX. Iron oxide nanoparticles for targeted cancer imaging and diagnostics. *Nanomedicine: Nanotechnology, Biology and Medicine* 2012, 8, 275-290.
[81] Rosen JE, Yoffe S, Meerasa A, Verma M, Gu FX. Nanotechnology and diagnostic imaging: new advances in contrast agent technology. *J. Nanomed. Nanotechnol.* 2011, 2, 1000115.
[82] Laurent S, Forge D, Port M, Roch A, Robic C, Vander Elst L, Muller RN. Magnetic iron oxide nanoparticles: synthesis, stabilization, vectorization, physicochemical characterizations, and biological applications. *Chem Rev* 2008, 108, 2064-2110.
[83] Semelka RC, Helmberger TK. Contrast agents for MR imaging of the liver. *Radiology* 2001, 218, 27-38.
[84] Kiessling F. Noninvasive cell tracking. *Handb Exp Pharmacol* 2008, 305-321.
[85] Berthault P, Huber G, Desvaux H. Biosensing using laser-polarized xenon NMR/MRI. *Prog. Nucl. Magn. Reson. Spectrosc.* 2009, 55, 35-60.
[86] Tang TY, Muller KH, Graves MJ, Li ZY, Walsh SR, Young V, Sadat U, Howarth SPS, Gillard JH. Iron Oxide Particles for Atheroma Imaging. *Arterioscler., Thromb., Vasc. Biol.* 2009, 29, 1001-1008.
[87] Cooper KL, Meng Y, Harnan S, Ward SE, Fitzgerald P, Papaioannou D, Wyld L, Ingram C, Wilkinson ID, et al. Positron emission tomography (PET) and magnetic resonance imaging (MRI) for the assessment of axillary lymph node metastases in early breast cancer: systematic review and economic evaluation. *Health Technol Assess* 2011, 15, iii-iv, 1-134.
[88] Harnan SE, Cooper KL, Meng Y, Ward SE, Fitzgerald P, Papaioannou D, Ingram C, Lorenz E, Wilkinson ID, et al. Magnetic resonance for assessment of axillary lymph node status in early breast cancer: a systematic review and meta-analysis. *Eur J Surg Oncol* 2011, 37, 928-936.
[89] Mattei A, Danuser H. Contemporary imaging analyses of pelvic lymph nodes in the prostate cancer patient. *Curr Opin Urol* 2011, 21, 211-218.
[90] Skotland T. Molecular imaging: challenges of bringing imaging of intracellular targets into common clinical use. *Contrast Media Mol. Imaging* 2012, 7, 1-6.
[91] Sosnovik DE, Nahrendorf M, Weissleder R. Magnetic nanoparticles for MR imaging: agents, techniques and cardiovascular applications. *Basic Res. Cardiol.* 2008, 103, 122-130.
[92] Rosenblum LT, Kosaka N, Mitsunaga M, Choyke PL, Kobayashi H. In vivo molecular imaging using nanomaterials: General in vivo characteristics of nano-sized reagents and applications for cancer diagnosis (Review). *Mol. Membr. Biol.* 2010, 27, 274-285.
[93] Park JY, Choi HJ, Nam G-E, Cho K-S, Son J-H. In vivo dual-modality terahertz/magnetic resonance imaging using superparamagnetic iron oxide nanoparticles as a dual contrast agent. *IEEE Trans. Terahertz Sci. Technol.* 2012, 2, 93-98.
[94] Goodwill PW, Saritas EU, Croft LR, Kim TN, Krishnan KM, Schaffer DV, Conolly SM. X-Space MPI: Magnetic Nanoparticles for Safe Medical Imaging. *Adv. Mater. (Weinheim, Ger.)* 2012, 24, 3870-3877.
[95] Hogemann-Savellano D, Bos E, Blondet C, Sato F, Abe T, Josephson L, Weissleder R, Gaudet J, Sgroi D, et al. The transferrin receptor: a potential molecular imaging marker for human cancer. *Neoplasia* 2003, 5, 495-506.
[96] Narayanan S, Sathy BN, Mony U, Koyakutty M, Nair SV, Menon D. Biocompatible Magnetite/Gold Nanohybrid Contrast Agents via Green Chemistry for MRI and CT Bioimaging. *ACS Appl. Mater. Interfaces* 2012, 4, 251-260.

[97] Jun Y-w, Huh Y-M, Choi J-s, Lee J-H, Song H-T, Kim S, Yoon S, Kim K-S, Shin J-S, et al. Nanoscale size effect of magnetic nanocrystals and their utilization for cancer diagnosis via magnetic resonance imaging. *J. Am. Chem. Soc.* 2005, 127, 5732-5733.
[98] Lu AH, Salabas EL, Schueth F. Magnetic nanoparticles: synthesis, protection, functionalization, and application. *Angew. Chem., Int. Ed.* 2007, 46, 1222-1244.
[99] Pinho SLC, Laurent S, Rocha J, Roch A, Delville M-H, Mornet S, Carlos LD, Vander EL, Muller RN, et al. Relaxometric Studies of γ-Fe2O3@SiO2 Core Shell Nanoparticles: When the Coating Matters. *J. Phys. Chem. C* 2012, 116, 2285-2291.
[100] Pinho SLC, Pereira GA, Voisin P, Kassem J, Bouchaud V, Etienne L, Peters JA, Carlos L, Mornet S, et al. Fine Tuning of the Relaxometry of γ-Fe2O3@SiO2 Nanoparticles by Tweaking the Silica Coating Thickness. *ACS Nano* 2010, 4, 5339-5349.
[101] Suzuki Y, Cunningham CH, Noguchi K-i, Chen IY, Weissman IL, Yeung AC, Robbins RC, Yang PC. In vivo serial evaluation of superparamagnetic iron-oxide labeled stem cells by off-resonance positive contrast. *Magnetic Resonance in Medicine* 2008, 60, 1269-1275.
[102] Cunningham CH, Arai T, Yang PC, McConnell MV, Pauly JM, Conolly SM. Positive contrast magnetic resonance imaging of cells labeled with magnetic nanoparticles. *Magn. Reson. Med.* 2005, 53, 999-1005.
[103] Senpan A, Caruthers SD, Rhee I, Mauro NA, Pan D, Hu G, Scott MJ, Fuhrhop RW, Gaffney PJ, et al. Conquering the Dark Side: Colloidal Iron Oxide Nanoparticles. *ACS Nano* 2009, 3, 3917-3926.
[104] Kattel K, Park JY, Xu W, Kim HG, Lee EJ, Bony BA, Heo WC, Jin S, Baeck JS, et al. Paramagnetic dysprosium oxide nanoparticles and dysprosium hydroxide nanorods as T2 MRI contrast agents. *Biomaterials* 2012, 33, 3254-3261.
[105] Das GK, Johnson NJJ, Cramen J, Blasiak B, Latta P, Tomanek B, van Veggel FCJM. NaDyF4 Nanoparticles as T2 Contrast Agents for Ultrahigh Field Magnetic Resonance Imaging. *The Journal of Physical Chemistry Letters* 2012, 3, 524-529.
[106] Lee J-H, Huh Y-M, Jun Y-w, Seo J-w, Jang J-t, Song H-T, Kim S, Cho E-J, Yoon H-G, et al. Artificially engineered magnetic nanoparticles for ultra-sensitive molecular imaging. *Nat Med* 2007, 13, 95-99.
[107] Winter PM. Magnetic resonance chemical exchange saturation transfer imaging and nanotechnology. *Wiley Interdisciplinary Reviews: Nanomedicine and Nanobiotechnology* 2012, 4, 389-398.
[108] Cai K, Kiefer GE, Caruthers SD, Wickline SA, Lanza GM, Winter PM. Quantification of water exchange kinetics for targeted PARACEST perfluorocarbon nanoparticles. *NMR in Biomedicine* 2012, 25, 279-285.
[109] Evbuomwan OM, Merritt ME, Kiefer GE, Dean SA. Nanoparticle-based PARACEST agents: the quenching effect of silica nanoparticles on the CEST signal from surface-conjugated chelates. *Contrast Media Mol. Imaging* 2012, 7, 19-25.
[110] Bouchard L-S, Anwar MS, Liu GL, Hann B, Xie ZH, Gray JW, Wang X, Pines A, Chen FF. Picomolar sensitivity MRI and photoacoustic imaging of cobalt nanoparticles. *Proc. Natl. Acad. Sci. U. S. A.* 2009, 106, 4085-4089.
[111] Yang H, Zhou H, Zhang C, Li X, Hu H, Wu H, Yang S. Water-soluble magnetic CoO nanocrystals functionalized with surfactants as T2-weighed MRI contrast agents in vitro. *Dalton Trans.* 2011, 40, 3616-3621.
[112] He X, Wang K, Cheng Z. In vivo near-infrared fluorescence imaging of cancer with nanoparticle-based probes. *Wiley Interdiscip. Rev.: Nanomed. Nanobiotechnol.* 2010, 2, 349-366.
[113] Altinoglu EI, Adair JH. Near infrared imaging with nanoparticles. *Wiley Interdiscip. Rev.: Nanomed. Nanobiotechnol.* 2010, 2, 461-477.

[114] Wittenberg NJ, Haynes CL. Using nanoparticles to push the limits of detection. *Wiley Interdisciplinary Reviews: Nanomedicine and Nanobiotechnology* 2009, 1, 237-254.
[115] Valizadeh A, Mikaeili H, Samiei M, Farkhani SM, Zarghami N, Kouhi M, Akbarzadeh A, Davaran S. Quantum dots: synthesis, bioapplications, and toxicity. *Nanoscale Res Lett* 2012, 7, 7-480.
[116] Hama Y, Koyama Y, Urano Y, Choyke PL, Kobayashi H. Simultaneous two-color spectral fluorescence lymphangiography with near infrared quantum dots to map two lymphatic flows from the breast and the upper extremity. *Breast cancer research and treatment* 2007, 103, 23-28.
[117] Kobayashi H, Hama Y, Koyama Y, Barrett T, Regino CAS, Urano Y, Choyke PL. Simultaneous Multicolor Imaging of Five Different Lymphatic Basins Using Quantum Dots. *Nano Lett.* 2007, 7, 1711-1716.
[118] Liu C-P, Cheng S-H, Chen N-T, Lo L-W. Intra/Inter-Particle Energy Transfer of Luminescence Nanocrystals for Biomedical Applications. *Journal of Nanomaterials* 2012, 2012, 9.
[119] So M-K, Xu C, Loening AM, Gambhir SS, Rao J. Self-illuminating quantum dot conjugates for in vivo imaging. *Nat Biotech* 2006, 24, 339-343.
[120] Clift MJD, Stone V. Quantum Dots: An Insight and Perspective of Their Biological Interaction and How This Relates to Their Relevance for Clinical Use *Theranostics* 2012, 2, 668-680.
[121] Kim S, Lim YT, Soltesz EG, De GAM, Lee J, Nakayama A, Parker JA, Mihaljevic T, Laurence RG, et al. Near-infrared fluorescent type II quantum dots for sentinel lymph node mapping. *Nat. Biotechnol.* 2004, 22, 93-97.
[122] Ye L, Yong K-T, Liu L, Roy I, Hu R, Zhu J, Cai H, Law W-C, Liu J, et al. A pilot study in non-human primates shows no adverse response to intravenous injection of quantum dots. *Nat Nano* 2012, 7, 453-458.
[123] Quan B, Choi K, Kim Y-H, Kang KW, Chung DS. Near infrared dye indocyanine green doped silica nanoparticles for biological imaging. *Talanta* 2012, 99, 387-393.
[124] Huang X, Zhang F, Lee S, Swierczewska M, Kiesewetter DO, Lang L, Zhang G, Zhu L, Gao H, et al. Long-term multimodal imaging of tumor draining sentinel lymph nodes using mesoporous silica-based nanoprobes. *Biomaterials* 2012, 33, 4370-4378.
[125] Bonacchi S, Genovese D, Juris R, Montalti M, Prodi L, Rampazzo E, Sgarzi M, Zaccheroni N. Luminescent Chemosensors Based on Silica Nanoparticles. In: *Prodi L, Montalti M, Zaccheroni N,* editors.: Springer Berlin / Heidelberg, 2011, pp. 93-138.
[126] Kuo W-S, Chang Y-T, Cho K-C, Chiu K-C, Lien C-H, Yeh C-S, Chen S-J. Gold nanomaterials conjugated with indocyanine green for dual-modality photodynamic and photothermal therapy. *Biomaterials* 2012, 33, 3270-3278.
[127] Altinoglu EI, Russin TJ, Kaiser JM, Barth BM, Eklund PC, Kester M, Adair JH. Near-Infrared Emitting Fluorophore-Doped Calcium Phosphate Nanoparticles for In Vivo Imaging of Human Breast Cancer. *ACS Nano* 2008, 2, 2075-2084.
[128] Kobayashi H, Ogawa M, Alford R, Choyke PL, Urano Y. New Strategies for Fluorescent Probe Design in Medical Diagnostic Imaging. *Chemical Reviews* 2009, 110, 2620-2640.
[129] Kim HM, Cho BR. Two-Photon Probes for Intracellular Free Metal Ions, Acidic Vesicles, And Lipid Rafts in Live Tissues. *Accounts of Chemical Research* 2009, 42, 863-872.
[130] Bachmann PK, Hummel H, Juestel T, Merikhi J, Ronda CR, Weiler V. Near-infrared luminescent nanomaterials for in-vivo optical imaging. *Journal of Nanophotonics* 2008, 2, 021920-021920.

[131] Zhou J, Liu Z, Li F. Upconversion nanophosphors for small-animal imaging. *Chem. Soc. Rev.* 2012, 41, 1323-1349.
[132] Zeng S, Tsang M-K, Chan C-F, Wong K-L, Fei B, Hao J. Dual-modal fluorescent/magnetic bioprobes based on small sized upconversion nanoparticles of amine-functionalized BaGdF5:Yb/Er. *Nanoscale* 2012, 4, 5118-5124.
[133] Yu X-F, Chen L-D, Li M, Xie M-Y, Zhou L, Li Y, Wang Q-Q. Highly efficient fluorescence of NdF3/SiO2 core/shell nanoparticles and the applications for in vivo NIR detection. *Adv. Mater.* 2008, 20, 4118-4123.
[134] Soga K, Nagasaki Y. Polyscale technology for developing near infrared fluorescence bioimaging system based on novel synthese approaches for rare-earth doped nanophospors. *Mater. Res. Innovations* 2010, 14, 51-55.
[135] Chatterjee DK, Rufaihah AJ, Zhang Y. Upconversion fluorescence imaging of cells and small animals using lanthanide doped nanocrystals. *Biomaterials* 2008, 29, 937-943.
[136] Soga K, Tokuzen K, Tsuji K, Yamano T, Venkatachalam N, Hyodo H, Kishimoto H, Jiang S, Digonnet MJF, et al. Application of ceramic phosphors for near infrared biomedical imaging technologies. *Proc. SPIE* 2010, 7598, 759807/759801-759807/759809.
[137] Zhou J, Yu M, Sun Y, Zhang X, Zhu X, Wu Z, Wu D, Li F. Fluorine-18-labeled Gd3+/Yb3+/Er3+ co-doped NaYF4 nanophosphors for multimodality PET/MR/UCL imaging. *Biomaterials* 2011, 32, 1148-1156.
[138] Hilderbrand SA, Shao F, Salthouse C, Mahmood U, Weissleder R. Upconverting luminescent nanomaterials: application to in vivo bioimaging. *Chemical Communications* 2009, 4188-4190.
[139] Zako T, Hyodo H, Tsuji K, Tokuzen K, Kishimoto H, Ito M, Kaneko K, Maeda M, Soga K. Development of Near Infrared-Fluorescent Nanophosphors and Applications for Cancer Diagnosis and Therapy. *Journal of Nanomaterials* 2010, 2010.
[140] Venkatachalam N, Okumura Y, Soga K, Fukuda R, Tsuji T. Bioimaging of M1 cells using ceramic nanophosphors: Synthesis and toxicity assay of Y 2 O 3 nanoparticles. *Journal of Physics: Conference Series* 2009, 191, 012002.
[141] Wang L, Zhang Y, Zhu Y. One-pot synthesis and strong near-infrared upconversion luminescence of poly(acrylic acid)-functionalized YF3:Yb3+/Er3+ nanocrystals. *Nano Res.* 2010, 3, 317-325.
[142] Chen G, Shen J, Ohulchanskyy TY, Patel NJ, Kutikov A, Li Z, Song J, Pandey RK, Ågren H, et al. (α-NaYbF4:Tm3+)/CaF2 Core/Shell Nanoparticles with Efficient Near-Infrared to Near-Infrared Upconversion for High-Contrast Deep Tissue Bioimaging. *ACS Nano* 2012, 6, 8280-8287.
[143] Welsher K, Liu Z, Sherlock SP, Robinson JT, Chen Z, Daranciang D, Dai H. A route to brightly fluorescent carbon nanotubes for near-infrared imaging in mice. *Nat Nano* 2009, 4, 773-780.
[144] Huang H, Zou M, Xu X, Liu F, Li N, Wang X. Near-infrared fluorescence spectroscopy of single-walled carbon nanotubes and its applications. *TrAC, Trends Anal. Chem.* 2011, 30, 1109-1119.
[145] Liu Z, Yang K, Lee S-T. Single-walled carbon nanotubes in biomedical imaging. *J. Mater. Chem.* 2011, 21, 586-598.
[146] Bandaru NM, Voelcker NH. Glycoconjugate-functionalized carbon nanotubes in biomedicine. *Journal of Materials Chemistry* 2012, 22, 8748-8758.
[147] Esteves da Silva JCG, Goncalves HMR. Analytical and bioanalytical applications of carbon dots. *TrAC, Trends Anal. Chem.* 2011, 30, 1327-1336.
[148] Dong Y, Wang R, Li G, Chen C, Chi Y, Chen G. Polyamine-Functionalized Carbon Quantum Dots as Fluorescent Probes for Selective and Sensitive Detection of Copper Ions. *Analytical Chemistry* 2012, 84, 6220-6224.

[149] Liu J-M, Lin L-p, Wang X-X, Lin S-Q, Cai W-L, Zhang L-H, Zheng Z-Y. Highly selective and sensitive detection of Cu2+ with lysine enhancing bovine serum albumin modified-carbon dots fluorescent probe. *Analyst* 2012, 137, 2637-2642.
[150] Huang P, Lin J, Wang X, Wang Z, Zhang C, He M, Wang K, Chen F, Li Z, et al. Light-Triggered Theranostics Based on Photosensitizer-Conjugated Carbon Dots for Simultaneous Enhanced-Fluorescence Imaging and Photodynamic Therapy. *Advanced Materials* 2012, 24, 5104-5110.
[151] Cao L, Yang S, Wang X, Luo P, Liu J, Sahu S, Liu Y, Sun Y. Competitive Performance of Carbon "Quantum" Dots in Optical Bioimaging. . *Theranostics* 2012, 2, 295-301.
[152] Sun Y-P, Zhou B, Lin Y, Wang W, Fernando KAS, Pathak P, Meziani MJ, Harruff BA, Wang X, et al. Quantum-Sized Carbon Dots for Bright and Colorful Photoluminescence. *Journal of the American Chemical Society* 2006, 128, 7756-7757.
[153] Yang S-T, Wang X, Wang H, Lu F, Luo PG, Cao L, Meziani MJ, Liu J-H, Liu Y, et al. Carbon Dots as Nontoxic and High-Performance Fluorescence Imaging Agents. *J. Phys. Chem. C* 2009, 113, 18110-18114.
[154] Hui YY, Cheng C-L, Chang H-C. Nanodiamonds for optical bioimaging. *J. Phys. D: Appl. Phys.* 2010, 43, 374021/374021-374021/374011.
[155] Mochalin VN, Shenderova O, Ho D, Gogotsi Y. The properties and applications of nanodiamonds. *Nat Nano* 2012, 7, 11-23.
[156] Barnard AS. Diamond standard in diagnostics: nanodiamond biolabels make their mark. *Analyst (Cambridge, U. K.)* 2009, 134, 1751-1764.
[157] Xing Y, Dai L. Nanodiamonds for nanomedicine. *Nanomedicine* 2009, 4, 207-218.
[158] Shen J, Zhu Y, Yang X, Li C. Graphene quantum dots: emergent nanolights for bioimaging, sensors, catalysis and photovoltaic devices. *J Chem. Soc. Chem. Commun.* 2012, 48, 3686-3699.
[159] Zhu S, Tang S, Zhang J, Yang B. Control the size and surface chemistry of graphene for the rising fluorescent materials. *Chemical Communications* 2012, 48, 4527-4539.
[160] Park J-H, Gu L, von MG, Ruoslahti E, Bhatia SN, Sailor MJ. Biodegradable luminescent porous silicon nanoparticles for in vivo applications. *Nat. Mater.* 2009, 8, 331-336.
[161] Wang Y, Liu Y, Luehmann H, Xia X, Brown P, Jarreau C, Welch M, Xia Y. Evaluating the Pharmacokinetics and In Vivo Cancer Targeting Capability of Au Nanocages by Positron Emission Tomography Imaging. *ACS Nano* 2012, 6, 5880-5888.
[162] Miller PW, Long NJ, Vilar R, Gee AD. Synthesis of 11C, 18F, 15O, and 13N radiolabels for positron emission tomography. *Angew. Chem., Int. Ed.* 2008, 47, 8998-9033.
[163] Sioka C, Fotopoulos A, Kyritsis A. Recent advances in PET imaging for evaluation of Parkinson's disease. *Eur J Nucl Med Mol Imaging* 2010, 37, 1594-1603.
[164] Liu Y, Welch MJ. Nanoparticles Labeled with Positron Emitting Nuclides: Advantages, Methods, and Applications. *Bioconjugate Chem.* 2012, 23, 671-682.
[165] Sun Y, Yu M, Liang S, Zhang Y, Li C, Mou T, Yang W, Zhang X, Li B, et al. Fluorine-18 labeled rare-earth nanoparticles for positron emission tomography (PET) imaging of sentinel lymph node. *Biomaterials* 2011, 32, 2999-3007.
[166] Duconge F, Pons T, Pestourie C, Herin L, Theze B, Gombert K, Mahler B, Hinnen F, Kuhnast B, et al. Fluorine-18-labeled phospholipid quantum dot micelles for in vivo multimodal imaging from whole body to cellular scales *Bioconjugate Chem.* 2008, 19, 1921.
[167] Schipper ML, Iyer G, Koh AL, Cheng Z, Ebenstein Y, Aharoni A, Keren S, Bentolila LA, Li J, et al. Particle size, surface coating, and PEGylation influence the biodistribution of quantum dots in living mice. *Small* 2009, 5, 126.
[168] Tu C, Ma X, House A, Kauzlarich SM, Louie AY. PET imaging and biodistribution of silicon quantum dots in

mice. *ACS Med. Chem. Lett.* 2011, 2, 285.
[169] Nahrendorf M, Keliher E, Marinelli B, Leuschner F, Robbins CS, Gerszten RE, Pittet MJ, Swirski FK, Weissleder R. Detection of Macrophages in Aortic Aneurysms by Nanoparticle Positron Emission Tomography-Computed Tomography. *Arterioscler., Thromb., Vasc. Biol.* 2011, 31, 750-757.
[170] Glaus C, Rossin R, Welch MJ, Bao G. In vivo evaluation of (64)Cu-labeled magnetic nanoparticles as a dual modalityPET/MR imaging agent. *Bioconjugate Chem.* 2010, 21, 715.
[171] Xie J, Chen K, Huang J, Lee S, Wang J, Gao J, Li X, Chen X. PET/NIRF/MRI triple functional iron oxide nanoparticles. *Biomaterials* 2010, 31, 3016-3022.
[172] Patel D, Kell A, Simard B, Xiang B, Lin HY, Tian G. The cell labeling efficacy, cytotoxicity and relaxivity of copper-activated MRI/PET imaging contrast agents. *Biomaterials* 2011, 32, 1167-1176.
[173] Martin dRRT, Tavare R, Paul RL, Jauregui-Osoro M, Protti A, Glaria A, Varma G, Szanda I, Blower PJ. Synthesis of 64CuII-Bis(dithiocarbamatebisphosphonate) and Its Conjugation with Superparamagnetic Iron Oxide Nanoparticles: In Vivo Evaluation as Dual-Modality PET-MRI Agent. *Angew. Chem., Int. Ed.* 2011, 50, 5509-5513, S5509/5501-S5509/5524.
[174] Stelter L, Pinkernelle JG, Michel R, Schwartlander R, Raschzok N, Morgul MH, Koch M, Denecke T, Ruf J, et al. Modification of aminosilanized superparamagnetic nanoparticles: feasibility of multimodal etection using 3T MRI, small animal PET, and fluorescence imaging. *Mol. Imaging Biol.* 2010, 12, 25.
[175] Yang X, Hong H, Grailer JJ, Rowland IJ, Javadi A, Hurley SA, Xiao Y, Yang Y, Zhang Y, et al. cRGD-functionalized, DOX-conjugated, and 64Cu-labeled superparamagnetic iron oxide nanoparticles for targeted anticancer drug delivery and PET/MR imaging. *Biomaterials* 2011, 32, 4151-4160.
[176] Hwang DW, Ko HY, Kim S-K, Kim D, Lee DS, Kim S. Development of a Quadruple Imaging Modality by Using Nanoparticles. *Chem.--Eur. J.* 2009, 15, 9387-9393, S9387/9381-S9387/9386.
[177] Choi JS, Park JC, Nah H, Woo S, Oh J, Kim KM, Cheon GJ, Chang Y, Yoo J, et al. A hybrid nanoparticle probe for dual-modality positron emission tomography and magnetic esonance imaging. *Angew. Chem., Int. Ed. Engl.* 2008, 47, 6259.
[178] Jauregui-Osoro M, Williamson PA, Glaria A, Sunassee K, Charoenphun P, Green MA, Mullen GED, Blower PJ. Biocompatible inorganic nanoparticles for [18F]-fluoride binding with applications in PET imaging. *Dalton Trans.* 2011, 40, 6226-6237.
[179] Liu Q, Sun Y, Li C, Zhou J, Yang T, Zhang X, Yi T, Wu D, Li F. (18)F-labeled magnetic-upconversion nanophosphors
via rare-earth cation-assisted ligand assembly. *ACS Nano* 2011, 5, 3146.
[180] Xie H, Wang ZJ, Bao A, Goins B, Phillips WT. In vivo PET imaging and biodistribution of radiolabeled gold nanoshells in rats with tumor xenografts. *Int. J. Pharm.* 2010, 395, 324.
[181] Xie H, Wang ZJ, Bao A, Goins B, Phillips WT. Radiolabeled gold nanoshells for in vivo imaging: example of methodology for initial evaluation of biodistribution of a novel nanoparticle. *Pan Stanford Ser. Biomed. Nanotechnol.* 2011, 2, 213-224.
[182] Cartier R, Kaufner L, Paulke BR, Wustneck R, Pietschmann S, Michel R, Bruhn H, Pison U. Latex nanoparticles for multimodal imaging and detection in vivo. *Nanotechnology* 2007, 18, 195102.
[183] Petersen AL, Binderup T, Rasmussen P, Henriksen JR, Elema DR, Kjaer A, Andresen TL. 64Cu loaded liposomes as positron emission tomography imaging agents. *Biomaterials* 2011, 32, 2334.

[184] Seo JW, Mahakian LM, Kheirolomoom A, Zhang H, Meares CF, Ferdani R, Anderson CJ, Ferrara KW. Liposomal Cu-64 labeling method using bifunctional chelators: poly(ethylene glycol) spacer and chelator effects. *Bioconjugate Chem.* 2010, 21, 1206.
[185] Seo JW, Zhang H, Kukis DL, Meares CF, Ferrara KW. A novel method to label preformed liposomes with 64Cu for positron emission tomography (PET) imaging. *Bioconjugate Chem.* 2008, 19, 2577.
[186] Oku N, Yamashita M, Katayama Y, Urakami T, Hatanaka K, Shimizu K, Asai T, Tsukada H, Akai S, et al. PET imaging of brain cancer with positron emitter-labeled liposomes. *Int. J. Pharm.* 2011, 403, 170-177.
[187] Rygh CB, Qin S, Seo JW, Mahakian LM, Zhang H, Adamson R, Chen JQ, Borowsky AD, Cardiff RD, et al. Longitudinal Investigation of Permeability and Distribution of Macromolecules in Mouse Malignant Transformation Using PET. *Clin. Cancer Res.* 2011, 17, 550-559.
[188] Marik J, Tartis MS, Zhang H, Fung JY, Kheirolomoom A, Sutcliffe JL, Ferrara KW. Long-circulating liposomes radiolabeled with [18F]fluorodipalmitin ([18F]FDP). *Nucl. Med. Biol.* 2007, 34, 165.
[189] Helbok A, Decristoforo C, Dobrozemsky G, Rangger C, Diederen E, Stark B, Prassl R, von Guggenberg E. Radiolabeling of lipid-based nanoparticles for diagnostics and therapeutic applications: a comparison using different radiometals. *J. Liposome Res.* 2009, 20, 219.
[190] Andreozzi E, Seo JW, Ferrara K, Louie A. Novel method to label solid lipid nanoparticles with (64)cu for positron emission tomography imaging. *Bioconjugate Chem.* 2011, 22, 808.
[191] Almutairi A, Rossin R, Shokeen M, Hagooly A, Ananth A, Capoccia B, Guillaudeu S, Abendschein D, Anderson CJ, et al. Biodegradable dendritic positron-emitting nanoprobes for the noninvasive imaging of ngiogenesis. *Proc. Natl. Acad. Sci. U. S. A.* 2009, 106, 685.
[192] Sun G, Xu J, Hagooly A, Rossin R, Li Z, Moore DA, Hawker CJ, Welch MJ, Wooley KL. Strategies for optimized radiolabeling of nanoparticles for in vivo PET imaging. *Adv. Mater.* 2007, 19, 3157.
[193] Herth MM, Barz M, Moderegger D, Allmeroth M, Jahn M, Thews O, Zentel R, Rosch F. Radioactive labeling of defined HPMA-based polymeric structures using [18F]FETos for in vivo imaging by positron emission tomography. *Biomacromolecules* 2009, 10, 1697.
[194] Simone EA, Zern BJ, Chacko A-M, Mikitsh JL, Blankemeyer ER, Muro S, Stan RV, Muzykantov VR. Endothelial targeting of polymeric nanoparticles stably labeled with the PET imaging radioisotope iodine-124. *Biomaterials* 2012, 33, 5406-5413.
[195] Liu Z, Cai W, He L, Nakayama N, Chen K, Sun X, Chen X, Dai H. In vivo biodistribution and highly efficient tumour targeting of carbon nanotubes in mice. *Nat. Nanotechnol.* 2007, 2, 47.
[196] Ruggiero A, Villa CH, Holland JP, Sprinkle SR, May C, Lewis JS, Scheinberg DA, McDevitt MR. Imaging and treating tumor vasculature with targeted radiolabeled carbon nanotubes. *Int. J. Nanomed.* 2010, 5, 783.
[197] McDevitt MR, Chattopadhyay D, Jaggi JS, Finn RD, Zanzonico PB, Villa C, Rey D, Mendenhall J, Batt CA, et al. PET imaging of soluble yttrium-86-labeled carbon nanotubes in mice. *PLoS One* 2007, 2, e907.
[198] Hong H, Zhang Y, Engle JW, Nayak TR, Theuer CP, Nickles RJ, Barnhart TE, Cai W. In vivo targeting and positron emission tomography imaging of tumor vasculature with 66Ga-labeled nano-graphene. *Biomaterials* 2012, 33, 4147-4156.
[199] Huang W-Y, Davis JJ. Multimodality and nanoparticles in medical imaging. *Dalton Trans.* 2011, 40, 6087-6103.

[200] Sharma P, Singh A, Brown S, Bengtsson N, Walter G, Grobmyer S, Iwakuma N, Santra S, Scott E, et al. Multimodal Nanoparticulate Bioimaging Contrast Agents. In: *Grobmyer SR, Moudgil BM,* editors. Cancer Nanotechnology: Humana Press, 2010, pp. 67-81.
[201] Jarzyna PA, Gianella A, Skajaa T, Knudsen G, Deddens LH, Cormode DP, Fayad ZA, Mulder WJM. Multifunctional imaging nanoprobes. *Wiley Interdiscip. Rev.: Nanomed. Nanobiotechnol.* 2010, 2, 138-150.
[202] Nahrendorf M, Zhang H, Hembrador S, Panizzi P, Sosnovik DE, Aikawa E, Libby P, Swirski FK, Weissleder R. Nanoparticle PET-CT Imaging of Macrophages in Inflammatory Atherosclerosis. *Circulation* 2008, 117, 379-387.
[203] Benezra M, Penate-Medina O, Zanzonico PB, Schaer D, Ow H, Burns A, DeStanchina E, Longo V, Herz E, et al. Multimodal silica nanoparticles are effective cancer-targeted probes in a model of human melanoma. *J Clin Invest* 2011, 121, 2768-2780.
[204] Kumar R, Roy I, Ohulchanskky TY, Vathy LA, Bergey EJ, Sajjad M, Prasad PN. In Vivo Biodistribution and Clearance Studies Using Multimodal Organically Modified Silica Nanoparticles. *ACS Nano* 2010, 4, 699-708.
[205] Chen K, Li Z-B, Wang H, Cai W, Chen X. Dual-modality optical and positron emission tomography imaging of vascular endothelial growth factor receptor on tumor vasculature using quantum dots. *Eur J Nucl Med Mol Imaging* 2008, 35, 2235-2244.
[206] Lee YK, Jeong JM, Hoigebazar L, Yang BY, Lee Y-S, Lee BC, Youn H, Lee DS, Chung J-K, et al. Nanoparticles modified by encapsulation of ligands with a long alkyl chain to affect multispecific and multimodal imaging. *J. Nucl. Med.* 2012, 53, 1462-1470.
[207] Psimadas D, Georgoulias P, Valotassiou V, Loudos G. Molecular nanomedicine towards cancer: 111In-labeled nanoparticles. *J Pharm Sci* 2012, 101, 2271-2280.
[208] Chen HH, Josephson L, Sosnovik DE. Imaging of apoptosis in the heart with nanoparticle technology. *Wiley Interdiscip. Rev.: Nanomed. Nanobiotechnol.* 2011, 3, 86-99.
[209] Makino A, Kimura S. Preparation of peptide- and protein-based molecular assemblies and their utilizations as nanocarriers for tumor imaging. *Reactive and Functional Polymers* 2011, 71, 272-279.
[210] Hong SY, Tobias G, Al-Jamal KT, Ballesteros B, Ali-Boucetta H, Lozano-Perez S, Nellist PD, Sim RB, Finucane C, et al. Filled and glycosylated carbon nanotubes for in vivo radio-emitter localization and imaging. *Nat. Mater.* 2010, 9, 485-490.
[211] Becker N, Liebermann D, Wesch H, Van Kaick G. Mortality among Thorotrast-exposed patients and an unexposed comparison group in the German Thorotrast study. *European Journal of Cancer* 2008, 44, 1259-1268.
[212] Liu Y, Ai K, Lu L. Nanoparticulate X-ray Computed Tomography Contrast Agents: From Design Validation to in Vivo Applications. *Accounts of Chemical Research* 2012, 45, 1817-1827.
[213] Galperin A, Margel D, Baniel J, Dank G, Biton H, Margel S. Radiopaque iodinated polymeric nanoparticles for X-ray imaging applications. *Biomaterials* 2007, 28, 4461-4468.
[214] Hallouard F, Anton N, Choquet P, Constantinesco A, Vandamme T. Iodinated blood pool contrast media for preclinical X-ray applications - A review. *Biomaterials* 2010, 31, 6249-6268.
[215] de Vries A, Custers E, Lub J, van dBS, Nicolay K, Gruell H. Block-copolymer-stabilized iodinated emulsions for use as CT contrast agents. *Biomaterials* 2010, 31, 6537-6544.
[216] Kong WH, Lee WJ, Cui ZY, Bae KH, Park TG, Kim JH, Park K, Seo SW. Nanoparticulate carrier containing water-insoluble iodinated oil as a multifunctional contrast agent for computed tomography imaging. *Biomaterials* 2007, 28, 5555-5561.

[217] Bakan DA, Weichert JP, Longino MA, Counsell RE. Polyiodinated triglyceride lipid emulsions for use as hepatoselective contrast agents in CT: effects of physicochemical properties on biodistribution and imaging profiles. *Invest. Radiol.* 2000, 35, 158-169.
[218] Hallouard F, Briancon S, Anton N, Li X, Vandamme T, Fessi H. Iodinated nano-emulsions as contrast agents for preclinical X-ray imaging, impact of the free surfactants on the pharmacokinetics. *Eur J Pharm Biopharm* 2012.
[219] Badea CT, Athreya KK, Espinosa G, Clark D, Ghafoori AP, Li Y, Kirsch DG, Johnson GA, Annapragada A, et al. Computed tomography imaging of primary lung cancer in mice using a liposomal-iodinated contrast agent. *PLoS One* 2012, 7, e34496.
[220] Elrod DB, Partha R, Danila D, Casscells SW, Conyers JL. An iodinated liposomal computed tomographic contrast agent prepared from a diiodophosphatidylcholine lipid. *Nanomedicine (N. Y., NY, U. S.)* 2009, 5, 42-45.
[221] Dunne M, Zheng J, Rosenblat J, Jaffray DA, Allen C. APN/CD13-targeting as a strategy to alter the tumor accumulation of liposomes. *J. Controlled Release* 2011, 154, 298-305.
[222] Montet X, Pastor CM, Vallee J-P, Becker CD, Geissbuhler A, Morel DR, Meda P. Improved Visualization of Vessels and Hepatic Tumors by Micro-Computed Tomography (CT) Using Iodinated Liposomes. *Invest. Radiol.* 2007, 42, 652-658.
[223] Samei E, Saunders RS, Badea CT, Ghaghada KB, Hedlund LW, Qi Y, Yuan H, Bentley RC, Mukundan S, Jr. Micro-CT imaging of breast tumors in rodents using a liposomal, nanoparticle contrast agent. *Int. J. Nanomed.* 2009, 4, 277-282.
[224] Skajaa T, Cormode DP, Falk E, Mulder WJM, Fisher EA, Fayad ZA. High-Density Lipoprotein-Based Contrast Agents for Multimodal Imaging of Atherosclerosis. *Arterioscler., Thromb., Vasc. Biol.* 2010, 30, 169-176.
[225] Hill ML, Corbin IR, Levitin RB, Cao W, Mainprize JG, Yaffe MJ, Zheng G. In vitro assessment of poly-iodinated triglyceride reconstituted low-density lipoprotein: initial steps toward CT molecular imaging. *Acad Radiol* 2010, 17, 1359-1365.
[226] Gazelle GS, Wolf GL, McIntire GL, Bacon ER, Na G, Halpern EF, Toner JL. Hepatic imaging with iodinated nanoparticles: a comparison with iohexol in rabbits. *Acad Radiol* 1995, 2, 700-704.
[227] McIntire GL, Bacon ER, Toner JL, Cornacoff JB, Losco PE, Illig KJ, Nikula KJ, Muggenburg BA, Ketai L. Pulmonary Delivery of Nanoparticles of Insoluble, Iodinated CT X-ray Contrast Agents to Lung Draining Lymph Nodes in Dogs. *J. Pharm. Sci.* 1998, 87, 1466-1470.
[228] Hyafil F, Cornily J-C, Feig JE, Gordon R, Vucic E, Amirbekian V, Fisher EA, Fuster V, Feldman LJ, et al. Noninvasive detection of macrophages using a nanoparticulate contrast agent for computed tomography. *Nat. Med. (N. Y., NY, U. S.)* 2007, 13, 636-641.
[229] deKrafft KE, Xie Z, Cao G, Tran S, Ma L, Zhou OZ, Lin W. Iodinated Nanoscale Coordination Polymers as Potential Contrast Agents for Computed Tomography. *Angew. Chem., Int. Ed.* 2009, 48, 9901-9904, S9901/9901-S9901/9918.
[230] Aviv H, Bartling S, Kieslling F, Margel S. Radiopaque iodinated copolymeric nanoparticles for X-ray imaging applications. *Biomaterials* 2009, 30, 5610-5616.
[231] Cai Q-Y, Kim SH, Choi KS, Kim SY, Byun SJ, Kim KW, Park SH, Juhng SK, Yoon K-H. Colloidal Gold Nanoparticles as a Blood-Pool Contrast Agent for X-ray Computed Tomography in Mice. *Invest. Radiol.* 2007, 42, 797-806.
[232] Xu C, Tung GA, Sun S. Size and Concentration Effect of Gold Nanoparticles on X-ray Attenuation As Measured on Computed Tomography. *Chem. Mater.* 2008, 20, 4167-4169.
[233] Margel S, Galperin A, Aviv H, Bartling S, Kiessling F. Radiopaque polymeric nanoparticles for X-ray medical imaging. Wiley-VCH Verlag GmbH & Co. KGaA; 2011. p. 343-364.

[234] Oh KS, Lee S, Na JH, Kim J-Y, Kim D-E, Kim K, Kwon IC, Yuk SH, Jeong SY. Blood-pool multifunctional nanoparticles formed by temperature-induced phase transition for cancer-targeting therapy and molecular imaging. *Int. J. Pharm. (Amsterdam, Neth.)* 2012, 437, 192-202.
[235] Park J-C, Yu M-K, An G-I, Park S-I, Oh J-M, Kim H-J, Kim J-H, Wang E-K, Hong I-H, et al. Facile Preparation of a Hybrid Nanoprobe for Triple-Modality Optical/PET/MR Imaging. *Small* 2010, 6, 2863-2868.
[236] Jackson PA, Rahman WNWA, Wong CJ, Ackerly T, Geso M. Potential dependent superiority of gold nanoparticles in comparison to iodinated contrast agents. *European Journal of Radiology* 2010, 75, 104-109.
[237] Peng C, Li K, Cao X, Xiao T, Hou W, Zheng L, Guo R, Shen M, Zhang G, et al. Facile formation of dendrimer-stabilized gold nanoparticles modified with diatrizoic acid for enhanced computed tomography imaging applications. *Nanoscale* 2012, 4, 6768-6778.
[238] Popovtzer R, Agrawal A, Kotov NA, Popovtzer A, Balter J, Carey TE, Kopelman R. Targeted Gold Nanoparticles Enable Molecular CT Imaging of Cancer. *Nano Lett.* 2008, 8, 4593-4596.
[239] Kim D, Park S, Lee JH, Jeong YY, Jon S. Antibiofouling Polymer-Coated Gold Nanoparticles as a Contrast Agent for in Vivo X-ray Computed Tomography Imaging. *J. Am. Chem. Soc.* 2007, 129, 7661-7665.
[240] Sun I-C, Eun D-K, Na JH, Lee S, Kim I-J, Youn I-C, Ko C-Y, Kim H-S, Lim D, et al. Heparin-Coated Gold Nanoparticles for Liver-Specific CT Imaging. *Chem.--Eur. J.* 2009, 15, 13341-13347, S13341/13341-S13341/13345.
[241] Park Y-S, Kasuya A, Dmytruk A, Yasuto N, Takeda M, Ohuchi N, Sato Y, Tohji K, Uo M, et al. Concentrated colloids of silica-encapsulated gold nanoparticles: colloidal stability, cytotoxicity, and X-ray absorption. *J. Nanosci. Nanotechnol.* 2007, 7, 2690-2695.
[242] Park Y-S, Liz-Marzan LM, Kasuya A, Kobayashi Y, Nagao D, Konno M, Mamykin S, Dmytruk A, Takeda M, et al. X-ray absorption of gold nanoparticles with thin silica shell. *J. Nanosci. Nanotechnol.* 2006, 6, 3503-3506.
[243] Guo R, Wang H, Peng C, Shen M, Zheng L, Zhang G, Shi X. Enhanced X-ray attenuation property of dendrimer-entrapped gold nanoparticles complexed with diatrizoic acid. *J. Mater. Chem.* 2011, 21, 5120-5127.
[244] Guo R, Wang H, Peng C, Shen M, Pan M, Cao X, Zhang G, Shi X. X-ray Attenuation Property of Dendrimer-Entrapped Gold Nanoparticles. *J. Phys. Chem. C* 2010, 114, 50-56.
[245] Beija M, Li Y, Duong HT, Laurent S, Vander EL, Muller RN, Lowe AB, Davis TP, Boyer C. Polymer-gold nanohybrids with potential use in bimodal MRI/CT: enhancing the relaxometric properties of Gd(iii) complexes. *J. Mater. Chem.* 2012, 22, 21382-21386.
[246] Luo T, Huang P, Gao G, Shen G, Fu S, Cui D, Zhou C, Ren Q. Mesoporous silica-coated gold nanorods with embedded indocyanine green for dual mode X-ray CT and NIR fluorescence imaging. *Opt. Express* 2011, 19, 17030-17039.
[247] Xiao M, Nyagilo J, Arora V, Kulkarni P, Xu D, Sun X, Dave DP. Gold nanotags for combined multi-colored Raman spectroscopy and X-ray computed tomography. *Nanotechnology* 2010, 21, 035101/035101-035101/035108.
[248] Nyagilo J, Xiao M, Sun X-K, Dave DP. Gold nanoprobes for multi-modality tumor imaging. *Proc. SPIE* 2010, 7576, 75760X/75761-75760X/75764.
[249] Hossain M, Su M. Nanoparticle Location and Material-Dependent Dose Enhancement in X-ray Radiation Therapy. *J. Phys. Chem. C* 2012, 116, 23047-23052.
[250] Kannan R, Zambre A, Chanda N, Kulkarni R, Shukla R, Katti K, Upendran A, Cutler C, Boote E, et al. Functionalized radioactive gold nanoparticles in tumor therapy. *Wiley Interdiscip. Rev.: Nanomed. Nanobiotechnol.* 2012, 4, 42-51.

[251] Rahman WN, Wong CJ, Ackerly T, Yagi N, Geso M. Polymer gels impregnated with gold nanoparticles implemented for measurements of radiation dose enhancement in synchrotron and conventional radiotherapy type beams. *Australas Phys Eng Sci Med* 2012, 35, 301-309.
[252] Jain S, Hirst DG, O'Sullivan JM. Gold nanoparticles as novel agents for cancer therapy. *Br J Radiol* 2012, 85, 101-113.
[253] Rabin O, Manuel PJ, Grimm J, Wojtkiewicz G, Weissleder R. An X-ray computed tomography imaging agent based on long-circulating bismuth sulphide nanoparticles. *Nat. Mater.* 2006, 5, 118-122.
[254] Kinsella JM, Jimenez RE, Karmali PP, Rush AM, Kotamraju VR, Gianneschi NC, Ruoslahti E, Stupack D, Sailor MJ. X-Ray Computed Tomography Imaging of Breast Cancer by using Targeted Peptide-Labeled Bismuth Sulfide Nanoparticles. *Angew. Chem., Int. Ed.* 2011, 50, 12308-12311, S12308/12301-S12308/12315.
[255] Mongan J, Rathnayake S, Fu Y, Wang R, Jones EF, Gao D-W, Yeh BM. In Vivo Differentiation of Complementary Contrast Media at Dual-Energy CT. *Radiology* 2012, 265, 267-272.
[256] Lee N, Cho HR, Oh MH, Lee SH, Kim K, Kim BH, Shin K, Ahn T-Y, Choi JW, et al. Multifunctional Fe3O4/TaOx Core/Shell Nanoparticles for Simultaneous Magnetic Resonance Imaging and X-ray Computed Tomography. *Journal of the American Chemical Society* 2012, 134, 10309-10312.
[257] Ajeesh M, Francis BF, Annie J, Varma PRH. Nano iron oxide-hydroxyapatite composite ceramics with enhanced radiopacity. *J. Mater. Sci.: Mater. Med.* 2010, 21, 1427-1434.
[258] Mahmoudi M, Serpooshan V, Laurent S. Engineered nanoparticles for biomolecular imaging. *Nanoscale* 2011, 3, 3007-3026.
[259] Cai H, Li K, Shen M, Wen S, Luo Y, Peng C, Zhang G, Shi X. Facile assembly of Fe3O4@Au nanocomposite particles for dual mode magnetic resonance and computed tomography imaging applications. *J. Mater. Chem.* 2012, 22, 15110-15120.
[260] Torres AS, Bonitatibus PJ, Jr., Colborn RE, Goddard GD, FitzGerald PF, Lee BD, Marino ME. Biological Performance of a Size-Fractionated Core-Shell Tantalum Oxide Nanoparticle X-Ray Contrast Agent. *Invest. Radiol.* 2012, 47, 578-587.
[261] Xia A, Chen M, Gao Y, Wu D, Feng W, Li F. Gd3+ complex-modified NaLuF4-based upconversion nanophosphors for trimodality imaging of NIR-to-NIR upconversion luminescence, X-Ray computed tomography and magnetic resonance. *Biomaterials* 2012, 33, 5394-5405.
[262] Cheung ENM, Alvares RDA, Oakden W, Chaudhary R, Hill ML, Pichaandi J, Mo GCH, Yip C, MacDonald PM, et al. Polymer-Stabilized Lanthanide Fluoride Nanoparticle Aggregates as Contrast Agents for Magnetic Resonance Imaging and Computed Tomography. *Chem. Mater.* 2010, 22, 4728-4739.
[263] Xing H, Bu W, Ren Q, Zheng X, Li M, Zhang S, Qu H, Wang Z, Hua Y, et al. A NaYbF4: Tm3+ nanoprobe for CT and NIR-to-NIR fluorescent bimodal imaging. *Biomaterials* 2012, 33, 5384-5393.
[264] Zhang G, Liu Y, Yuan Q, Zong C, Liu J, Lu L. Dual modal in vivo imaging using upconversion luminescence and enhanced computed tomography properties. *Nanoscale* 2011, 3, 4365-4371.
[265] Liu Y, Ai K, Liu J, Yuan Q, He Y, Lu L. A High-Performance Ytterbium-Based Nanoparticulate Contrast Agent for In Vivo X-Ray Computed Tomography Imaging. *Angew. Chem., Int. Ed.* 2012, 51, 1437-1442, S1437/1431-S1437/1415.

[266] Pan D, Schirra CO, Senpan A, Schmieder AH, Stacy AJ, Roessl E, Thran A, Wickline SA, Proska R, et al. An Early Investigation of Ytterbium Nanocolloids for Selective and Quantitative "Multicolor" Spectral CT Imaging. *ACS Nano* 2012, 6, 3364-3370.
[267] Dayton PA, Rychak JJ. Molecular ultrasound imaging using microbubble contrast agents. *Front. Biosci.* 2007, 12, 5124-5142.
[268] Gessner R, Dayton PA. Advances in molecular imaging with ultrasound. *Mol Imaging* 2010, 9, 117-127.
[269] Choyke PL. Science to practice: angiogenic marker expression during tumor growth--can targeted US microbubbles help monitor molecular changes in the microvasculature? *Radiology* 2011, 258, 655-656.
[270] Zheng Y, Zhang Y, Ao M, Zhang P, Zhang H, Li P, Qing L, Wang Z, Ran H. Hematoporphyrin encapsulated PLGA microbubble for contrast enhanced ultrasound imaging and sonodynamic therapy. *J. Microencapsulation* 2012, 29, 437-444.
[271] Prajapati JV, Agrawal YK. Synthesis, characterization and application of microbubbles: a review. *Int. J. Pharm. Sci. Res.* 2012, 3, 1532-1543.
[272] Anderson DR, Duryee MJ, Garvin RP, Boska MD, Thiele GM, Klassen LW. A method for the making and utility of gadolinium-labeled albumin microbubbles. *Magn. Reson. Imaging* 2012, 30, 96-103.
[273] Mukdadi OM, Kim H-B, Hertzberg J, Shandas R. Numerical modeling of microbubble backscatter to optimize ultrasound particle image velocimetry imaging: initial studies. *Ultrasonics* 2004, 42, 1111-1121.
[274] Alkan-Onyuksel H, Demos SM, Lanza GM, Vonesh MJ, Klegerman ME, Kane BJ, Kuszak J, McPherson DD. Development of inherently echogenic liposomes as an ultrasonic contrast agent. *J Pharm Sci* 1996, 85, 486-490.
[275] Tiukinhoy-Laing SD, Buchanan K, Parikh D, Huang S, MacDonald RC, McPherson DD, Klegerman ME. Fibrin targeting of tissue plasminogen activator-loaded echogenic liposomes. *Journal of drug targeting* 2007, 15, 109-114.
[276] Klegerman ME, Zou Y, McPherson DD. Fibrin targeting of echogenic liposomes with inactivated tissue plasminogen activator. *Journal of liposome research* 2008, 18, 95-112.
[277] Marsh JN, Partlow KC, Abendschein DR, Scott MJ, Lanza GM, Wickline SA. Molecular imaging with targeted perfluorocarbon nanoparticles: quantification of the concentration dependence of contrast enhancement for binding to sparse cellular epitopes. *Ultrasound in medicine & biology* 2007, 33, 950-958.
[278] Rapoport N. Phase-shift, stimuli-responsive perfluorocarbon nanodroplets for drug delivery to cancer. *Wiley Interdiscip. Rev.: Nanomed. Nanobiotechnol.* 2012, 4, 492-510.
[279] Rapoport N, Nam K-H. Droplet-to-bubble transition in phase-shift nanoemulsions for tumor chemotherapy. *Int. J. Transp. Phenom.* 2011, 12, 51-62.
[280] Sheeran PS, Luois SH, Mullin LB, Matsunaga TO, Dayton PA. Design of ultrasonically-activatable nanoparticles using low boiling point perfluorocarbons. *Biomaterials* 2012, 33, 3262-3269.
[281] Xu RX. Multifunctional microbubbles and nanobubbles for photoacoustic imaging. *Contrast Media Mol. Imaging* 2011, 6, 401-411.
[282] Hwang T-L, Lin Y-K, Chi C-H, Huang T-H, Fang J-Y. Development and evaluation of perfluorocarbon nanobubbles for apomorphine delivery. *J. Pharm. Sci.* 2009, 98, 3735-3747.
[283] Cavalli R, Bisazza A, Giustetto P, Civra A, Lembo D, Trotta G, Guiot C, Trotta M. Preparation and characterization of dextran nanobubbles for oxygen delivery. *Int. J. Pharm.* 2009, 381, 160-165.
[284] Cavalli R, Bisazza A, Rolfo A, Balbis S, Madonnaripa D, Caniggia I, Guiot C. Ultrasound-mediated oxygen delivery from chitosan nanobubbles. *Int. J. Pharm.* 2009, 378, 215-217.

[285] Lee C-H, Lin C-AJ, Rajendram R, Chang WH. Use of Microbubbles and Nanobubbles for Diagnostic Vascular Molecular Imaging and Therapeutic Applications. Science Publishers, Inc.; 2012. p. 303-323.
[286] Lapotko D. Plasmonic nanobubbles as tunable cellular probes for cancer theranostics. *Cancers* 2011, 3, 802-840.
[287] Watanabe Y, Horie S, Funaki Y, Kikuchi Y, Yamazaki H, Ishii K, Mori S, Vassaux G, Kodama T. Delivery of Na/I symporter gene into skeletal muscle using nanobubbles and ultrasound: visualization of gene expression by PET. *J. Nucl. Med.* 2010, 51, 951-958.
[288] Horie S, Watanabe Y, Ono M, Mori S, Kodama T. Evaluation of antitumor effects following tumor necrosis factor-α gene delivery using nanobubbles and ultrasound. *Cancer Sci.* 2011, 102, 2082-2089.
[289] Akif TM. Transcranial Doppler ultrasound in neurovascular diseases: diagnostic and therapeutic aspects. *J Neurochem* 2012, 123 Suppl 2, 39-51.
[290] Seo M, Gorelikov I, Williams R, Matsuura N. Microfluidic Assembly of Monodisperse, Nanoparticle-Incorporated Perfluorocarbon Microbubbles for Medical Imaging and Therapy. *Langmuir* 2010, 26, 13855-13860.
[291] Chonpathompikunlert P, Fan C-H, Ozaki Y, Yoshitomi T, Yeh C-K, Nagasaki Y. Redox nanoparticle treatment protects against neurological deficit in focused ultrasound-induced intracerebral hemorrhage. *Nanomedicine (London, U. K.)* 2012, 7, 1029-1043.
[292] Tachibana K, Feril LB, Ikeda-Dantsuji Y. Sonodynamic therapy. *Ultrasonics* 2008, 48, 253-259.
[293] Xu B, Lu R, Dou H, Tao K, Sun K, Qiu Y, Ding J, Zhang D, Li J, et al. Exploring the structure-property relationships of ultrasonic/MRI dual imaging magnetite/PLA microbubbles: magnetite@Cavity versus magnetite@Shell systems. *Colloid Polym. Sci.* 2012, 290, 1617-1626.
[294] Owen J, Pankhurst Q, Stride E. Magnetic targeting and ultrasound mediated drug delivery: Benefits, limitations and combination. *Int. J. Hyperthermia* 2012, 28, 362-373.
[295] Mannell H, Pircher J, Fochler F, Stampnik Y, Raethel T, Gleich B, Plank C, Mykhaylyk O, Dahmani C, et al. Site directed vascular gene delivery in vivo by ultrasonic destruction of magnetic nanoparticle coated microbubbles. *Nanomedicine (New York, NY, U. S.)* 2012, 8, 1309-1318.
[296] Mannell H, Pircher J, Raethel T, Schilberg K, Zimmermann K, Pfeifer A, Mykhaylyk O, Gleich B, Pohl U, et al. Targeted Endothelial Gene Delivery by Ultrasonic Destruction of Magnetic Microbubbles Carrying Lentiviral Vectors. *Pharm. Res.* 2012, 29, 1282-1294.
[297] Lin C-Y, Li J-R, Tseng H-C, Wu M-F, Lin W-L. Enhancement of focused ultrasound with microbubbles on the treatments of anticancer nanodrug in mouse tumors. *Nanomedicine (New York, NY, U. S.)* 2012, 8, 900-907.
[298] He W, Yang F, Wu Y, Wen S, Chen P, Zhang Y, Gu N. Microbubbles with surface coated by superparamagnetic iron oxide nanoparticles. *Mater. Lett.* 2012, 68, 64-67.
[299] Cai X, Yang F, Gu N. Applications of magnetic microbubbles for theranostics. *Theranostics* 2012, 2, 103-112.
[300] Wang X, Chen H, Zheng Y, Ma M, Chen Y, Zhang K, Zeng D, Shi J. Au-nanoparticle coated mesoporous silica nanocapsule-based multifunctional platform for ultrasound mediated imaging, cytoclasis and tumor ablation. *Biomaterials* 2012, http://dx.doi.org/10.1016/j.biomaterials.2012.11.044,.
[301] Yao J, Wang LV. Photoacoustic tomography: fundamentals, advances and prospects. *Contrast Media Mol. Imaging* 2011, 6, 332-345.
[302] Xu M, Wang LV. Photoacoustic imaging in biomedicine. *Review of Scientific Instruments* 2006, 77, 041101-041122.

[303] Wang LV. Multiscale photoacoustic microscopy and computed tomography. *Nat. Photonics* 2009, 3, 503-509.
[304] Yang X, Stein EW, Ashkenazi S, Wang LV. Nanoparticles for photoacoustic imaging. *Wiley Interdiscip. Rev.: Nanomed. Nanobiotechnol.* 2009, 1, 360-368.
[305] Yang X, Skrabalak SE, Li Z-Y, Xia Y, Wang LV. Photoacoustic Tomography of a Rat Cerebral Cortex in vivo with Au Nanocages as an Optical Contrast Agent. *Nano Lett.* 2007, 7, 3798-3802.
[306] Wang Y, Xie X, Wang X, Ku G, Gill KL, O'Neal DP, Stoica G, Wang LV. Photoacoustic Tomography of a Nanoshell Contrast Agent in the in Vivo Rat Brain. *Nano Lett.* 2004, 4, 1689-1692.
[307] Wang X, Pang Y, Ku G, Xie X, Stoica G, Wang LV. Noninvasive laser-induced photoacoustic tomography for structural and functional in vivo imaging of the brain. *Nat. Biotechnol.* 2003, 21, 803-806.
[308] Wells PNT, Liang H-D, Young TP. Ultrasonic imaging technologies in perspective. *J Med Eng Technol* 2011, 35, 289-299.
[309] Wang L, Wu H. Biomedical optics: Principles and imaging. *Wiley-In* 2007.
[310] Kruger RA, Reinecke DR, Kruger GA. Thermoacoustic computed tomography--technical considerations. *Med Phys* 1999, 26, 1832-1837.
[311] Qin H, Xu D, Yang S. Dextran-coated Fe3O4 magnetic nanoparticles as a contrast agent in thermoacoustic tomography for hepatocellular carcinoma detection. *J. Phys.: Conf. Ser.* 2011, 277, 012028/012021-012028/012027, 012010.011088/011742-016596/012277/012021/012028.
[312] Meissner KE, Majithiaa R, Brown RA, Wang LV, Maffeis TGG. Microwaves and nanoparticles: from synthesis to imaging. *Proc. SPIE* 2011, 7909, 79091E/79091-79091E/79096.
[313] Nie L, Ou Z, Yang S, Xing D. Thermoacoustic molecular tomography with magnetic nanoparticle contrast agents for targeted tumor detection. *Med. Phys.* 2010, 37, 4193-4200.
[314] Zhou T, Wu B, Xing D. Bio-modified Fe3O4 core/Au shell nanoparticles for targeting and multimodal imaging of cancer cells. *J. Mater. Chem.* 2012, 22, 470-477.
[315] Nam SY, Ricles LM, Sokolov K, Suggs LJ, Emelianov SY. Ultrasound and photoacoustic imaging to monitor mesenchymal stem cells labeled with gold nanoparticles. *Proc. SPIE* 2011, 7899, 78991Z/78991-78991Z/78997.
[316] Sharma R, Sharma A. Gold nanoparticles and emerging applications in imaging. CRC Press; 2010. p. 73-76.
[317] Kim C, Cho EC, Chen J, Song KH, Au L, Favazza CP, Zhang Q, Cobley CM, Xia Y, et al. Molecular photoacoustic imaging using gold nanoparticles as a contrast agent. *Proc. SPIE* 2010, 7564, 75641V/75641-75641V/75645.
[318] Mallidi S, Larson T, Tam J, Joshi PP, Karpiouk A, Sokolov K, Emelianov S. Multiwavelength Photoacoustic Imaging and Plasmon Resonance Coupling of Gold Nanoparticles for Selective Detection of Cancer. *Nano Lett.* 2009, 9, 2825-2831.
[319] Zhang Q, Iwakuma N, Sharma P, Moudgil BM, Wu C, McNeill J, Jiang H, Grobmyer SR. Gold nanoparticles as a contrast agent for in vivo tumor imaging with photoacoustic tomography. *Nanotechnology* 2009, 20, 395102.
[320] Sharma P, Brown SC, Bengtsson N, Zhang Q, Walter GA, Grobmyer SR, Santra S, Jiang H, Scott EW, et al. Gold-Speckled Multimodal Nanoparticles for Noninvasive Bioimaging. *Chem. Mater.* 2008, 20, 6087-6094.
[321] Manohar S, Ungureanu C, Van LTG. Gold nanorods as molecular contrast agents in photoacoustic imaging: the promises and the caveats. *Contrast Media Mol. Imaging* 2011, 6, 389-400.

[322] Ito T, Kusaka E, Isobe Y, Nishimoto S-i. Synthesis of gold nanoparticles coated with pH-responsive polymers and evaluation of the cellular uptake. *MRS Online Proc. Libr.* 2011, 1416, No pp. given.
[323] Chen Y-S, Frey W, Kim S, Homan K, Kruizinga P, Sokolov K, Emelianov S. Enhanced thermal stability of silica-coated gold nanorods for photoacoustic imaging and image-guided therapy. *Opt. Express* 2010, 18, 8867-8877.
[324] Pan D, Pramanik M, Senpan A, Wickline SA, Wang LV, Lanza GM. A facile synthesis of novel self-assembled gold nanorods designed for near-infrared imaging. *J. Nanosci. Nanotechnol.* 2010, 10, 8118-8123.
[325] Chen L-C, Wei C-W, Souris JS, Cheng S-H, Chen C-T, Yang C-S, Li P-C, Lo L-W. Enhanced photoacoustic stability of gold nanorods by silica matrix confinement. *J. Biomed. Opt.* 2010, 15, 016010/016011-016010/016016.
[326] Cho EC, Kim C, Zhou F, Cobley CM, Song KH, Chen J, Li Z-Y, Wang LV, Xia Y. Measuring the Optical Absorption Cross Sections of Au-Ag Nanocages and Au Nanorods by Photoacoustic Imaging. *J. Phys. Chem. C* 2009, 113, 9023-9028.
[327] Li P-C, Wang C-RC, Shieh D-B, Wei C-W, Liao C-K, Poe C, Jhan S, Ding A-A, Wu Y-N. In vivo photoacoustic molecular imaging with simultaneous multiple selective targeting using antibody-conjugated gold nanorods. *Opt. Express* 2008, 16, 18605-18615.
[328] Kim C, Song H-M, Cai X, Yao J, Wei A, Wang LV. In vivo photoacoustic mapping of lymphatic systems with plasmon-resonant nanostars. *J. Mater. Chem.* 2011, 21, 2841-2844.
[329] Au L, Cobley CM, Chen J, Xia Y. Gold nanocages: A multifunctional platform for molecular optical imaging and photothermal treatment. John Wiley & Sons, Inc.; 2011. p. 615-638.
[330] Xia Y, Li W, Cobley CM, Chen J, Xia X, Zhang Q, Yang M, Cho EC, Brown PK. Gold Nanocages: From Synthesis to Theranostic Applications. *Acc. Chem. Res.* 2011, 44, 914-924.
[331] Li W, Brown PK, Wang LV, Xia Y. Gold nanocages as contrast agents for photoacoustic imaging. *Contrast Media Mol. Imaging* 2011, 6, 370-377.
[332] Cai X, Li W, Kim C-H, Yuan Y, Wang LV, Xia Y. In Vivo Quantitative Evaluation of the Transport Kinetics of Gold Nanocages in a Lymphatic System by Noninvasive Photoacoustic Tomography. *ACS Nano* 2011, 5, 9658-9667.
[333] Song KH, Kim C, Cobley CM, Xia Y, Wang LV. Near-Infrared Gold Nanocages as a New Class of Tracers for Photoacoustic Sentinel Lymph Node Mapping on a Rat Model. *Nano Lett.* 2009, 9, 183-188.
[334] Kim C, Cho EC, Chen J, Song KH, Au L, Favazza C, Zhang Q, Cobley CM, Gao F, et al. In Vivo Molecular Photoacoustic Tomography of Melanomas Targeted by Bioconjugated Gold Nanocages. *ACS Nano* 2010, 4, 4559-4564.
[335] Lu W, Huang Q, Ku G, Wen X, Zhou M, Guzatov D, Brecht P, Su R, Oraevsky A, et al. Photoacoustic imaging of living mouse brain vasculature using hollow gold nanospheres. *Biomaterials* 2010, 31, 2617-2626.
[336] Li M-L, Wang JC, Schwartz JA, Gill-Sharp KL, Stoica G, Wang LV. In-vivo photoacoustic microscopy of nanoshell extravasation from solid tumor vasculature. *Journal of Biomedical Optics* 2009, 14, 010507-010507.
[337] Liu H, Liu T, Wu X, Li L, Tan L, Chen D, Tang F. Targeting Gold Nanoshells on Silica Nanorattles: a Drug Cocktail to Fight Breast Tumors via a Single Irradiation with Near-Infrared Laser Light. *Adv. Mater. (Weinheim, Ger.)* 2012, 24, 755-761.
[338] Pan D, Pramanik M, Wickline SA, Wang LV, Lanza GM. Recent advances in colloidal gold nanobeacons for molecular photoacoustic imaging. *Contrast Media Mol. Imaging* 2011, 6, 378-388.

[339] Pan D, Pramanik M, Senpan A, Ghosh S, Wickline SA, Wang LV, Lanza GM. Near infrared photoacoustic detection of sentinel lymph nodes with gold nanobeacons. *Biomaterials* 2010, 31, 4088-4093.
[340] Kalele S, Gosavi SW, Urban J, Kulkarni SK. Nanoshell particles: synthesis, properties and applications. *Curr. Sci.* 2006, 91, 1038-1052.
[341] Huang X, Neretina S, El-Sayed MA. Gold Nanorods: From Synthesis and Properties to Biological and Biomedical Applications. *Adv. Mater. (Weinheim, Ger.)* 2009, 21, 4880-4910.
[342] Ji X, Shao R, Elliott AM, Stafford RJ, Esparza-Coss E, Bankson JA, Liang G, Luo Z-P, Park K, et al. Bifunctional Gold Nanoshells with a Superparamagnetic Iron Oxide-Silica Core Suitable for Both MR Imaging and Photothermal Therapy. *J. Phys. Chem. C* 2007, 111, 6245-6251.
[343] Huang G, Yuan Y, Xing D. Antibiofouling polymer coated gold nanoparticles as a dual modal contrast agent for X-ray and photoacoustic imaging. *J. Phys.: Conf. Ser.* 2011, 277, 012012/012011-012012/012016, 012010.011088/011742-016596/012277/012011/012012.
[344] Chen Y-S, Frey W, Kim S, Kruizinga P, Homan K, Emelianov S. Silica-coated gold nanorods as photoacoustic signal nanoamplifiers. *Nano Lett.* 2011, 11, 348-354.
[345] Zhang JZ. Biomedical Applications of Shape-Controlled Plasmonic Nanostructures: A Case Study of Hollow Gold Nanospheres for Photothermal Ablation Therapy of Cancer. *J. Phys. Chem. Lett.* 2010, 1, 686-695.
[346] Choi J, Yang J, Jang E, Suh J-S, Huh Y-M, Lee K, Haam S. Gold nanostructures as photothermal therapy agent for cancer. *Anti-Cancer Agents Med. Chem.* 2011, 11, 953-964.
[347] Lu W, Melancon MP, Li C. Theranostic applications of gold core - shell structured nanoparticles. John Wiley & Sons, Inc.; 2011. p. 683-708.
[348] Hu M, Chen J, Li Z-Y, Au L, Hartland GV, Li X, Marquez M, Xia Y. Gold nanostructures: engineering their plasmonic properties for biomedical applications. *Chem. Soc. Rev.* 2006, 35, 1084-1094.
[349] Eghtedari M, Oraevsky A, Copland JA, Kotov NA, Conjusteau A, Motamedi M. High Sensitivity of In Vivo Detection of Gold Nanorods Using a Laser Optoacoustic Imaging System. *Nano Lett.* 2007, 7, 1914-1918.
[350] Song KH, Kim C, Maslov K, Wang LV. Noninvasive in vivo spectroscopic nanorod-contrast photoacoustic mapping of sentinel lymph nodes. *Eur J Radiol* 2009, 70, 227-231.
[351] Jokerst JV, Thangaraj M, Kempen PJ, Sinclair R, Gambhir SS. Photoacoustic Imaging of Mesenchymal Stem Cells in Living Mice via Silica-Coated Gold Nanorods. *ACS Nano* 2012, 6, 5920-5930.
[352] Alkilany AM, Murphy CJ. Toxicity and cellular uptake of gold nanoparticles: what we have learned so far? *J. Nanopart. Res.* 2010, 12, 2313-2333.
[353] Alkilany AM, Thompson LB, Boulos SP, Sisco PN, Murphy CJ. Gold nanorods: Their potential for photothermal therapeutics and drug delivery, tempered by the complexity of their biological interactions. *Adv. Drug Delivery Rev.* 2012, 64, 190-199.
[354] Thakor AS, Jokerst J, Zaveleta C, Massoud TF, Gambhir SS. Gold Nanoparticles: A Revival in Precious Metal Administration to Patients. *Nano Lett.* 2011, 11, 4029-4036.
[355] Murphy CJ, Gole AM, Stone JW, Sisco PN, Alkilany AM, Goldsmith EC, Baxter SC. Gold Nanoparticles in Biology: Beyond Toxicity to Cellular Imaging. *Acc. Chem. Res.* 2008, 41, 1721-1730.
[356] Cole JR, Mirin NA, Knight MW, Goodrich GP, Halas NJ. Photothermal Efficiencies of Nanoshells and Nanorods for Clinical Therapeutic Applications. *J. Phys. Chem. C* 2009, 113, 12090-12094.
[357] Foldvari M, Bagonluri M. Carbon nanotubes as functional excipients for nanomedicines: I. Pharmaceutical properties. *Nanomedicine (N. Y., NY, U. S.)* 2008, 4, 173-182.

[358] Foldvari M, Bagonluri M. Carbon nanotubes as functional excipients for nanomedicines: II. Drug delivery and biocompatibility issues. *Nanomedicine (N. Y., NY, U. S.)* 2008, 4, 183-200.
[359] Hong H, Gao T, Cai W. Molecular imaging with single-walled carbon nanotubes. *Nano Today* 2009, 4, 252-261.
[360] Depan D, Misra RDK. Hybrid nanoparticle architecture for cellular uptake and bioimaging: direct crystallization of a polymer immobilized with magnetic nanoparticles on carbon nanotubes. *Nanoscale* 2012, 4, 6325-6335.
[361] Khandare JJ, Jalota-Badhwar A, Satavalekar SD, Bhansali SG, Aher ND, Kharas F, Banerjee SS. PEG-conjugated highly dispersive multifunctional magnetic multi-walled carbon nanotubes for cellular imaging. *Nanoscale* 2012, 4, 837-844.
[362] Hu Z, Pantos GD, Kuganathan N, Arrowsmith RL, Jacobs RMJ, Kociok-Koehn G, O'Byrne J, Jurkschat K, Burgos P, et al. Interactions between Amino acid-Tagged Naphthalenediimide and Single Walled Carbon Nanotubes for the Design and Construction of New Bioimaging Probes. *Adv. Funct. Mater.* 2012, 22, 503-518.
[363] de la Zerda A, Bodapati S, Teed R, May SY, Tabakman SM, Liu Z, Khuri-Yakub BT, Chen X, Dai H, et al. Family of Enhanced Photoacoustic Imaging Agents for High-Sensitivity and Multiplexing Studies in Living Mice. *ACS Nano* 2012, 6, 4694-4701.
[364] Avti PK, Hu S, Favazza C, Mikos AG, Jansen JA, Shroyer KR, Wang LV, Sitharaman B. Detection, mapping, and quantification of single walled carbon nanotubes in histological specimens with photoacoustic microscopy. *PLoS One* 2012, 7, e35064.
[365] Cai X, Paratala BS, Hu S, Sitharaman B, Wang LV. Multiscale Photoacoustic Microscopy of Single-Walled Carbon Nanotube-Incorporated Tissue Engineering Scaffolds. *Tissue Eng., Part C* 2012, 18, 310-317.
[366] Wang C, Ma X, Ye S, Cheng L, Yang K, Guo L, Li C, Li Y, Liu Z. Protamine Functionalized Single-Walled Carbon Nanotubes for Stem Cell Labeling and In Vivo Raman/Magnetic Resonance/Photoacoustic Triple-Modal Imaging. *Adv. Funct. Mater.* 2012, 22, 2363-2375.
[367] Zhou F, Wu S, Yuan Y, Chen WR, Xing D. Mitochondria-Targeting Photoacoustic Therapy Using Single-Walled Carbon Nanotubes. *Small* 2012, 8, 1543-1550.
[368] Zanganeh S, Aguirre A, Biswal NC, Pavlik C, Smith MB, Alqasemi U, Li H, Zhu Q. Hypoxia targeted carbon nanotubes as a sensitive contrast agent for photoacoustic imaging of tumors. *Proc. SPIE* 2011, 7899, 78991S/78991-78991S/78996.
[369] Cai X, Hu S, Paratala B, Sitharaman B, Wang LV. Dual-mode photoacoustic microscopy of carbon nanotube incorporated scaffolds in blood and biological tissues. *Proc. SPIE* 2011, 7899, 78992I/78991-78992I/78996.
[370] Khodakovskaya MV, de SK, Nedosekin DA, Dervishi E, Biris AS, Shashkov EV, Galanzha EI, Zharov VP. Complex genetic, photothermal, and photoacoustic analysis of nanoparticle-plant interactions. *Proc. Natl. Acad. Sci. U. S. A.* 2011, 108, 1028-1033, S1028/1021-S1028/1011.
[371] de la Zerda A, Liu Z, Bodapati S, Teed R, Vaithilingam S, Khuri-Yakub BT, Chen X, Dai H, Gambhir SS. Ultrahigh Sensitivity Carbon Nanotube Agents for Photoacoustic Molecular Imaging in Living Mice. *Nano Lett.* 2010, 10, 2168-2172.
[372] Lee IYS, Hayama Y, Suzuki H, Osawa T. Photoacoustic Sensitization and Laser-Induced Cavitation in Polymer Solutions by Carbon Nanotubes. *J. Phys. Chem. C* 2010, 114, 22392-22397.
[373] Pramanik M, Swierczewska M, Green D, Sitharaman B, Wang LV. Single-walled carbon nanotubes as a multimodal-thermoacoustic and photoacoustic-contrast agent. *J. Biomed. Opt.* 2009, 14, 034018/034011-034018/034018.

[374] O'Connell MJ, Bachilo SM, Huffman CB, Moore VC, Strano MS, Haroz EH, Rialon KL, Boul PJ, Noon WH, et al. Band gap fluorescence from individual single-walled carbon nanotubes. *Science* 2002, 297, 593-596.
[375] Berciaud S, Cognet L, Poulin P, Weisman RB, Lounis B. Absorption spectroscopy of individual single-walled carbon nanotubes. *Nano Lett* 2007, 7, 1203-1207.
[376] De La Zerda A, Zavaleta C, Keren S, Vaithilingam S, Bodapati S, Liu Z, Levi J, Smith BR, Ma T-J, et al. Carbon nanotubes as photoacoustic molecular imaging agents in living mice. *Nat. Nanotechnol.* 2008, 3, 557-562.
[377] Xiang L, Yuan Y, Xing D, Ou Z, Yang S, Zhou F. Photoacoustic molecular imaging with antibody-functionalized single-walled carbon nanotubes for early diagnosis of tumor. *J Biomed Opt* 2009, 14, 021008.
[378] Pramanik M, Song KH, Swierczewska M, Green D, Sitharaman B, Wang LV. In vivo carbon nanotube-enhanced non-invasive photoacoustic mapping of the sentinel lymph node. *Physics in Medicine and Biology* 2009, 54, 3291.
[379] de la Zerda A, Kim J-W, Galanzha EI, Gambhir SS, Zharov VP. Advanced contrast nanoagents for photoacoustic molecular imaging, cytometry, blood test and photothermal theranostics. *Contrast Media Mol. Imaging* 2011, 6, 346-369.
[380] Kim J-W, Galanzha EI, Shashkov EV, Moon H-M, Zharov VP. Golden carbon nanotubes as multimodal photoacoustic and photothermal high-contrast molecular agents. *Nat. Nanotechnol.* 2009, 4, 688-694.
[381] Algar WR, Prasuhn DE, Stewart MH, Jennings TL, Blanco-Canosa JB, Dawson PE, Medintz IL. The Controlled Display of Biomolecules on Nanoparticles: A Challenge Suited to Bioorthogonal Chemistry. *Bioconjugate Chemistry* 2011, 22, 825-858.
[382] Galanzha EI, Shashkov EV, Kelly T, Kim J-W, Yang L, Zharov VP. In vivo magnetic enrichment and multiplex photoacoustic detection of circulating tumor cells. *Nat. Nanotechnol.* 2009, 4, 855-860.
[383] Yang K, Hu L, Ma X, Ye S, Cheng L, Shi X, Li C, Li Y, Liu Z. Multimodal Imaging Guided Photothermal Therapy using Functionalized Graphene Nanosheets Anchored with Magnetic Nanoparticles. *Advanced Materials* 2012, 24, 1868-1872.
[384] Sharma P, Brown S, Walter G, Santra S, Moudgil B. Nanoparticles for bioimaging. *Adv. Colloid Interface Sci.* 2006, 123-126, 471-485.
[385] Akers WJ, Kim C, Berezin M, Guo K, Fuhrhop R, Lanza GM, Fischer GM, Daltrozzo E, Zumbusch A, et al. Noninvasive Photoacoustic and Fluorescence Sentinel Lymph Node Identification using Dye-Loaded Perfluorocarbon Nanoparticles. *ACS Nano* 2011, 5, 173-182.
[386] Kohl Y, Kaiser C, Bost W, Stracke F, Thielecke H, Wischke C, Lendlein A, Kratz K, Lemor R. Near-infrared dye-loaded PLGA nanoparticles prepared by spray drying for photoacoustic applications. *Int. J. Artif. Organs* 2011, 34, 249-254.
[387] Ray A, Wang X, Koo LY-E, Hah HJ, Kim G, Chen T, Orrienger D, Sagher O, Kopelman R. Photo-acoustic imaging of blue nanoparticle targeted brain tumor for intra-operative glioma delineation. *Proc. SPIE* 2011, 8089, 808906/808901-808906/808906.
[388] Chouikrat R, Seve A, Vanderesse R, Benachour H, Barberi-Heyob M, Richeter S, Raehm L, Durand JO, Verelst M, et al. Non polymeric nanoparticles for photodynamic therapy applications: recent developments. *Curr. Med. Chem.* 2012, 19, 781-792.
[389] Cheng S-H, Lo L-W. Inorganic nanoparticles for enhanced photodynamic cancer therapy. *Curr. Drug Discovery Technol.* 2011, 8, 269-276.
[390] Mazzaglia A. Photodynamic tumor therapy with cyclodextrin nanoassemblies. John Wiley & Sons, Inc.; 2011. p. 343-361,, 346 plates.
[391] Nann T. Nanoparticles in photodynamic therapy. *Nano Biomed. Eng.* 2011, 3, 137-143.

[392] Wang X, Ku G, Wegiel MA, Bornhop DJ, Stoica G, Wang LV. Noninvasive photoacoustic angiography of animal brains in vivo with near-infrared light and an optical contrast agent. *Opt Lett* 2004, 29, 730-732.
[393] Qu M, Kim S, Mehrmohammadi M, Mallidi S, Joshi P, Homan K, Chen Y-S, Emelianov S, Oraevsky AA, et al. Combined photoacoustic and magneto-motive ultrasound imaging. *Proc. SPIE* 2010, 7564, 756433/756431-756433/756437.
[394] Qu M, Mehrmohammadi M, Emelianov S. Detection of Nanoparticle Endocytosis Using Magneto-Photoacoustic Imaging. *Small* 2011, 7, 2858-2862.
[395] Alwi R, Telenkov S, Mandelis A, Leshuk T, Gu F, Oladepo S, MichAlian K. Silica-coated super paramagnetic iron oxide nanoparticles (SPION) as biocompatible contrast agent in biomedical photoacoustics. *Biomed. Opt. Express* 2012, 3, 2500-2509.
[396] Doiron AL, Homan KA, Emelianov S, Brannon-Peppas L. Poly(Lactic-co-Glycolic) Acid as a Carrier for Imaging Contrast Agents. *Pharm. Res.* 2009, 26, 674-682.
[397] Huynh E, Lovell JF, Helfield BL, Jeon M, Kim C, Goertz DE, Wilson BC, Zheng G. Porphyrin Shell Microbubbles with Intrinsic Ultrasound and Photoacoustic Properties. *Journal of the American Chemical Society* 2012, 134, 16464-16467.
[398] Oh SJ, Choi J, Maeng I, Park JY, Lee K, Huh Y-M, Suh J-S, Haam S, Son J-H. Molecular imaging with terahertz waves. *Opt. Express* 2011, 19, 4009-4016.
[399] Oh SJ, Kang J, Maeng I, Suh J-S, Huh Y-M, Haam S, Son J-H. Nanoparticle-enabled terahertz imaging for cancer diagnosis. *Opt. Express* 2009, 17, 3469-3475.
[400] Lee D-K, Kim H, Kim T, Cho B, Lee K, Son J-H. Characteristics of Gadolinium Oxide Nanoparticles as Contrast Agents for Terahertz Imaging. *J Infrared Milli Terahz Waves* 2011, 32, 506-512.
[401] Larue C, Khodja H, Herlin-Boime N, Brisset F, Flank AM, Fayard B, Chaillou S, Carriere M. Investigation of titanium dioxide nanoparticles toxicity and uptake by plants. *J. Phys.: Conf. Ser.* 2011, 304, 012057/012051-012057/012057.
[402] Homma-Takeda S, Nishimura Y, Watanabe Y, Yukawa M, Ueno S. Lobe-specific changes in zinc levels in the prostate of rats exposed to tributyltin chloride. *Int. J. PIXE* 2005, 15, 131-138.
[403] Morawski M, Reinert T, Meinecke C, Arendt T, Butz T. Antibody meets the microbeam - or how to find neurofibrillary tangles. *Nucl. Instrum. Methods Phys. Res., Sect. B* 2005, 231, 229-233.
[404] Harada S, Tamakawa Y, Ishii K, Tanaka A, Satoh T, Matsuyama S, Yamazaki H, Komori Y, Kamiya T, et al. The kinetics of Fe and Ca for the development of radiation-induced apoptosis by micro-PIXE imaging. *Nucl. Instrum. Methods Phys. Res., Sect. B* 2003, 210, 383-387.
[405] Homma-Takeda S, Nishimura Y, Watanabe Y, Imaseki H, Yukawa M. Elemental imaging of rat epididymis by micro-PIXE analysis. *Nucl. Instrum. Methods Phys. Res., Sect. B* 2003, 210, 368-372.
[406] Pinheiro T, Alves LC, Barreiros A, Araujo F, Bohic S, Simionovici A. Imaging and quantification of trace metals in thin biological specimens using microprobe techniques: Synchrotron induced X-ray fluorescence microprobe and nuclear microprobe. *J. Phys. IV* 2003, 104, 321-324.
[407] Yukawa M, Imaseki H. Imaging of elemental distribution in the small area of biological samples -micro-PIXE analysis. *Biomed. Res. Trace Elem.* 2003, 14, 11-16.
[408] Harada S, Tamakawa Y, Ishii K, Tanaka A, Satoh T, Matsuyama S, Yamazaki H, Kamiya T, Sakai T, et al. The kinetics of Fe and Ca for the development of radiation-induced apoptosis by micro-PIXE imaging. *Nucl. Instrum. Methods Phys. Res., Sect. B* 2002, 189, 437-442.

[409] Gontier E, Ynsa M-D, Bíró T, Hunyadi J, Kiss B, Gáspár K, Pinheiro T, Silva J-N, Filipe P, et al. Is there penetration of titania nanoparticles in sunscreens through skin? A comparative electron and ion microscopy study. *Nanotoxicology* 2008, 2, 218-231.
[410] Simon M, Barberet P, Moretto P, Bacqueville D, Mavon A, Seznec H. The skin barrier function: a micro-PIXE study. *X-Ray Spectrometry* 2009, 38, 132-137.
[411] Menzel F, Reinert T, Vogt J, Butz T. Investigations of percutaneous uptake of ultrafine TiO2 particles at the high energy ion nanoprobe LIPSION. *Nucl. Instrum. Methods Phys. Res., Sect. B* 2004, 219-220, 82-86.
[412] Sakai N, Matsui Y, Yamamoto S, Sera K, Fujimaki H, Uchiyama I. Biodistribution of ultrafine particles of titanium dioxide by intratracheal administration to mice. *J. UOEH* 2008, 30, 27-38.
[413] Abe S, Koyama C, Uo M, Akasaka T, Kuboki Y, Watari F. Time-dependence and visualization of TiO2 and Pt particle biodistribution in mice. *J. Nanosci. Nanotechnol.* 2009, 9, 4988-4991.
[414] Kim J-K, Seo S-J, Kim K-H, Kim T-J, Chung M-H, Kim K-R, Yang T-K. Therapeutic application of metallic nanoparticles combined with particle-induced X-ray emission effect. *Nanotechnology* 2010, 21, 425102/425101-425102/425110.
[415] Bradley DA, Farquharson MJ, Gundogdu O, Al-Ebraheem A, Che IE, Kaabar W, Bunk O, Pfeiffer F, Falkenberg G, et al. Applications of condensed matter understanding to medical tissues and disease progression: Elemental analysis and structural integrity of tissue scaffolds. *Radiat. Phys. Chem.* 2009, 79, 162-175.
[416] Jiang X-M, Wang L-M, Wang J, Chen C-Y. Gold Nanomaterials: Preparation, Chemical Modification, Biomedical Applications and Potential Risk Assessment. *Appl. Biochem. Biotechnol.* 2012, 166, 1533-1551.
[417] Szikszai Z, Kertesz Z, Bodnar E, Major I, Borbiro I, Kiss AZ, Hunyadi J. Nuclear microprobe investigation of the penetration of ultrafine zinc oxide into intact and tape-stripped human skin. *Nucl. Instrum. Methods Phys. Res., Sect. B* 2010, 268, 2160-2163.
[418] Lekki J, Stachura Z, Dabros W, Stachura J, Menzel F, Reinert T, Butz T, Pallon J, Gontier E, et al. On the follicular pathway of percutaneous uptake of nanoparticles: Ion microscopy and autoradiography studies. *Nucl. Instrum. Methods Phys. Res., Sect. B* 2007, 260, 174-177.
[419] Deves G, Isaure MP, Le LP, Bourguignon J, Ortega R. Fully quantitative imaging of chemical elements in Arabidopsis thaliana tissues using STIM, PIXE and RBS. *Nucl. Instrum. Methods Phys. Res., Sect. B* 2005, 231, 117-122.
[420] Kertesz Z, Szikszai Z, Gontier E, Moretto P, Surleve-Bazeille JE, Kiss B, Juhasz I, Hunyadi J, Kiss AZ. Nuclear microprobe study of TiO2-penetration in the epidermis of human skin xenografts. *Nucl. Instrum. Methods Phys. Res., Sect. B* 2005, 231, 280-285.
[421] Simon M, Barberet P, Delville M-H, Moretto P, Seznec H. Titanium dioxide nanoparticles induced intracellular calcium homeostasis modification in primary human keratinocytes. Towards an in vitro explanation of titanium dioxide nanoparticles toxicity. *Nanotoxicology* 2011, 5, 125-139.
[422] Barberet P, Vianna F, Karamitros M, Brun T, Gordillo N, Moretto P, Incerti S, Seznec H. Monte-Carlo dosimetry on a realistic cell monolayer geometry exposed to alpha particles. *Physics in Medicine and Biology* 2012, 57, 2189.
[423] Le Trequesser Q, Saez G, Deves G, Barberet P, Delville M, Seznec H. unpublished work.
[424] Sharma P, Singh A, Brown SC, Walter GA, Santra S, Grobmyer SR, Scott EW, Moudgil BM. The emergence of magnetic and fluorescent multimodal nanoparticles as contrast agents in bioimaging. CRC Press; 2009. p. 353-392.

[425] Cherry SR, Louie AY, Jacobs RE. The integration of positron emission tomography with magnetic resonance imaging. *Proc. IEEE* 2008, 96, 416-438.
[426] Catana C, Wu Y, Judenhofer MS, Qi J, Pichler BJ, Cherry SR. Simultaneous acquisition of multislice PET and MR images: initial results with a MR-compatible PET scanner. *J Nucl Med* 2006, 47, 1968-1976.
[427] Schlemmer HP, Pichler BJ, Schmand M, Burbar Z, Michel C, Ladebeck R, Jattke K, Townsend D, Nahmias C, et al. Simultaneous MR/PET imaging of the human brain: feasibility study. *Radiology* 2008, 248, 1028-1035.
[428] Abe M. Nanomedicine: molecular imaging for in vivo diagnostics. *MTA Dialog* 2009, 10, 994-997.
[429] Hwang JY, Park J, Kang BJ, Lubow DJ, Chu D, Farkas DL, Shung KK, Medina-Kauwe LK. Multimodality imaging in vivo for preclinical assessment of tumor-targeted doxorubicin nanoparticles. *PLoS One* 2012, 7, e34463.
[430] Kim J, Piao Y, Hyeon T. Multifunctional nanostructured materials for multimodal imaging, and simultaneous imaging and therapy. *Chem. Soc. Rev.* 2009, 38, 372-390.
[431] Louie A. Multimodality Imaging Probes: Design and Challenges. *Chem. Rev. (Washington, DC, U. S.)* 2010, 110, 3146-3195.
[432] Masotti A. Multifuntional nanoparticles: preparation and applications in biomedicine and in non-invasive bioimaging. *Recent Pat. Nanotechnol.* 2010, 4, 53-62.
[433] Masotti A. Multifunctional nanoparticles, nanocages and degradable polymers as a potential novel generation of non-invasive molecular and cellular imaging systems. *Recent Pat. Nanotechnol.* 2011, 5, 163-177.
[434] McCarthy JR, Weissleder R. Multimodal imaging and therapy with magnethofluorescent nanoparticles. John Wiley & Sons, Inc.; 2011. p. 593-613.
[435] Wang L, O'Donoghue MB, Tan W. Nanoparticles for multiplex diagnostics and imaging. *Nanomedicine (London, U. K.)* 2006, 1, 413-426.
[436] Xing H, Bu W, Zhang S, Zheng X, Li M, Chen F, He Q, Zhou L, Peng W, et al. Multifunctional nanoprobes for upconversion fluorescence, MR and CT trimodal imaging. *Biomaterials* 2012, 33, 1079-1089.
[437] Yong K-T, Roy I, Swihart MT, Prasad PN. Multifunctional nanoparticles as biocompatible targeted probes for human cancer diagnosis and therapy. *J. Mater. Chem.* 2009, 19, 4655-4672.
[438] Zrazhevskiy P, Sena M, Gao X. Designing multifunctional quantum dots for bioimaging, detection, and drug delivery. *Chem. Soc. Rev.* 2010, 39, 4326-4354.
[439] Jennings LE, Long NJ. 'Two is better than one'--probes for dual-modality molecular imaging. *Chemical communications (Cambridge, England)* 2009, 3511-3524.
[440] Chen P-J, Hu S-H, Hsiao C-S, Chen Y-Y, Liu D-M, Chen S-Y. Multifunctional magnetically removable nanogated lids of Fe3O4-capped mesoporous silica nanoparticles for intracellular controlled release and MR imaging. *J. Mater. Chem.* 2011, 21, 2535-2543.
[441] Gindy ME, Prud'homme RK. Multifunctional nanoparticles for imaging, delivery and targeting in cancer therapy. *Expert Opin. Drug Delivery* 2009, 6, 865-878.
[442] Sharma R, Sharma A, Chen CJ. State of art on bioimaging by nanoparticles in hyperthermia and thermometry: visualization of tissue protein targeting. *Open Nanomed. J.* 2010, 3, 10-23.
[443] Cherry SR. Fundamentals of positron emission tomography and applications in preclinical drug development. *J. Clin. Pharmacol.* 2001, 41, 482-491.
[444] Cherry SR. The 2006 henry N. wagner lecture: of mice and men (and positrons)-advances in PET imaging technology. *J. Nucl. Med.* 2006, 47, 1735-1745.

[445] Kircher MF, de la Zerda A, Jokerst JV, Zavaleta CL, Kempen PJ, Mittra E, Pitter K, Huang R, Campos C, et al. A brain tumor molecular imaging strategy using a new triple-modality MRI-photoacoustic-Raman nanoparticle. *Nat Med* 2012, 18, 829-834.
[446] Kim D, Yu MK, Lee TS, Park JJ, Jeong YY, Jon S. Amphiphilic polymer-coated hybrid nanoparticles as CT/MRI dual contrast agents. *Nanotechnology* 2011, 22, 155101/155101-155101/155107, S155101/155101-S155101/155112.
[447] Janczewski D, Zhang Y, Das GK, Yi DK, Padmanabhan P, Bhakoo KK, Tan TTY, Selvan ST. Bimodal magnetic-fluorescent probes for bioimaging. *Microsc. Res. Tech.* 2011, 74, 563-576.
[448] Chen F, Huang P, Zhu Y-J, Wu J, Zhang C-L, Cui D-X. The photoluminescence, drug delivery and imaging properties of multifunctional Eu3+/Gd3+ dual-doped hydroxyapatite nanorods. *Biomaterials* 2011, 32, 9031-9039.
[449] Singh MP, Atkins TM, Muthuswamy E, Kamali S, Tu C, Louie AY, Kauzlarich SM. Development of Iron-Doped Silicon Nanoparticles As Bimodal Imaging Agents. *ACS Nano* 2012, 6, 5596-5604.
[450] Lim YT, Cho MY, Kim JK, Hwangbo S, Chung BH. Plasmonic magnetic nanostructure for bimodal imaging and photonic-based therapy of cancer cells. *ChemBioChem* 2007, 8, 2204-2209.
[451] Medarova Z, Kumar M, Ng S-w, Moore A. Development and application of a dual-purpose nanoparticle platform for delivery and imaging of siRNA in tumors. *Methods Mol. Biol. (Totowa, NJ, U. S.)* 2009, 555, 1-13.
[452] Wu S, Zhang L, Zhong J, Zhang Z. Dual contrast magnetic resonance imaging tracking of iron-labeled cells in vivo. *Cytotherapy* 2010, 12, 859-869.
[453] Pichler BJ, Wehrl HF, Kolb A, Judenhofer MS. Positron emission tomography/magnetic resonance imaging: the next generation of multimodality imaging? *Semin Nucl Med* 2008, 38, 199-208.
[454] Zaidi H, Del Guerra A. An outlook on future design of hybrid PET/MRI systems. *Med Phys* 2011, 38, 5667-5689.
[455] Uppal R, Ciesienski KL, Chonde DB, Loving GS, Caravan P. Discrete Bimodal Probes for Thrombus Imaging. *Journal of the American Chemical Society* 2012, 134, 10799-10802.
[456] Tran TD, Caruthers SD, Hughes M, Marsh JN, Cyrus T, Winter PM, Neubauer AM, Wickline SA, Lanza GM. Clinical applications of perfluorocarbon nanoparticles for molecular imaging and targeted therapeutics. *Int. J. Nanomed.* 2007, 2, 515-526.
[457] Oh MH, Lee N, Kim H, Park SP, Piao Y, Lee J, Jun SW, Moon WK, Choi SH, et al. Large-Scale Synthesis of Bioinert Tantalum Oxide Nanoparticles for X-ray Computed Tomography Imaging and Bimodal Image-Guided Sentinel Lymph Node Mapping. *J. Am. Chem. Soc.* 2011, 133, 5508-5515.
[458] Agarwal A, Huang SW, O'Donnell M, Day KC, Day M, Kotov N, Ashkenazi S. Targeted gold nanorod contrast agent for prostate cancer detection by photoacoustic imaging. *Journal of Applied Physics* 2007, 102, 064701-064704.
[459] Park JM, Gambhir SS. Multimodality Radionuclide, Fluorescence, and Bioluminescence Small-Animal Imaging. *Proceedings of the IEEE* 2005, 93, 771-783.
[460] Lin C-AJ, Chuang W-K, Huang Z-Y, Kang S-T, Chang C-Y, Chen C-T, Li J-L, Li JK, Wang H-H, et al. Rapid Transformation of Protein-Caged Nanomaterials into Microbubbles As Bimodal Imaging Agents. *ACS Nano* 2012, 6, 5111-5121.
[461] Zhu X, Zhou J, Chen M, Shi M, Feng W, Li F. Core-shell Fe3O4@NaLuF4:Yb,Er/Tm nanostructure for MRI, CT and upconversion luminescence tri-modality imaging. *Biomaterials* 2012, 33, 4618-4627.
[462] Barnett BP, Ruiz-Cabello J, Hota P, Ouwerkerk R, Shamblott MJ, Lauzon C, Walczak P, Gilson WD, Chacko VP, et al. Use of perfluorocarbon nanoparticles for non-invasive

multimodal cell tracking of human pancreatic islets. *Contrast Media Mol. Imaging* 2011, 6, 251-259.
[463] John R, Nguyen FT, Kolbeck KJ, Chaney EJ, Marjanovic M, Suslick KS, Boppart SA. Targeted multifunctional multimodal protein-shell microspheres as cancer imaging contrast agents. *Mol Imaging Biol* 2012, 14, 17-24.
[464] Koole R, Mulder WJM, van SMM, Strijkers GJ, Meijerink A, Nicolay K. Magnetic quantum dots for multimodal imaging. *Wiley Interdiscip. Rev.: Nanomed. Nanobiotechnol.* 2009, 1, 475-491.
[465] Erathodiyil N, Ying JY. Functionalization of Inorganic Nanoparticles for Bioimaging Applications. *Acc. Chem. Res.* 2011, 44, 925-935.
[466] Park G, Lee KG, Lee SJ, Park TJ, Wi R, Wang KW, Kim DH. Ultrasound-aided formation of gold nanoparticles on multi-walled carbon nanotubes functionalized with mercatobenzene moieties. *J. Nanosci. Nanotechnol.* 2011, 11, 6222-6226.
[467] Frey NA, Peng S, Cheng K, Sun S. Magnetic nanoparticles: synthesis, functionalization, and applications in bioimaging and magnetic energy storage. *Chem. Soc. Rev.* 2009, 38, 2532-2542.
[468] Tiwari PM, Vig K, Dennis VA, Singh SR. Functionalized gold nanoparticles and their biomedical applications. *Nanomaterials* 2011, 1, 31-63.
[469] Subbiah R, Veerapandian M, Yun KS. Nanoparticles: functionalization and multifunctional applications in biomedical sciences. *Curr Med Chem* 2010, 17, 4559-4577.
[470] Thanh NTK, Green LAW. Functionalisation of nanoparticles for biomedical applications. *Nano Today* 2010, 5, 213-230.
[471] Liu Y, Miyoshi H, Nakamura M. Nanomedicine for drug delivery and imaging: a promising avenue for cancer therapy and diagnosis using targeted functional nanoparticles. *Int J Cancer* 2007, 120, 2527-2537.
[472] Kong W-H, Bae K-H, Hong C-A, Lee Y-H, Hahn S-K, Park T-G. Multimerized siRNA Cross-linked by Gold Nanoparticles. *Bioconjugate Chem.* 2011, 22, 1962-1969.
[473] Hu R, Zhang X-B, Kong R-M, Zhao X-H, Jiang J, Tan W. Nucleic acid-functionalized nanomaterials for bioimaging applications. *J. Mater. Chem.* 2011, 21, 16323-16334.
[474] Koba W, Kim K, Lipton ML, Jelicks L, Das B, Herbst L, Fine E. Imaging devices for use in small animals. *Semin Nucl Med* 2011, 41, 151-165.
[475] Kong R-M, Zhang X-B, Chen Z, Tan W. Aptamer-Assembled Nanomaterials for Biosensing and Biomedical Applications. *Small* 2011, 7, 2428-2436.
[476] Lee JH, Yigit MV, Mazumdar D, Lu Y. Molecular diagnostic and drug delivery agents based on aptamer-nanomaterial conjugates. *Advanced Drug Delivery Reviews* 2010, 62, 592-605.
[477] Chen Y-S, Hung Y-C, Liau I, Huang GS. Assessment of the in vivo toxicity of gold nanoparticles. *Nanoscale Res. Lett.* 2009, 4, 858-864.
[478] Ferro-Flores G, Ramirez FdM, Melendez-Alafort L, Santos-Cuevas CL. Peptides for in vivo target-specific cancer imaging. *Mini-Rev. Med. Chem.* 2010, 10, 87-97.
[479] Filfil R, Jin A, Tolkatchev D, Tonan K, Gingras R, Barber PA, Ni F. Development of polyvalent peptide-conjugated magnetic nanoparticles for targeted in-vivo imaging of micro-thrombi. *Adv. Exp. Med. Biol.* 2009, 611, 415-416.
[480] Haidar ZS. Bio-inspired/-functional colloidal core-shell polymeric-based nanosystems: technology promise in tissue engineering, bioimaging and nanomedicine. *Polymers (Basel, Switz.)* 2010, 2, 323-352.
[481] Koo H, Huh MS, Sun I-C, Yuk SH, Choi K, Kim K, Kwon IC. In Vivo Targeted Delivery of Nanoparticles for Theranosis. *Acc. Chem. Res.* 2011, 44, 1018-1028.
[482] Li J, Wu D, Miao Z, Zhang Y. Preparation of quantum dot bioconjugates and their applications in bio-imaging. *Curr. Pharm. Biotechnol.* 2010, 11, 662-671.

[483] Cormode DP, Skajaa T, van Schooneveld MM, Koole R, Jarzyna P, Lobatto ME, Calcagno C, Barazza A, Gordon RE, et al. Nanocrystal Core High-Density Lipoproteins: A Multimodality Contrast Agent Platform. *Nano Letters* 2008, 8, 3715-3723.
[484] Wells MA, Abid A, Kennedy IM, Barakat AI. Serum proteins prevent aggregation of Fe2O3 and ZnO nanoparticles. *Nanotoxicology* 2012, 6, 837-846.
[485] Volden S, Lystvet SM, Halskau O, Glomm WR. Generally applicable procedure for in situ formation of fluorescent protein-gold nanoconstructs. *RSC Adv.* 2012, 2, 11704-11711.
[486] Tong S, Cradick TJ, Ma Y, Dai ZF, Bao G. Engineering imaging probes and molecular machines for nanomedicine. *Sci. China: Life Sci.* 2012, 55, 843-861.
[487] Aleksenko SS, Shmykov AY, Oszwaldowski S, Timerbaev AR. Interactions of tumour-targeting nanoparticles with proteins: potential of using capillary electrophoresis as a direct probe. *Metallomics* 2012, 4, 1141-1148.
[488] Mansur A, Mansur H, Gonzalez J. Enzyme-polymers conjugated to quantum-dots for sensing applications. *Sensors* 2011, 11, 9951-9972.
[489] Sun X, Zhao Y, Lin VSY, Slowing II, Trewyn BG. Luciferase and Luciferin Co-immobilized Mesoporous Silica Nanoparticle Materials for Intracellular Biocatalysis. *J. Am. Chem. Soc.* 2011, 133, 18554-18557.
[490] Lee D-E, Kim AY, Saravanakumar G, Koo H, Kwon IC, Choi K, Park JH, Kim K. Hyaluronidase-sensitive SPIONs for MR/optical dual imaging nanoprobes. *Macromol. Res.* 2011, 19, 861-867.
[491] Yang Y, Aw J, Chen K, Liu F, Padmanabhan P, Hou Y, Cheng Z, Xing B. Enzyme-Responsive Multifunctional Magnetic Nanoparticles for Tumor Intracellular Drug Delivery and Imaging. *Chem.--Asian J.* 2011, 6, 1381-1389.
[492] Eck W, Nicholson AI, Zentgraf H, Semmler W, Bartling S. Anti-CD4-targeted Gold Nanoparticles Induce Specific Contrast Enhancement of Peripheral Lymph Nodes in X-ray Computed Tomography of Live Mice. *Nano Lett.* 2010, 10, 2318.
[493] Khlebtsov N, Dykman L. Biodistribution and toxicity of engineered gold nanoparticles: a review of in vitro and in vivo studies. *Chemical Society Reviews* 2011, 40, 1647-1671.
[494] Liang F, Chen B. A review on biomedical applications of single-walled carbon nanotubes. *Curr. Med. Chem.* 2010, 17, 10-24.
[495] Oberdorster G, Stone V, Donaldson K. Toxicology of nanoparticles: A historical perspective. *Nanotoxicology* 2007, 1, 2-25.
[496] Park MVDZ, Lankveld DPK, van Loveren H, de Jong WH. The status of in vitro toxicity studies in the risk assessment of nanomaterials. *Nanomedicine* 2009, 4, 669-685.
[497] Han X, Corson N, Wade-Mercer P, Gelein R, Jiang J, Sahu M, Biswas P, Finkelstein JN, Elder A, et al. Assessing the relevance of in vitro studies in nanotoxicology by examining correlations between in vitro and in vivo data. *Toxicology* 2012, 297, 1-9.
[498] Sharma A, Madhunapantula SRV, Robertson GP. Toxicological considerations when creating nanoparticle-based drugs and drug delivery systems. *Expert Opin. Drug Metab. Toxicol.* 2012, 8, 47-69.
[499] Bardhan R, Lal S, Joshi A, Halas NJ. Theranostic Nanoshells: From Probe Design to Imaging and Treatment of Cancer. *Acc. Chem. Res.* 2011, 44, 936-946.
[500] Melancon MP, Zhou M, Li C. Cancer Theranostics with Near-Infrared Light-Activatable Multimodal Nanoparticles. *Acc. Chem. Res.* 2011, 44, 947-956.
[501] von MG, Park J-H, Agrawal A, Bandaru NK, Das SK, Sailor MJ, Bhatia SN. Computationally Guided Photothermal Tumor Therapy Using Long-Circulating Gold Nanorod Antennas. *Cancer Res.* 2009, 69, 3892-3900.
[502] Melancon MP, Lu W, Yang Z, Zhang R, Cheng Z, Elliot AM, Stafford J, Olson T, Zhang JZ, et al. In vitro and in vivo targeting of hollow gold nanoshells directed at epidermal

growth factor receptor for photothermal ablation therapy. *Mol. Cancer Ther.* 2008, 7, 1730-1739.
[503] Gobin AM, Lee MH, Halas NJ, James WD, Drezek RA, West JL. Near-Infrared Resonant Nanoshells for Combined Optical Imaging and Photothermal Cancer Therapy. *Nano Lett.* 2007, 7, 1929-1934.
[504] Kam NWS, O'Connell M, Wisdom JA, Dai H. Carbon nanotubes as multifunctional biological transporters and near-infrared agents for selective cancer cell destruction. *Proc. Natl. Acad. Sci. U. S. A.* 2005, 102, 11600-11605.
[505] Ishikawa M, Biju V. Luminescent quantum dots, making invisibles visible in bioimaging. *Prog. Mol. Biol. Transl. Sci.* 2011, 104, 53-99,, 54 plates.
[506] Azzazy HME, Mansour MMH, Kazmierczak SC. From diagnostics to therapy: Prospects of quantum dots. *Clinical Biochemistry* 2007, 40, 917-927.
[507] O'Neal DP, Hirsch LR, Halas NJ, Payne JD, West JL. Photo-thermal tumor ablation in mice using near infrared-absorbing nanoparticles. *Cancer Lett. (Amsterdam, Neth.)* 2004, 209, 171-176.
[508] Nagao T, Takahashi M, Matsuzaki K, Minamitani H. Application of bioimaging techniques to mechanistic studies on photodynamic therapy. *Bioimages* 2003, 11, 53-60.
[509] Couleaud P, Morosini V, Frochot C, Richeter S, Raehm L, Durand J-O. Silica-based nanoparticles for photodynamic therapy applications. *Nanoscale* 2010, 2, 1083-1095.
[510] Bae SW, Tan W, Hong J-I. Fluorescent dye-doped silica nanoparticles: new tools for bioapplications. *Chemical Communications* 2012, 48, 2270-2282.
[511] Li W, Lu W, Fan Z, Zhu X, Reed A, Newton B, Zhang Y, Courtney S, Tiyyagura PT, et al. Enhanced photodynamic selectivity of nano-silica-attached porphyrins against breast cancer cells. *Journal of Materials Chemistry* 2012, 22, 12701-12708.
[512] Heister E, Neves V, Tîlmaciu C, Lipert K, Beltrán VS, Coley HM, Silva SRP, McFadden J. Triple functionalisation of single-walled carbon nanotubes with doxorubicin, a monoclonal antibody, and a fluorescent marker for targeted cancer therapy. *Carbon* 2009, 47, 2152-2160.
[513] Fernandez-Fernandez A, Manchanda R, McGoron AJ. Theranostic Applications of Nanomaterials in Cancer: Drug Delivery, Image-Guided Therapy, and Multifunctional Platforms. *Appl. Biochem. Biotechnol.* 2011, 165, 1628-1651.
[514] Huang P, Bao L, Zhang C, Lin J, Luo T, Yang D, He M, Li Z, Gao G, et al. Folic acid-conjugated silica-modified gold nanorods for X-ray/CT imaging-guided dual-mode radiation and photo-thermal therapy. *Biomaterials* 2011, 32, 9796-9809.
[515] Liu Z, Lammers T, Ehling J, Fokong S, Bornemann J, Kiessling F, Gaetjens J. Iron oxide nanoparticle-containing microbubble composites as contrast agents for MR and ultrasound dual-modality imaging. *Biomaterials* 2011, 32, 6155-6163.
[516] Kim S, Chen Y-S, Luke GP, Emelianov SY. In vivo three-dimensional spectroscopic photoacoustic imaging for monitoring nanoparticle delivery. *Biomed Opt Express* 2011, 2, 2540-2550.
[517] Ghaghada KB, Badea CT, Karumbaiah L, Fettig N, Bellamkonda RV, Johnson GA, Annapragada A. Evaluation of tumor microenvironment in an animal model using a nanoparticle contrast agent in computed tomography imaging. *Acad Radiol* 2011, 18, 20-30.
[518] Byers RJ, Hitchman ER. Quantum dots brighten biological imaging. *Prog Histochem Cytochem* 2011, 45, 201-237.
[519] Zicha D. Quantitative imaging in metastasis research. *Int. Drug Discovery* 2010, 5, 68-71.
[520] Jacobsen B, Ploug M. The urokinase receptor and its structural homologue C4.4A in human cancer: expression, prognosis and pharmacological inhibition. *Curr. Med. Chem.* 2008, 15, 2559-2573.

[521] Chen K-J, Tang L, Garcia MA, Wang H, Lu H, Lin W-Y, Hou S, Yin Q, Shen CKF, et al. The therapeutic efficacy of camptothecin-encapsulated supramolecular nanoparticles. *Biomaterials* 2012, 33, 1162-1169.
[522] Tsai C-C, Chang C-H, Chen L-C, Chang Y-J, Lan K-L, Wu Y-H, Hsu C-W, Liu IH, Ho C-L, et al. Biodistribution and pharmacokinetics of 188Re-liposomes and their comparative therapeutic efficacy with 5-fluorouracil in C26 colonic peritoneal carcinomatosis mice. *Int. J. Nanomed.* 2011, 6, 2607-2619.
[523] Wu L, Wu X. Current application of nanotechnology in cancer prevention and treatment. *Zhonghua Zhongliu Fangzhi Zazhi* 2007, 14, 1740-1743.
[524] Rotomskis R, Streckyte G, Karabanovas V. Nanoparticles in diagnostics and therapy: towards nanomedicine. *Medicina (Kaunas)* 2006, 42, 542-558.
[525] Sukhanova A, Venteo L, Cohen JHM, Pluot M, Nabiev I. Nano-biocaptures for research and diagnostics in inflammation diseases and cancer. *Ann. Pharm. Fr.* 2006, 64, 125-134.
[526] Kircher MF, Weissleder R, Josephson L. A Dual Fluorochrome Probe for Imaging Proteases. *Bioconjugate Chem.* 2004, 15, 242-248.
[527] Yu MK, Jeong YY, Park J, Park S, Kim JW, Min JJ, Kim K, Jon S. Drug-loaded superparamagnetic iron oxide nanoparticles for combined cancer imaging and therapy in vivo. *Angew. Chem., Int. Ed.* 2008, 47, 5362-5365.
[528] Ma W-F, Wu K-Y, Tang J, Li D, Wei C, Guo J, Wang S-L, Wang C-C. Magnetic drug carrier with a smart pH-responsive polymer network shell for controlled delivery of doxorubicin. *J. Mater. Chem.* 2012, 22, 15206-15214.
[529] Aydin RST, Pulat M. 5-Fluorouracil encapsulated chitosan nanoparticles for pH-stimulated drug delivery: evaluation of controlled release kinetics. *J. Nanomater.* 2012, 313961, 313910 pp.
[530] Santra S, Kaittanis C, Perez JM. Biodegradable hyperbranched polyester: a new building block in the construction of multifunctional nanoparticles and nanocomposites for targeted cancer therapy and imaging. *Polym. Prepr. (Am. Chem. Soc., Div. Polym. Chem.)* 2010, 51, 212-213.
[531] Oishi M, Nagasaki Y. pH-responsive PEGylated nanogels as smart nanodevice for cancer diagnosis and therapy. *Polym. Prepr. (Am. Chem. Soc., Div. Polym. Chem.)* 2008, 49, 461-462.
[532] Shim MS, Kwon YJ. Stimuli-responsive polymers and nanomaterials for gene delivery and imaging applications. *Advanced Drug Delivery Reviews* 2012, 64, 1046-1059.
[533] Wijaya A, Schaffer SB, Pallares IG, Hamad-Schifferli K. Selective Release of Multiple DNA Oligonucleotides from Gold Nanorods. *ACS Nano* 2008, 3, 80-86.
[534] Braun GB, Pallaoro A, Wu G, Missirlis D, Zasadzinski JA, Tirrell M, Reich NO. Laser-Activated Gene Silencing via Gold Nanoshell-siRNA Conjugates. *ACS Nano* 2009, 3, 2007-2015.
[535] Lee SE, Liu GL, Kim F, Lee LP. Remote optical switch for localized and selective control of gene interference. *Nano Lett* 2009, 9, 562-570.
[536] Li J, Yu Z, Jiang H, Zou G, Zhang Q. Photo and pH dual-responsive polydiacetylene smart nanocontainer. *Mater. Chem. Phys.* 2012, 136, 219-224.
[537] Rastogi R, Gulati N, Kotnala RK, Sharma U, Jayasundar R, Koul V. Evaluation of folate conjugated pegylated thermosensitive magnetic nanocomposites for tumor imaging and therapy. *Colloids Surf., B* 2011, 82, 160-167.
[538] Zhang JL, Srivastava RS, Misra RDK. Core-Shell Magnetite Nanoparticles Surface Encapsulated with Smart Stimuli-Responsive Polymer: Synthesis, Characterization, and LCST of Viable Drug-Targeting Delivery System. *Langmuir* 2007, 23, 6342-6351.
[539] Knecht LD, Ali N, Wei Y, Hilt JZ, Daunert S. Nanoparticle-Mediated Remote Control of Enzymatic Activity. *ACS Nano* 2012, 6, 9079-9086.

[540] Nie L, Zeng X, Guo H, Zhang L. Poly(N-isopropylacrylamide)-coated thermoresponsive/magnetic/fluorescent multifunctional microspheres. *Adv. Sci. Lett.* 2012, 10, 202-207.
[541] Park S, Kim HS, Kim WJ, Yoo HS. Pluronic@Fe3O4 nanoparticles with robust incorporation of doxorubicin by thermo-responsiveness. *Int. J. Pharm. (Amsterdam, Neth.)* 2012, 424, 107-114.
[542] Baeza A, Guisasola E, Ruiz-Hernandez E, Vallet-Regi M. Magnetically Triggered Multidrug Release by Hybrid Mesoporous Silica Nanoparticles. *Chem. Mater.* 2012, 24, 517-524.
[543] Hiraiwa K, Ueda M, Takeuchi H, Oyama T, Irino T, Yoshikawa T, Kondo A, Kitagawa Y. Sentinel node mapping with thermoresponsive magnetic nanoparticles in rats. *J Surg Res* 2012, 174, 48-55.
[544] Li Q, Zhang L, Bai L, Zhang Z, Zhu J, Zhou N, Cheng Z, Zhu X. Multistimuli-responsive hybrid nanoparticles with magnetic core and thermoresponsive fluorescence-labeled shell via surface-initiated RAFT polymerization. *Soft Matter* 2011, 7, 6958-6966.
[545] Yu SS, Scherer RL, Ortega RA, Bell CS, O'Neil CP, Hubbell JA, Giorgio TD. Enzymatic- and temperature-sensitive controlled release of ultrasmall superparamagnetic iron oxides (USPIOs). *J. Nanobiotechnol.* 2011, 9, 7.
[546] Omer M, Haider S, Park S-Y. A novel route for the preparation of thermally sensitive core-shell magnetic nanoparticles. *Polymer* 2011, 52, 91-97.
[547] Lapointe J, Martel S. Thermoresponsive hydrogel with embedded magnetic nanoparticles for the implementation of shrinkable medical microrobots and for targeting and drug delivery applications. Engineering in Medicine and Biology Society, 2009. EMBC 2009. Annual International Conference of the IEEE2009. p. 4246-4249.
[548] Aznar E, Mondragon L, Ros-Lis JV, Sancenon F, Marcos MD, Martinez-Manez R, Soto J, Perez-Paya E, Amoros P. Finely Tuned Temperature-Controlled Cargo Release Using Paraffin-Capped Mesoporous Silica Nanoparticles. *Angew. Chem., Int. Ed.* 2011, 50, 11172-11175, S11172/11171-S11172/11112.
[549] Tagami T, Foltz WD, Ernsting MJ, Lee CM, Tannock IF, May JP, Li S-D. MRI monitoring of intratumoral drug delivery and prediction of the therapeutic effect with a multifunctional thermosensitive liposome. *Biomaterials* 2011, 32, 6570-6578.
[550] Qin S, Seo JW, Zhang H, Qi J, Curry F-RE, Ferrara KW. An imaging-driven model for liposomal stability and circulation. *Mol Pharm* 2010, 7, 12-21.
[551] Sugihara S, Ito S, Irie S, Ikeda I. Synthesis of Thermoresponsive Shell Cross-Linked Micelles via Living Cationic Polymerization and UV Irradiation. *Macromolecules (Washington, DC, U. S.)* 2010, 43, 1753-1760.
[552] Wang P, He J, Wang P-N, Chen J-Y. Poly (N-isopropylacrylamide)-coated multifunctional nanoparticles for cell tracking. *Photomed. Laser Surg.* 2010, 28, 201-205.
[553] Schroeder A, Goldberg MS, Kastrup C, Wang Y, Jiang S, Joseph BJ, Levins CG, Kannan ST, Langer R, et al. Remotely Activated Protein-Producing Nanoparticles. *Nano Lett.* 2012, 12, 2685-2689.
[554] Antipina MN, Sukhorukov GB. Remote control over guidance and release properties of composite polyelectrolyte based capsules. *Adv. Drug Delivery Rev.* 2011, 63, 716-729.
[555] He Z-W, Satarkar N, Xie T, Cheng Y-T, Hilt JZ. Remote Controlled Multishape Polymer Nanocomposites with Selective Radiofrequency Actuations. *Adv. Mater. (Weinheim, Ger.)* 2011, 23, 3192-3196.
[556] Lehner R, Wang X, Wolf M, Hunziker P. Designing switchable nanosystems for medical application. *J. Controlled Release* 2012, 161, 307-316.
[557] Chan A, Orme RP, Fricker RA, Roach P. Remote and local control of stimuli responsive materials for therapeutic applications. *Adv Drug Deliv Rev* 2012.

[558] Lee J-H, Jang J-t, Choi J-s, Moon SH, Noh S-h, Kim J-w, Kim J-G, Kim I-S, Park KI, et al. Exchange-coupled magnetic nanoparticles for efficient heat induction. *Nat. Nanotechnol.* 2011, 6, 418-422.
[559] Huang H, Delikanli S, Zeng H, Ferkey DM, Pralle A. Remote control of ion channels and neurons through magnetic-field heating of nanoparticles. *Nat. Nanotechnol.* 2010, 5, 602-606.
[560] Knoepfel T, Akemann W. Remote control of cells. *Nat. Nanotechnol.* 2010, 5, 560-561.
[561] Carling C-J, Nourmohammadian F, Boyer J-C, Branda NR. Remote-Control Photorelease of Caged Compounds Using Near-Infrared Light and Upconverting Nanoparticles. *Angew. Chem., Int. Ed.* 2010, 49, 3782-3785, S3782/3781-S3782/3789.

Caption to figures:

Figure 1. *In vivo* testing of the (Tf)-SPION conjugate in rats bearing 9L gliosarcoma tumors. Two tumors expressing either a high (9L3.9) or a low (9L4.2) level of the TfR were imaged before injection and 72 hours after injection of Tf-SPION particles. Reprinted with permission from [95]. Copyright (2003) Neoplasia Press.

Figure 2. *In vivo* five-color lymphatic drainage imaging pointing at five distinct lymphatic drainages. (a) *In vivo* and intra-surgical spectral fluorescence imaging of a mouse injected with five carboxyl QDs (565, blue; 605, green; 655, yellow; 705, magenta; 800, red) intra-cutaneously into the middle digits of the bilateral upper extremities, the bilateral ears, and at the median chin, as shown in the right hand side schema. Five primary draining lymph nodes were simultaneously visualized with different colors through the skin in the *in vivo* image and were more clearly seen in the image taken at the surgery. Reprinted, with permission, from Ref. [117], Copyright (2007) American Chemical Society.

Figure 3. a) *In vivo* images of LPSiNPs and Dextran-coated-LPSiNPs. The mice were imaged at multiple time points after intravenous injection of LPSiNPs and Dextran-coated-LPSiNPs (20 mg kg^{-1}). Arrowheads and arrows with solid lines indicate liver and bladder, respectively. b) Lateral image of the same mice shown in a), 8 h after LPSiNP or Dextran-coated-LPSiNP injection. Arrows with dashed lines indicate spleen. Reprinted by permission from Macmillan Publishers Ltd from Ref. [160]. Copyright (2009) Nature Publishing Group.

Figure 4: PET/CT images of the 30 nm ^{64}Cu-DOTA-PEG-Au NCs in a mouse bearing an EMT-6 tumor at 1, 4, and 24 h post- injection (3.7 MBq injection/mouse). T, tumor; B, bladder. The increase of tumor-to-muscle ratios was consistent with the biodistribution measurements. Reprinted, with permission, from Ref. [161]. Copyright (2012) American Chemical Society.

Figure 5. Dynamic PET/CT imaging of BALB/C mouse injected with ^{18}F-CLIO. Merged PET/CT coronal images at 2 h (**a**), 7 h (**b**), and 16 h (**c**) post-injection of ^{18}F-CLIO. PET only coronal images at 2 h (**d**), 7 h (**e**), and 16 h (**f**) post-injection of ^{18}F-CLIO. CT only coronal image (**g**). Three-dimensional merged PET-CT images at 2 h (**h**) and 16 h (**i**) post-injection. The *green arrow* indicates blood pool region of interest (ROI) and the *asterisk* indicates liver ROI. Reprinted, with permission, from Ref. [34]. Copyright (2009) American Chemical Society.

Figure 6. *In vivo* PET–MR imaging studies with [^{64}Cu(dtcbp)$_2$]-Fe_3O_4 NPs in mouse. A,B) Coronal (top) and short axis (bottom) MR images of the lower abdominal area and upper hind legs showing the popliteal lymph nodes (solid arrows) before (A) and after (B) footpad injection of [^{64}Cu(dtcbp)$_2$]-Fe_3O_4. C) Coronal (top) and short-axis (bottom) Nano PET–CT images of the same mouse as in (B) showing the uptake of the NPs in the popliteal (solid arrow) and iliac lymph nodes (hollow arrow). D) Whole-body NanoPET–CT images showing sole uptake of [^{64}Cu(dtcbp)$_2$]-Fe_3O_4in the popliteal and iliac lymph nodes. No translocation of radioactivity to other tissues was detected. Reprinted, with permission, from Ref. [173]. Copyright (2011) John Wiley and Sons.

Figure 7. Whole-animal SPECT/CT imaging, immediately after tail intravenous injection administration of filled, functionalized SWNTs (left hand side); and radionuclide alone (right hand side). Reprinted, with permission, from Ref. [210]. Copyright (2010) Nature Publishing Group.

Figure 8. Photo-acoustic detection of SWNT-ICG in living mice. (**a**) Mice were injected subcutaneously with SWNT-ICG at various concentrations - 0.82–200 nmol L^{-1}). The images represent ultrasound (gray) and photoacoustic (green) vertical slices through the subcutaneous injections (dotted black line). The skin is visualized in the ultrasound images, and the photoacoustic images show the SWNT-ICG distribution. The nanobeacons on the images illustrate the approximate edges of each inclusion. (**b**) The photoacoustic signal from each inclusion was calculated using 3D regions of interest and the "background" represents the endogenous signal measured from tissues. Linear regression ($R^2 = 0.97$) of the photoacoustic signal curve indicates that 170 pmol.L^{-1} SWNT-ICG will give the equivalent background signal of tissues. Reprinted, with permission, from Ref. [371], Copyright (2010) American Chemical Society.

Figure 9. Description of proton beam irradiation on tumor tissue in the presence of metallic NPs. Tumor-associated macrophage, distributed in tumor periphery, uptakes metallic nanoparticles, which produces a therapeutic effect potentially on TAM and infiltrated tumor cell by proton-induced X-ray emission (PIXE) effect. Reprinted, with permission, from Ref. [414]. Copyright (2010) IOP Publishing Ltd.

Figure 10. Sagittal cut through a hair follicle of porcine skin exposed to a formulation containing nanosized TiO_2. PIXE-data were taken with 2.25 MeV protons at 100 pA and a charge of 0.5 µC. The scan size is 400 µm×400 µm, on 256×256 pixels and a lateral resolution around 1 µm. The formulation with NPs (blue) is deeply pushed into the follicle. Reprinted, with permission, from Ref. [418]. Copyright (2007) Elsevier.

Figure 11. a) Density map (STIM) and *in situ* 2D chemical imaging (PIXE) of HaCat cells exposed to titanium oxide NPs. Control HaCat cells (left panel) and HaCat cells exposed to titanium oxide NPs (right panel) have been investigated using phase contrast imaging and STIM/PIXE analysis. The simultaneous combination of STIM and PIXE reveals the specific *in situ* chemical distribution in the whole cellular body. A specific pattern is observed for the phosphorus distribution which is mainly located in the cell nucleus. Titanium is only detected in exposed cells with disperse but punctuated distribution in the cellular body. Scale bar, 10 µm. b) High resolution confocal image of paraformaldehyde-fixed PHFK cells treated with Fluorecein-TiO_2-NPs (green) at a final concentration of 2 mg/cm^2 for 24 h and treated for immunofluorescence with propidium iodide (PI) (cytoplasm and nucleolus, red) and Hoechst^{33342} (nucleus, blue): top Fluorescence image, bottom 3D reconstruction.

Figure 12. Density map (STIM) and *in situ* chemical imaging (PIXE) of a lyophilized adult *C. elegans* exposed to titanium oxide nanoparticles. (top) STIM rendition of the whole *C. elegans* body. Regions of interest corresponding to buccal cavity, pharynx corpus (metacorpus), pharyngeal posterior part with terminal bulb and anterior part of the intestine (GUT) are shown. Intestinal cells can be also seen between gut and uterus which is full of fertilized eggs. (bottom) 2D maps of phosphorus (green), sulfur (red) and titanium (blue) in the whole *C. elegans* body. Co-localization map reveals a highly specific distribution of element in organs suggesting a link between chemical anatomical structure and their functions. The titanium oxide nanoparticles ingestion is demonstrated by the presence of titanium in the pharyngeal metacarpus and in the rectum. Phosphorus (green), sulfur (red) and titanium (blue). Scale bar, 20 μm.

Figure 13. Different types of surface functionalization and morphologies of inorganic NPs. Reprinted with permission from [12] Copyright (2012) John Wiley and Sons.

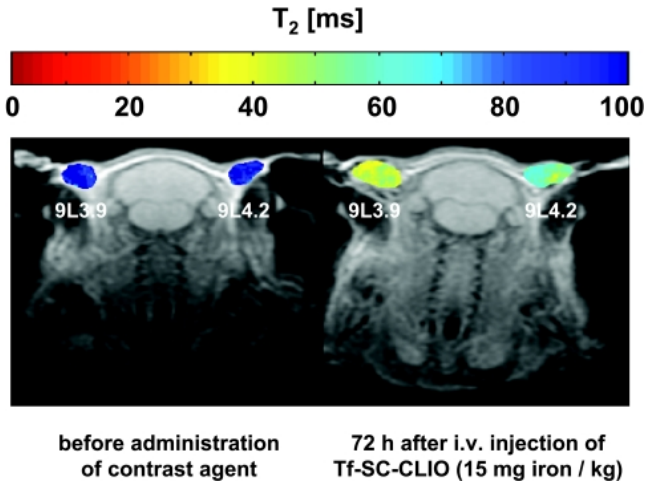

Figure 14. *In vivo* testing of the (Tf)-SPION conjugate in rats bearing 9L gliosarcoma tumors. Two tumors expressing either a high (9L3.9) or a low (9L4.2) level of the TfR were imaged before injection and 72 hours after injection of Tf-SPION particles. Reprinted with permission from [95]. Copyright (2003) Neoplasia Press.

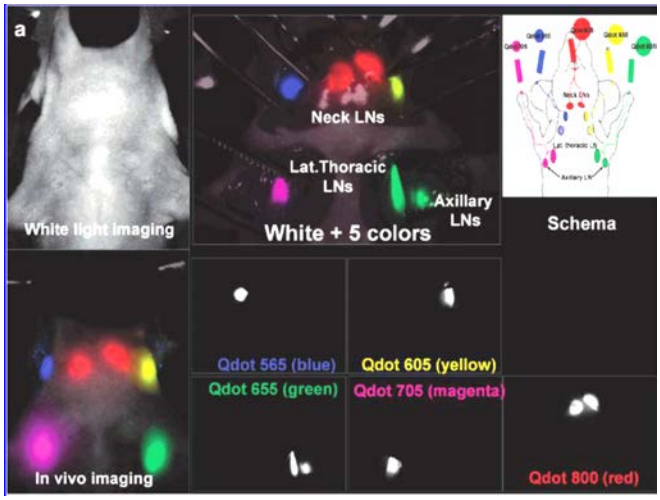

Figure 15. *In vivo* five-color lymphatic drainage imaging pointing at five distinct lymphatic drainages. (a) *In vivo* and intra-surgical spectral fluorescence imaging of a mouse injected with five carboxyl QDs (565, blue; 605, green; 655, yellow; 705, magenta; 800, red) intra-cutaneously into the middle digits of the bilateral upper extremities, the bilateral ears, and at the median chin, as shown in the right hand side schema. Five primary draining lymph nodes were simultaneously visualized with different colors through the skin in the *in vivo* image and were more clearly seen in the image taken at the surgery. (Reprinted, with permission, from Ref. [117], Copyright (2007) American Chemical Society)

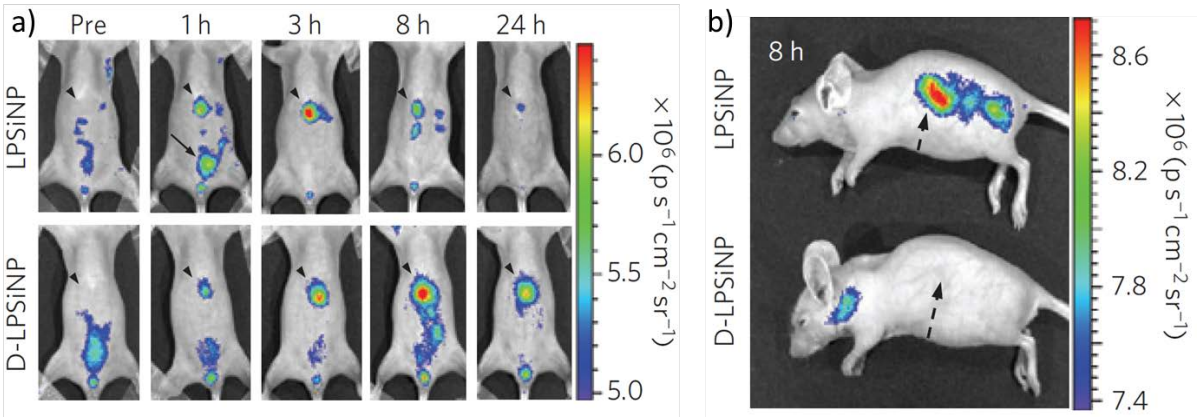

Figure 16. a) *In vivo* images of LPSiNPs and Dextran-coated-LPSiNPs. The mice were imaged at multiple time points after intravenous injection of LPSiNPs and Dextran-coated-LPSiNPs (20 mg kg^{-1}). Arrowheads and arrows with solid lines indicate liver and bladder, respectively. b) Lateral image of the same mice shown in a), 8 h after LPSiNP or Dextran-coated-LPSiNP injection. Arrows with dashed lines indicate spleen. Reprinted by permission from Macmillan Publishers Ltd from Ref. [160]. Nature Materials. Copyright 2009.

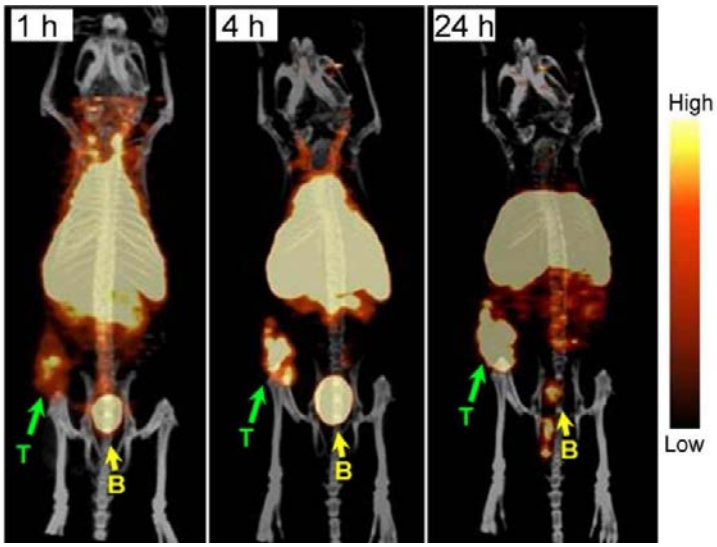

Figure 17: PET/CT images of the 30 nm ^{64}Cu-DOTA-PEG-Au NCs in a mouse bearing an EMT-6 tumor at 1, 4, and 24 h post- injection (3.7 MBq injection/mouse). T, tumor; B, bladder. The increase of tumor-to-muscle ratios was consistent with the biodistribution measurements. Reprinted, with permission, from Ref. [161], Copyright (2012) American Chemical Society.

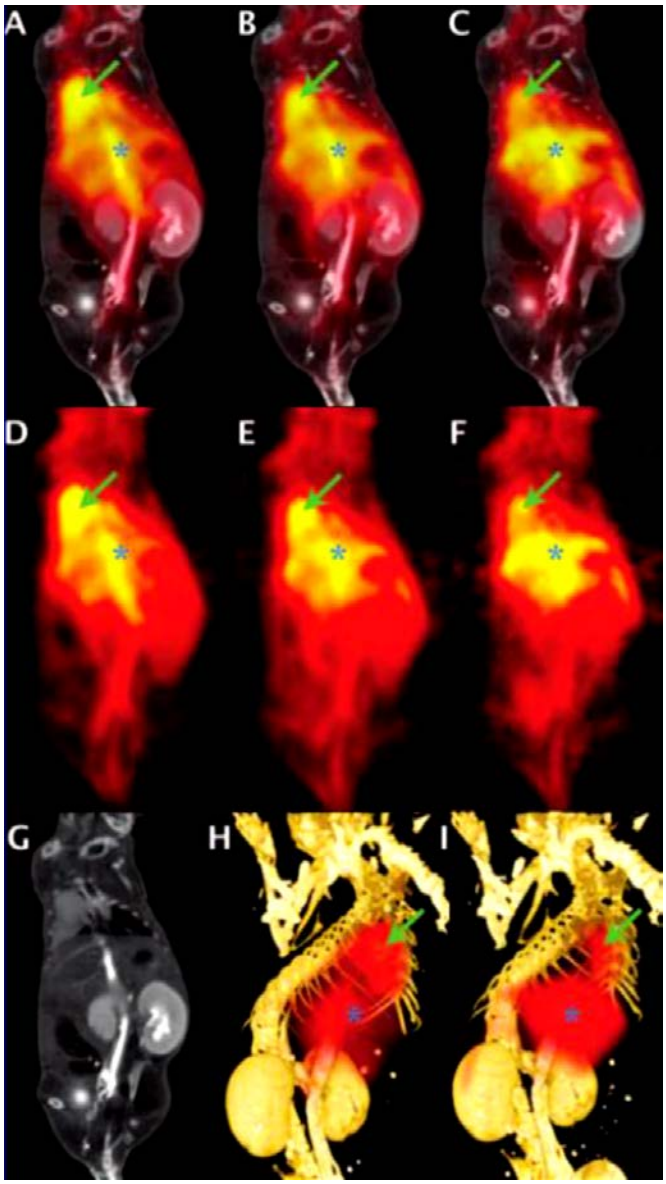

Figure 18. Dynamic PET/CT imaging of BALB/C mouse injected with ^{18}F-CLIO. Merged PET/CT coronal images at 2 h (**a**), 7 h (**b**), and 16 h (**c**) post-injection of ^{18}F-CLIO. PET only coronal images at 2 h (**d**), 7 h (**e**), and 16 h (**f**) post-injection of ^{18}F-CLIO. CT only coronal image (**g**). Three-dimensional merged PET-CT images at 2 h (**h**) and 16 h (**i**) post-injection. The *green arrow* indicates blood pool region of interest (ROI) and the *asterisk* indicates liver ROI. Reprinted, with permission, from Ref. [34], Copyright (2009) American Chemical Society.

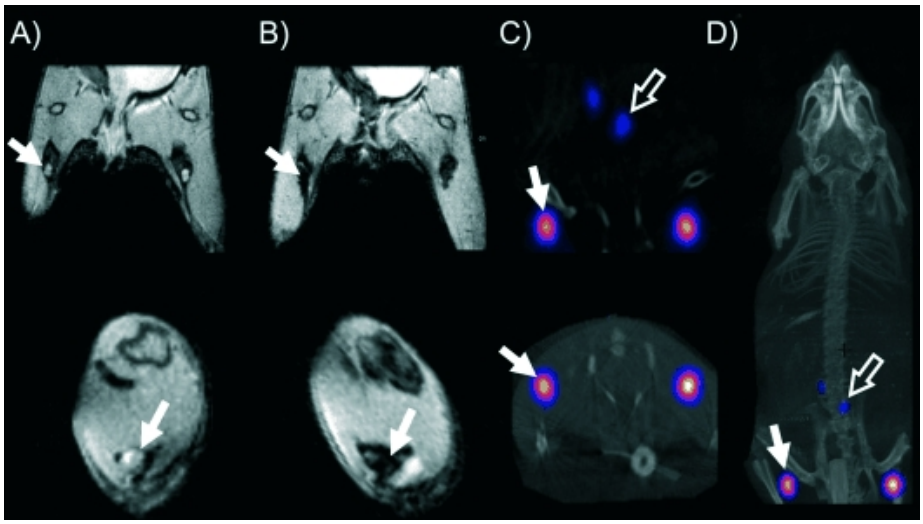

Figure 19. *In vivo* PET–MR imaging studies with [^{64}Cu(dtcbp)$_2$]-Fe_3O_4 NPs in mouse. A,B) Coronal (top) and short axis (bottom) MR images of the lower abdominal area and upper hind legs showing the popliteal lymph nodes (solid arrows) before (A) and after (B) footpad injection of [^{64}Cu(dtcbp)$_2$]-Fe_3O_4. C) Coronal (top) and short-axis (bottom) Nano PET–CT images of the same mouse as in (B) showing the uptake of the NPs in the popliteal (solid arrow) and iliac lymph nodes (hollow arrow). D) Whole-body NanoPET–CT images showing sole uptake of [^{64}Cu(dtcbp)$_2$]-Fe_3O_4in the popliteal and iliac lymph nodes. No translocation of radioactivity to other tissues was detected. Reprinted, with permission, from Ref. [173]. Copyright (2011) John Wiley and Sons.

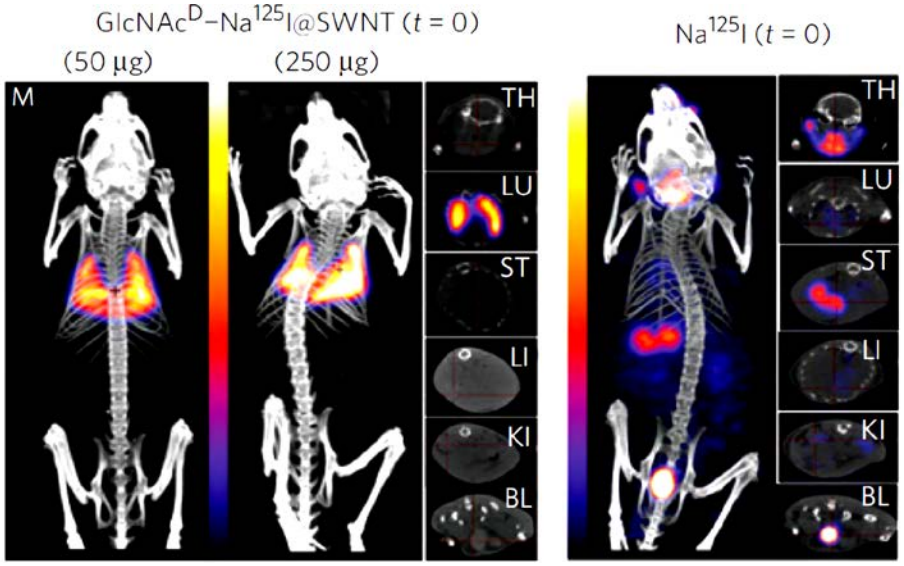

Figure 20. Whole-animal SPECT/CT imaging, immediately after tail intravenous injection administration of filled, functionalized SWNTs (left hand side); and radionuclide alone (right hand side). Reprinted, with permission, from Ref. [210]. Copyright (2010) Nature Publishing Group.

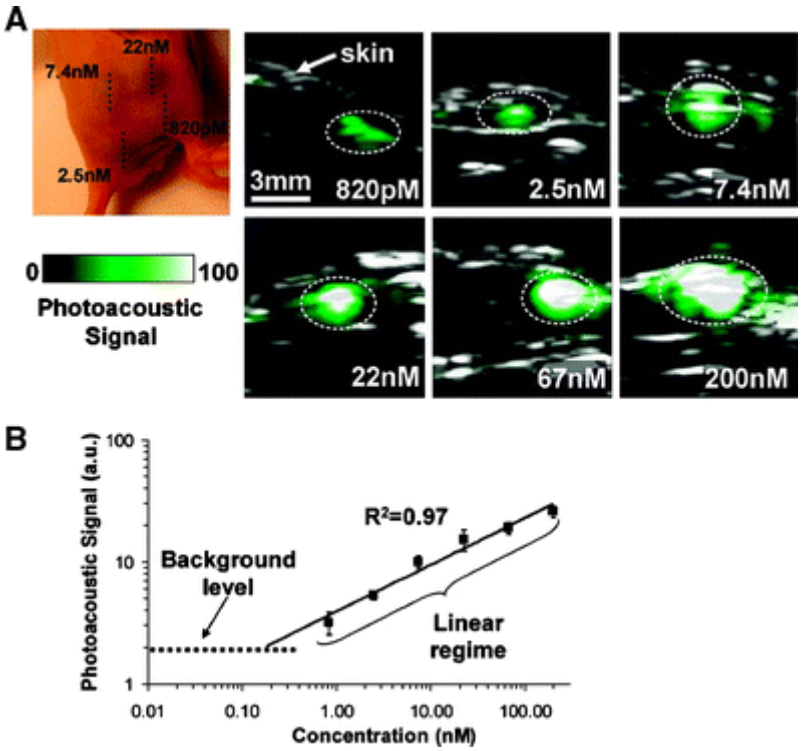

Figure 21. Photo-acoustic detection of SWNT-ICG in living mice. (**a**) Mice were injected subcutaneously with SWNT-ICG at various concentrations - 0.82–200 nmol L^{-1}). The images represent ultrasound (gray) and photoacoustic (green) vertical slices through the subcutaneous injections (dotted black line). The skin is visualized in the ultrasound images, and the photoacoustic images show the SWNT-ICG distribution. The nanobeacons on the images illustrate the approximate edges of each inclusion. (**b**) The photoacoustic signal from each inclusion was calculated using 3D regions of interest and the "background" represents the endogenous signal measured from tissues. Linear regression ($R^2 = 0.97$) of the photoacoustic signal curve indicates that 170 pmol.L^{-1} SWNT-ICG will give the equivalent background signal of tissues. Reprinted, with permission, from Ref. [371], Copyright (2010) American Chemical Society.

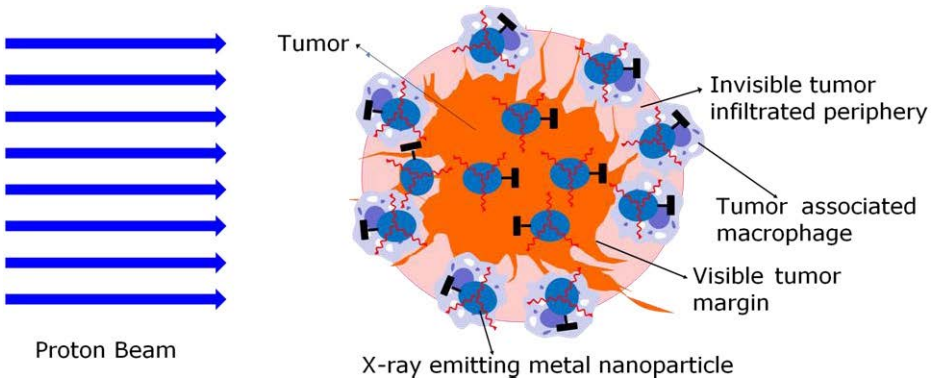

Figure 22. Description of proton beam irradiation on tumor tissue in the presence of metallic NPs. Tumor-associated macrophage, distributed in tumor periphery, uptakes metallic nanoparticles, which produces a therapeutic effect potentially on TAM and infiltrated tumor cell by proton-induced X-ray emission (PIXE) effect. Reprinted, with permission, from Ref. [414]. Copyright 2010 IOP Publishing Ltd.

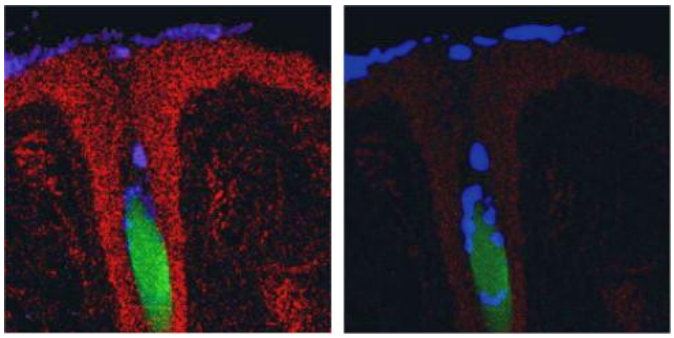

Figure 23. Sagittal cut through a hair follicle of porcine skin exposed to a formulation containing nanosized TiO_2. PIXE-data were taken with 2.25 MeV protons at 100 pA and a charge of 0.5 µC. The scan size is 400 µm×400 µm, on 256×256 pixels and a lateral resolution around 1 µm. The formulation with NPs (blue) is deeply pushed into the follicle. Reprinted, with permission, from Ref. [418]. Copyright 2007 Elsevier.

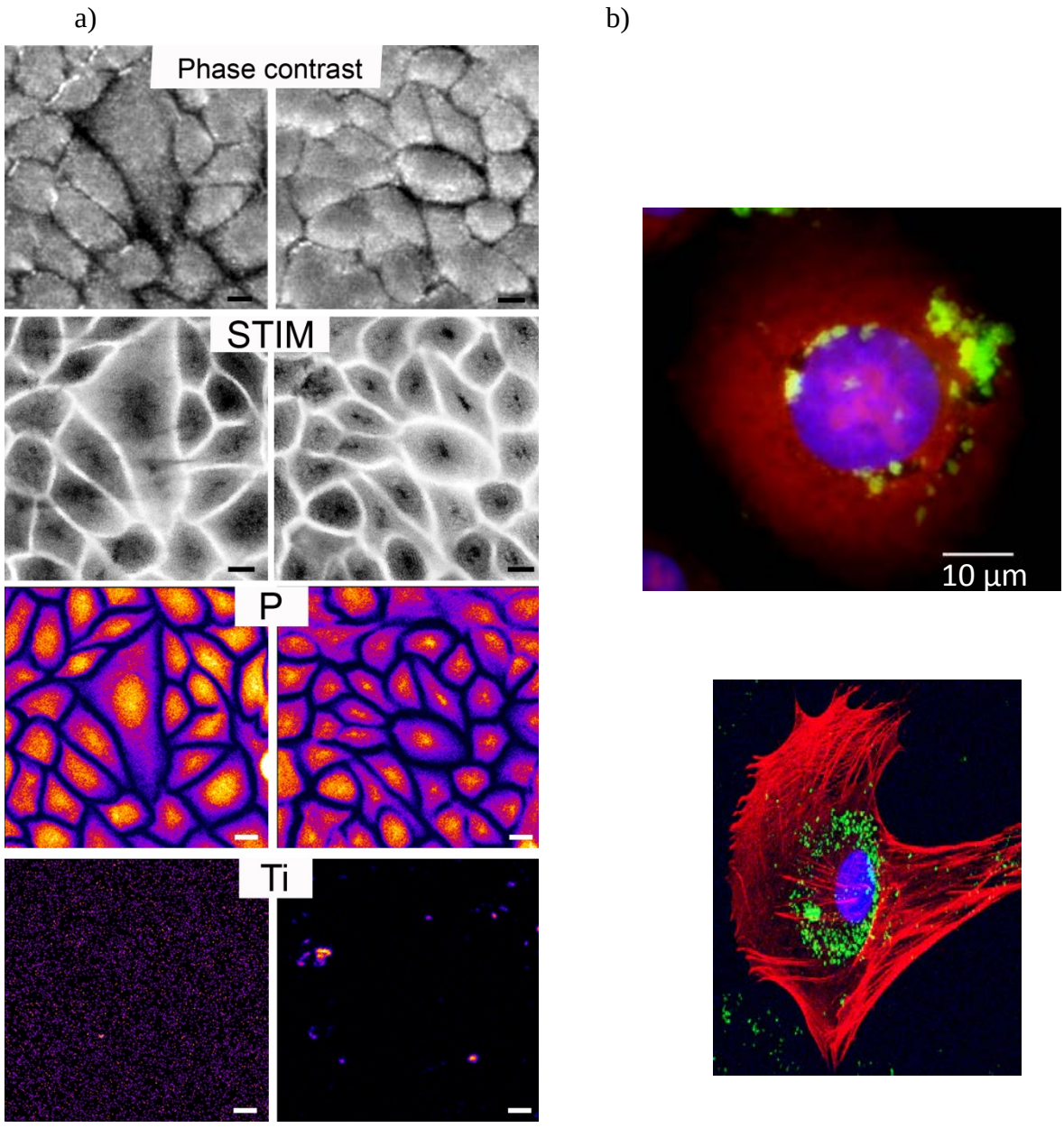

Figure 24. a) Density map (STIM) and *in situ* 2D chemical imaging (PIXE) of HaCat cells exposed to titanium oxide NPs. Control HaCat cells (left panel) and HaCat cells exposed to titanium oxide NPs (right panel) have been investigated using phase contrast imaging and STIM/PIXE analysis. The simultaneous combination of STIM and PIXE reveals the specific *in situ* chemical distribution in the whole cellular body. A specific pattern is observed for the phosphorus distribution which is mainly located in the cell nucleus. Titanium is only detected in exposed cells with disperse but punctuated distribution in the cellular body. Scale bar, 10 □m. b) High resolution confocal image of paraformaldehyde-fixed PHFK cells treated with Fluorecein-TiO_2-NPs (green) at a final concentration of 2 mg/cm^2 for 24 h and treated for

immunofluorescence with propidium iodide (PI) (cytoplasm and nucleolus, red) and Hoechst[33342] (nucleus, blue): top Fluorescence image, bottom 3D reconstruction.

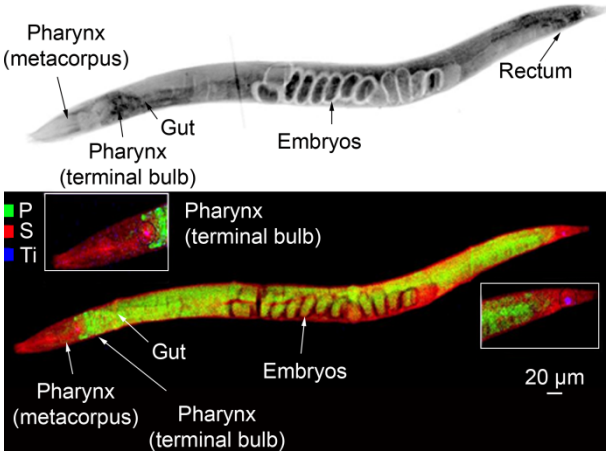

Figure 25. – Density map (STIM) and *in situ* chemical imaging (PIXE) of a lyophilized adult *C. elegans* exposed to titanium oxide nanoparticles. (top) STIM rendition of the whole *C. elegans* body. Regions of interest corresponding to buccal cavity, pharynx corpus (metacorpus), pharyngeal posterior part with terminal bulb and anterior part of the intestine (GUT) are shown. Intestinal cells can be also seen between gut and uterus which is full of fertilized eggs. (bottom) 2D maps of phosphorus (green), sulfur (red) and titanium (blue) in the whole *C. elegans* body. Co-localization map reveals a highly specific distribution of element in organs suggesting a link between chemical anatomical structure and their functions. The titanium oxide nanoparticles ingestion is demonstrated by the presence of titanium in the pharyngeal metacarpus and in the rectum. Phosphorus (green), sulfur (red) and titanium (blue). Scale bar, 20 µm.

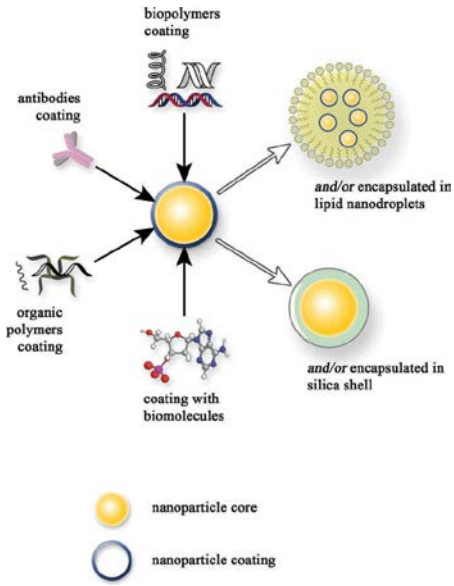

Figure 26. Different types of surface functionalization and morphologies of inorganic NPs. Reprinted with permission from [12] Copyright 2012 John Wiley and Sons.

Quentin Le Trequesser is a PhD student sharing is time between the Institute for Solid State Chemistry Bordeaux (ICMCB, France) and the center of nuclear studies of Bordeaux-Gradignan (CENBG, France). His current research involves synthesis and characterization of TiO_2 nanoparticles with highly controlled morphologies in order to study their mechanisms of internalization and toxicity in biological systems.

Hervé Seznec is research associate CNRS/IN2P3/University of Bordeaux at the Centre Etudes Nucléaires de Bordeaux Grandignan, UMR 5797) in Gradignan, France. He received his doctorate (PhD) in Human Molecular Genetics from the University of Paris, France in 2001. His area of research includes biology/genetics, biophyscis and biochemistry. His current research interests focus on the development of cell irradiation and correlative cell imaging methodologies based on charged particle microbeam for studying the cellular physiology of *in vitro* and *in vivo* biological systems. One of the major objectives of his research is to address the toxicology of metal oxide nanoparticles using human cell culture or as nematode *C. elegans*.

Marie-Hélène DELVILLE is a Senior Researcher at French National Centre for Scientific Research CNRS since 1985. She had been working for 10 years in organometallic chemistry before moving to the Institute of Condensed Matter of Bordeaux in 1996, where she is currently working. Her research interests are focused on the fundamental and practical aspects involved in the synthesis of organic–inorganic colloidal nanoobjects with special emphasis on the synthesis, control of shape, surface functionalization of mineral oxide particles and sol–gel chemistry. Her research also includes, at the interface between chemistry and biology, their use in biomedical applications, focusing on the synthesis of multimodal nanoparticles for imaging and therapy purposes with some insight in toxicity approaches.